Forest-atmosphere exchange of reactive nitrogen in a low polluted area – Part I: Measuring temporal dynamics

Pascal Wintjen[1], Frederik Schrader[1], Martijn Schaap[2,3], Burkhard Beudert[4], and Christian Brümmer[1]

[1]Thünen Institute of Climate-Smart Agriculture, Bundesallee 68, 38116, Braunschweig, Germany
[2]TNO, Climate Air and Sustainability, Utrecht, 3584 CB, The Netherlands
[3]Institute of Meteorology, Freie Universität Berlin, 12165 Berlin, Germany
[4]Bavarian Forest National Park, 94481, Grafenau, Germany

Correspondence: Pascal Wintjen (pascal.wintjen@thuenen.de)

Abstract. ~~Understanding the biosphere-atmosphere exchange characteristics of nitrogen is essential for the parameterization of modern deposition routines. For investigating temporal dynamics and responses of reactive nitrogen compounds to micrometeorology and biophysical factors, long-term flux measurements are needed.~~ Long-term dry deposition flux measurements of reactive nitrogen based on the eddy-covariance or the aerodynamic gradient method are scarce. Due to the large diversity of reactive nitrogen compounds and high technical requirements for the measuring devices, simultaneous measurements of individual reactive nitrogen compounds are not affordable.~~In this study~~Hence, we ~~investigate~~ examined the exchange patterns of total reactive nitrogen (ΣN_r) and determined annual dry deposition budgets based on measured data at a low-polluted mixed forest located in the Bavarian Forest National Park (NPBW), Germany. Flux measurements of ΣN_r were carried out with a Total Reactive Atmospheric Nitrogen Converter (TRANC) coupled to a chemiluminescence dectector (CLD) for 2.5 years.

The average ΣN_r concentration was 3.1 µg N m^{-3}. Denuder measurements with DELTA samplers and chemiluminescence measurements of nitrogen oxides (NO_x) have shown that NO_x has the highest contribution to ΣN_r ($\sim$ 51.4%), followed by ammonia (NH_3) ($\sim$ 2~~1~~0.0%), ammonium (NH_4^+) ($\sim$ 15.3%), nitrate NO_3^- ($\sim$ 7.0%), and nitric acid (HNO_3) ($\sim$ 6.3%). Only slight seasonal changes were found in the ΣN_r concentration level whereas a seasonal pattern was observed for the contribution of NH_3 and NO_x. NH_3 showed highest contributions to ΣN_r in spring and summer, NO_x in autumn and winter.

We observed ~~mostly~~ deposition fluxes at the measurement site with median fluxes ranging from -15 to -5 ng N m^{-2} s^{-1} (negative fluxes indicate deposition). Median deposition velocities ranged from 0.2 to 0.5 cm s^{-1}. In general, highest deposition velocities were recorded during high incident radiation, in particular from May to September. Our results suggest that seasonal changes in ~~concentrations~~ composition of ~~the~~ ΣN_r ~~compounds~~,~~and~~ global radiation (R_g) and other drivers correlated with R_g were most likely influencing the deposition velocity (v_d). We found that from May to September higher temperatures, lower relative humidity, and dry leaf surfaces~~, and no precipitation~~ increase v_d of ΣN_r. At the measurement site, ΣN_r concentration did not emerge as a driver for the ΣN_r v_d. ~~The effective canopy resistance ($R_{c,eff}$) was slightly lower at low relative humidity and higher ΣN_r concentrations. Aerodynamic (R_a) and boundary-layer resistance (R_b) showed a negligible contribution to v_d in comparison to $R_{c,eff}$ highlighting the importance of the surface resistance to the uptake of ΣN_r. Presumably, stomatal uptake seemed to be most responsible for ΣN_r during those months.~~

~~During rain and in periods of lower radiation, v_d was significantly lower and sometimes even negative indicating emission phases of ΣN_r. In those times, $R_{c,eff}$ increased, and R_a and R_b were in same order of magnitude as $R_{c,eff}$, and thus atmospheric resistances seemed to be as important as the surface resistance for the ΣN_r exchange. In periods of lower radiation and rain, cuticular or soil processes appeared to be relevant for the ΣN_r exchange.~~

No significant influence of temperature, humidity, friction velocity, or ~~precipitation~~ wind speed on ΣN_r dry deposition sums were found ~~with differences between deposition estimates being within their uncertainty ranges~~. We used the Mean-Diurnal-Variation (MDV) approach for filling gaps of up to five days. Remaining gaps were replaced by a monthly average of the specific half-hour value. From June 2016 to May 2017 and June 2017 to May 2018, we estimated dry deposition sums of 3.8~~±0.8 kg N ha^{-1}~~ and 4.~~1~~0~~±1.1~~ kg N ha^{-1} a^{-1} , respectively. ~~Mean total wet depositions were 8.0 kg N ha^{-1} and 6.8 kg N ha^{-1} for the timeframes 2016/2017 and 2017/2018, respectively.~~ Adding results from the wet deposition measurements ~~to the measurement years~~, we determined ~~11.8~~12.2 ~~kg N ha^{-1}~~ and 10.9 kg N ha^{-1} a^{-1} as total nitrogen deposition~~, respectively.~~in the two years of observation.

~~Our findings provide a better understanding of exchange dynamics at low-polluted, natural ecosystems, thereby providing opportunities for further development of deposition models.~~This work encompasses (one of) the first long-term flux measurements of ΣN_r using novel measurement techniques for estimating annual nitrogen dry deposition of a forest ecosystem.

1 Introduction

Reactive nitrogen (N_r) compounds are essential nutrients for plants. However, an intensive supply of nitrogen by fertilisation or atmospheric deposition is harmful for natural ecosystems and leads to a loss of biodiversity through soil acidification and eutrophication (Krupa, 2003; Galloway et al., 2003) and may also threaten human health by acting as precoursors for ozone (O_3) and PM~~2.5~~$_{2.5}$ (Erisman et al., 2013). Atmospheric nitrogen load increased significantly during the last century due to intensive crop production and livestock farming (Sutton et al., 2011; Flechard et al., 2011, 2013; Sutton et al., 2013) (mainly through ammonia) and fossil fuel combustion by traffic and industry (mainly through nitrogen dioxide and ~~nitrogen~~ nitric oxide). The additional amount of N_r enhances biosphere-atmosphere exchange of N_r (Flechard et al., 2011), affects plant health (Sutton et al., 2011) and influences the carbon sequestration of ecosystems such as forests (Magnani et al., 2007; Högberg, 2007; Sutton et al., 2008; Flechard et al., 2020), although the impact of increasing nitrogen deposition on forests carbon sequestration is still under investigation.

For estimating the biosphere-atmosphere exchange of N_r compounds such as nitrogen dioxide (NO_2), ~~nitrogen monoxide~~ nitric oxide (NO), ~~nitrogen dioxide (NO_2),~~ ammonia (NH_3), nitrous acid (HONO), nitric acid (HNO_3) and ~~particulate ammonium nitrate (NH_4NO_3)~~ particulate ammonium (NH_4^+) and nitrate (NO_3^-), micrometeorological methods such as the eddy-covariance (EC) and the aerodynamic gradient (GM) approach ~~has~~ have proven ~~its~~ their applicability on various ecosystems. The sum of these compounds is called total reactive nitrogen (ΣN_r) throughout this manuscript. The EC method is the common method for estimating greenhouse gas fluxes (Aubinet et al., 1999; Baldocchi, 2003) in flux monitoring networks (FLUXNET (Baldocchi et al., 2001), ICOS (Heiskanen et al., 2021)) and also suitable for measuring the exchange of N_r compounds. However, the

EC method requires fast-response analyzers. For evaluating fluxes of NO and NO_2 the EC technique has been tested in earlier studies (Delany et al., 1986; Eugster and Hesterberg, 1996; Civerolo and Dickerson, 1998; Li et al., 1997; Rummel et al., 2002; Horii et al., 2004; Stella et al., 2013; Min et al., 2014). In recent years, progress has been made in EC measurements of NH_3 (Famulari et al., 2004; Whitehead et al., 2008; Ferrara et al., 2012; Zöll et al., 2016; Moravek et al., 2019). First attempts in applying EC had been made on HNO_3, organic nitrogen molecules, nitrate (NO_3^-), and ammonium aerosols (NH_4^+) (Farmer et al., 2006; Nemitz et al., 2008; Farmer and Cohen, 2008; Farmer et al., 2011). Due to typically low concentrations, high reactivity, and water solubility, measuring fluxes of N_r compounds is still challenging since instruments need a low detection limit and a response time of $< 1\,s$ (Ammann et al., 2012). Thus, fast-response instruments for measuring N_r compounds like HNO_3 or NH_3 are equipped with a special inlet and short heated tubes to prevent interaction with tube walls (see Farmer et al., 2006; Zöll et al., 2016). However, these instruments need regular maintenance, have a high power consumption, and need a ~~climate~~ temperature controlled environment for a stable performance. Considering the high technical requirements of these instruments, measuring fluxes of HNO_3 or NH_3 with these instrument is still challenging.

The Total Reactive Atmospheric Nitrogen Converter (TRANC) (Marx et al., 2012) converts all above mentioned N_r compounds to NO. In combination with a fast-response chemiluminescence detector (CLD), the system allows measurements of ΣN_r with a high sampling frequency. Due to a low detection limit and a response time of about 0.3 s, the TRANC-CLD system can be used for flux calculation based on the eddy-covariance (EC) technique. The key advantage of the TRANC is that only one device is needed for a quantification of the nitrogen dry deposition instead of running several instruments for each compound individually. The TRANC-CLD system has been shown to be suitable for EC measurements above a number of different ecosystems (see Ammann et al., 2012; Brümmer et al., 2013; Zöll et al., 2019; Wintjen et al., 2020).

~~Prior EC studies of ΣN_r or its compounds were carried out above managed field sites or close to agricultural or industrial emission hotspots, in order to focus on measuring the impact of environmental pollution or fertilization on (crop) plants. Only a few studies were conducted at remote locations, but were mainly focusing only on single N_r compounds (e.g., Wyers and Erisman, 1998; He~~

~~At remote sites, concentrations of reactive N_r compounds are typically low and close to the detection limit of the deployed instruments. Zöll et al. (2019) demonstrated that the TRANC-CLD system is able to detect concentrations and fluctuations of ΣN_r accurately even at low ambient levels. It was the first study presenting short-term flux measurements of ΣN_r conducted with the same instrumentation at the measurement site with a focus on establishing a link between the drivers of both ΣN_r and CO_2. The authors identified incident radiation as primary driver for ΣN_r and CO_2 fluxes. Investigations on light response curves exhibited a reversal point for ΣN_r highlighting the existence of a canopy compensation point. The overall concentration of ΣN_r was identified as secondary driver for the ΣN_r exchange showing that processes affecting the physical and chemical properties of ΣN_r are more relevant than other micrometeorological drivers for the ΣN_r fluxes. Further analyses on deposition velocities and corresponding aerodynamic, boundary layer, and canopy resistances of ΣN_r allow to examine if the exchange is driven by turbulent or canopy processes. These investigations were formerly made for individual components of ΣN_r. For example, Wolff et al. (2010) found that aerosol fluxes of total ammonium and total nitrate were driven by aerodynamic processes. NH_3 features bidirectional exchange through stomata and cuticles (e.g., Farquhar, Graham D. and Firth, Peter M. and Wetselaar, Robbert and W~~

~~NO_2 exhibits mainly stomatal and insignificant cuticular deposition (e.g., Rondon et al., 1993; Alberto Rondón and Lennart Granat, 1994;~~

whereas NO emissions are driven by soil microbial activities, which are influenced by soil temperature, soil moisture, and soil nitrogen (e.g., A. Remde and F. Slemr and R. Conrad, 1989; Remde, Armin and Conrad, Ralf, 1993; David Fowler and Chris Flechard and

Since N_r species exhibit an interannual variability and various reaction pathways, the exchange mechanisms of ΣN_r change through the seasons. With the availability of long-term flux measurements at a remote location, we were able to investigate seasonal changes in deposition velocities and resistances at low concentrations of ΣN_r and its components. An evaluation could be important for inferential deposition models in order to validate bidirectional resistance schemes.

Only a few long-term studies have been conducted to derive annual inputs with micrometeorological methods at (remote) forest ecosystems. Munger et al. (1996) conducted EC measurements of NO_y, which refers to the sum of all oxidized N_r compounds, e.g., NO_2, NO, HNO_3, dinitrogen pentoxide (N_2O_5), peroxyacyl nitrates (PAN), aerosol nitrates, above a mixed deciduous forest for five years. Averaged NO_x concentrations were at 0.62 and 4.26 ppb (0.36 and 2.44 µg N m^{-3}) during summer and winter, respectively, if wind was blowing from Northwest. During southwesterly winds, mean NO_x concentrations were 1.25 and 9.48 ppb (0.72 and 5.43 µg N m^{-3}) during summer and winter, respectively, indicating a varying pollution climate. The authors reported an annual net dry deposition of NO_y covering 1990 to 1994 of 2.49 kg N ha^{-1} a^{-1}. Munger et al. (1998) reported an annual reactive N deposition of wet + dry deposition measurements of 6.4 kg N ha^{-1} a^{-1} for the period 1990 to 1996 at the same site. Dry deposition of NO_y contributed 34% to total deposition. Wet deposition of NH_4^+ was comparatively low estimated to 1.1 kg N ha^{-1} a^{-1}. Neirynck et al. (2007) and Erisman et al. (1996) conducted GM measurements in order to estimate dry deposition of NO_x and NH_3. Neirynck et al. (2007) published GM measurements from July 1999 to November 2001 above mixed coniferous/deciduous forest, which was in close proximity of a highway and the city of Antwerp leading to mean NO_2 and NH_3 concentrations of 8.7 and 3.0 µg N m^{-3}, respectively. The authors determined an annual NH_3 dry deposition of 19.6 kg N ha^{-1} a^{-1} and NO_x emission of 2.7 kg N ha^{-1} a^{-1}. NO_x emissions were probably related to a strong contribution of soil-emitted NO. Erisman et al. (1996) reported NO_x and NH_3 fluxes above a Douglas Fir stand of 2.5 ha surrounded by a larger forested area of 50 km^2 for 1995. Mean NH_3 concentration was 4.5 µg N m^{-3} possibly related to livestock farming in the surroundings of the site. They estimated annual dry depositions of 17.9 kg N ha^{-1} a^{-1} and 2.8 kg N ha^{-1} a^{-1} for NH_3 and NO_x, respectively. These were the few long-term micrometeorological measurements of N_r species above forests. No recent reports on long-term flux measurements of N_r were found. Since several N_r compounds contribute to ΣN_r each with different chemical and physical properties, a complex arrangement of different, highly specialized measurement devices would be needed for quantifying ΣN_r exchange. To our knowledge, there is no publication available reporting annual ΣN_r deposition at (remote) forest ecosystems using micrometeorological methods. As stated above, the true benefit of the TRANC is that the most relevant N_r species are converted, and a single instrument is sufficient for deriving dry nitrogen deposition. Therewith, we were able to determine annual dry deposition and show seasonal changes in the ΣN_r flux pattern.

During a measurement campaign instrumental performance issues and/or periods of insufficient turbulence arise, which require a quality flagging of processed fluxes. Afterwards, the resulting gaps in the measured time-series need to be filled in order to properly estimate long-term deposition budgets. Known gap-filling strategies include the Mean-Diurnal-Variation (MDV) method (Falge et al., 2001), look-up tables (LUT) (Falge et al., 2001), non-linear regression (NLR) (Falge et al., 2001),

marginal distribution sampling (MDS) (Reichstein et al., 2005), and artificial neural networks (Moffat et al., 2007). However, most of these methods have in common that they were originally designed for carbon dioxide (CO_2) or other inert gases. MDS requires a short-term stability of fluxes and micrometeorological parameters. This condition is not necessarily fulfilled for ΣN_r and its components. Their exchange patterns are characterized by a higher variability for different time scales leading to a lower autocorrelation and non-stationarities in flux time series compared to inert gases like CO_2. It is, on the other hand, possible to use statistical methods like MDV or linear interpolation to fill short gaps in flux time series. This was done by Brümmer et al. (2013), but filling long gaps with this technique is not recommended. Since exchange patterns of ΣN_r can substantially vary each day depending on the composition of ΣN_r and micrometeorology, it is questionable if statistical methods are suitable for ΣN_r considering the high reactivity and chemical properties of its compounds.

The study presented here is the first one showing long-term flux measurements of ΣN_r using the EC technique in combination with novel measurement techniques above a remote forest ~~focusing on the impact of environmental controls on fluxes, deposition velocities, and resistances~~. We discuss the observed flux pattern of ΣN_r (1), ~~investigate~~ show the influence of micrometeorology on ~~determined~~ deposition velocities, ~~and (canopy) resistances~~ (2), and ~~show the influence of micrometeorological parameters on~~ determine dry deposition sums estimated with the MDV approach while considering the influence of micrometeorological parameters (3). Wet deposition results obtained from bulk and wet-only sampler measurements are complementarily used to estimate total deposition.

Part II of the paper will present the usage of the acquired dataset in a modeling framework to estimate annual N budgets. Modeled fluxes and deposition velocities of the ΣN_r components will be compared to values reported in literature. Similar to Part I, the influence of micrometeorology on modeled fluxes~~,~~ and deposition velocities~~, and resistance~~ will be investigated. Dry depositions estimated with the EC method will be compared to results from modeling approaches using in-situ and modeled input parameters and to ~~canopy outflow~~ nitrogen throughfall measurements. We will discuss the ecological impact of nitrogen deposition on forest ecosystems. A comparison to annual N budgets reported for other forest ecosystems will be carried out.

2 Materials and Methods

2.1 Site and meteorological conditions

Measurements were made in the Bavarian Forest National Park (NPBW) (48°56'N 13°25'E, 807 m a.s.l) in southeast Germany. The unmanaged site is located in the Forellenbach catchment ($\sim 0.69\,km^2$ (Beudert and Breit, 2010)), is surrounded by a natural, mixed forest, and is about 3 km away from the Czech border. Due to the absence of emission sources of N_r in the surroundings of the measurement site, mean annual concentrations of NO_2 (2.1-4.8 ppb (1.2-2.8 µg N m^{-3})), NO (0.4-1.6 ppb (0.2-0.9 µg N m^{-3})) and NH_3 (1.4 ppb (0.8 µg N m^{-3})) are low (Beudert and Breit, 2010). The site is characterized by low annual temperatures (6.1°C) and high annual precipitation (1327 mm) measured at 945 m a.s.l. Annual temperature in 2016, 2017, and 2018 was 6.8°C, 6.9°C, and 8.0°C and precipitation was 1208 mm, 1345 mm, and 1114 mm, respectively. There are no industries or power plants nearby, only small villages with moderate animal housing and farming (Beudert et al., 2018). Due to these site characteristics, measurements of the ΣN_r background deposition are possible. For monitoring air quality and

micrometeorology a 50 m tower was installed in the 1980s. Measurements of ozone, sulphur dioxide, and NO_x, the sum of NO and NO_2, have been conducted since 1990 (Beudert and Breit, 2010). The Forellenbach site is part of the International Cooperative Program on Integrated Monitoring of Air pollution Effects on Ecosystems (ICP IM) within the framework of the Geneva Convention on Long-Range Transboundary Air Pollution (UNECE, 2020) and belongs to the Long Term Ecological Research (LTER) network (LTER, 2020). The Federal Environment Agency (UBA) and NPBW Administration have been carrying out this monitoring program in the Forellenbach catchment. The flux footprint consists of Norway spruce (*Picea abies*) and European beech (*Fagus sylvatica*) covering approximately 80% and 20% of the footprint, respectively (Zöll et al., 2019). During the study period, maximum stand height was less than 20 m since the dominating Norway spruce ~~are~~ is recovering from a complete dieback by bark beetle in the mid-1990s and 2000s (Beudert and Breit, 2014).

2.2 Experimental setup

Flux measurements of ΣN_r were made from January 2016 until end of June 2018 at a height of 30 m above ground. A custom-built ΣN_r converter (total reactive atmospheric nitrogen converter, TRANC) after Marx et al. (2012) and a 3-D ultrasonic anemometer (GILL-R3, Gill Instruments, Lymington, UK) were attached on different booms close to each other at 30 m height. The horizontal and vertical sensor separations were 32 cm and 20 cm, respectively (Wintjen et al., 2020). The TRANC was connected via a 45 m opaque PTFE tube to a fast-response chemiluminescence detector (CLD 780 TR, ECO PHYSICS AG, Dürnten, Switzerland), which was housed in an air-conditioned box at the bottom of the tower. The CLD was coupled to a dry vacuum scroll pump (BOC Edwards XDS10, Sussex, UK), which was placed at ground level, too. The inlet of the TRANC is designed after Marx et al. (2012) and Ammann et al. (2012). The conversion of ΣN_r to NO is split in two steps. First~~ly~~, a thermal conversion occurs in an iron-nickel-chrome tube at 870°C~~. The thermal conversion of NH_4NO_3 leads to gaseous NH_3 and HNO_3.~~ leading to a split up of NH_4^+ and NO_3^- aerosols such as ammonium sulfate, ammonium nitrate, sodium and calcium nitrate into their subcomponents. In case of NH_4NO_3, it is thermally converted to NH_3 and HNO_3 (Marx et al., 2012). The latter is split up into to NO_2, H_2O, and O_2. NH_3 is oxidized by O_2 at a platinum gauze to NO. HONO is split up to NO and a hydroxyl radical (OH). In a second step, a gold tube passively heated to 300°C catalytically converts the remaining oxidized N_r species to NO. In this process, carbon monoxide (CO) is acting as a reducing agent. More details about the chemical conversion steps can be found in Marx et al. (2012). A critical orifice was mounted at the TRANC's outlet and restricted the mass flow to 2.1 $L\,min^{-1}$ after the critical orifice assuring low pressure along the tube. ~~The mass flow rate before the critical orifice was the same as after the critical orifice. Since mass flow was equal to both sides of the critical orifice, a difference in flow velocity was induced due to the reduction in pressure. Flow velocities were not measured for the different sections.~~The pressure gradient from the critical orifice to the CLD was not measured. Thus, only assumptions about the turbulent flow regime can be made. Considering tube length and lag time minus residence time in the converter, the latter assumed to 2 sec at maximum due to tube length and platinum mesh as an additional flow resistance, flow speed was at 2.7 ms^{-1} at maximum. Using an inner diameter of 4.4 mm and a kinematic viscosity at 15°C ($1.485 \cdot 10^{-5}$ m^2 s^{-1}), we calculated a Reynolds number of 800 indicating an overall laminar flow. We cannot provide a reasonable explanation to the low Reynolds number since pressure gradient was not measured. Generally, the flow type inside the tube affects high-frequency attenuation

(Massman, 1991; Lenshow and Raupach, 1991; Moncrieff et al., 1997). High-frequency attenuation was corrected with an empirical method based fully on measured cospectra (Wintjen et al., 2020). Since an empirical approach was used to estimate the high-frequency damping, effects originating from the low Reynolds number and from physical and chemical processes occurred after the critical orifice were considered in the flux analysis.

The conversion efficiency of the TRANC had been investigated by Marx et al. (2012). They found 99% for NO_2, 95% for NH_3, and 97% for a gas mixture of NO_2 and NH_3. Conversion efficiencies for sodium nitrate ($NaNO_3$), ammonium nitrate (NH_4NO_3), and ammonium sulfate ($(NH_4)_2SO_4$) were 78%, 142%, and 91%, respectively. Overall, the results indicate that the TRANC is able to convert aerosols and gases efficiently to NO. For further details we refer to the publication of Marx et al. (2012).

For determining local turbulence - wind speed, wind direction, friction velocity (u_*) - measurements of the wind components (u, v, and w) were conducted using the sonic anemometer. Close to the sonic, an open-path LI-7500 infrared gas analyzer (IRGA) for measuring CO_2 and H_2O concentrations was installed.

For investigating the local meteorology, air temperature and relative humidity sensors (HC2S3, Campbell Scientific, Logan, Utah, USA) were mounted at four different heights (10, 20, 40, and 50 m above ground). At the same levels, wind propeller anemometers (R.M. Young, Wind Monitor Model 05103VM-45, Traverse City, Michigan, USA) were mounted on booms. Leaf wetness sensors designed after the shape of a leaf (Decagon, LWS, n=6, Pullman, Washington, USA) were attached to branches of a spruce and a beech tree near the tower. Sensors of the beech tree were at heights of approximately 2.1 m, 5.6 m, and 6.1 m, sensors of the spruce tree were at heights of 2.1 m, 4.6 m, and 6.9 m. These measurements started in April 2016. Due to a wetting of the sensor's surface, the electric conductivity of the material changes. This signal, the leaf wetness, was converted by the instrument to dimensionless counts. Based on the number and range of counts, different wetness states could be defined. Half-hourly leaf wetness values were in the range from 0 to 270. In this study, we defined the wetness states "dry" and "wet". The condition wet can be induced by the accumulation of hygroscopic particles extending the duration of the wetness state or water droplets. In order to classify a leaf as dry or wet, we determined a threshold value based on the medians of leaf wetness values. During daylight (global radiation $> 20\,\mathrm{W\,m^{-2}}$), medians ranged from 1.1 to 2.0 and were between 4.1 and 9.4 during nighttime. During nighttime, medians are higher due to dew formation. According to the values determined during daylight, we set the threshold value to 1.5 for all sensors. If the leave wetness value was lower than 1.5, the leaf was considered as dry. Otherwise, the leaf surface was considered as wet. To take differences between the sensors into account, all sensors were used to derive a common wetness Boolean. Therefore, the number of dry sensors were counted for each half-hour: If at least three sensors were considered as dry, the corresponding half-hour was considered as mostly dry. A cleaning of sensors was not conducted because contamination effects could be corrected by implemented algorithms. The derived wetness Boolean was used in the analysis of deposition velocities ~~and resistances~~ (Sec. 3.2).

Ambient NH_3 was collected by passive samplers at ground level (1.5), 10, 20, 30, and 50 m from January 2016 to June 2018. Measurements at 40 m started in July 2016. The collector at ground level was moved to 40 m. Passive samplers of the IVL type (Ferm, 1991) were used for NH_3, and the ~~exposition~~ exposure duration was approximately one month at a time. DELTA measurements (DEnuder for Long-Term Atmospheric sampling (e.g., Sutton et al., 2001; Tang et al., 2009)) of NH_3, HNO_3,

SO_2, NO_3^-, and NH_4^+ were taken at the 30-m platform. The DELTA measurements had the same sampling duration as the passive samplers. The denuder preparation and subsequent analyzing of the samples was identical to the procedure for KAPS denuders (Kananaskis Atmospheric Pollutant Sampler, (Peake, 1985; Peake and Legge, 1987)) given in Dämmgen et al. (2010) and Hurkuck et al. (2014). Basic denuders were coated with sodium carbonate to collect HNO_3, SO_2, and HCl. Citric acid was applied to acid denuders for removing NH_3. Two cellulose filter papers (Whatman No. 1, 25 mm diameter) were used for collecting aerosols. The first filter was prepared with potassium carbonate in glycerol, the second filter with citric acid. During operation, ~~We~~ we controlled the pump to keep flow at a constant level and checked the pipes for contamination effects before analyzing. Blank values were used as additional quality control.

Fast-response measurements of NH_3 were performed with a NH_3 Quantum Cascade Laser (QCL) (model mini QC-TILDAS-76 from Aerodyne Research, Inc. (ARI, Billerica, MA, USA)) at 30 m height, too. The setup of the QCL was the same as described in Zöll et al. (2016). In contrast to Zöll et al. (2016), we were not able to calculate NH_3 fluxes with the QCL using the EC method (see Sec. 2.3). Further details about the location and specifications of the installed instruments can be found in Zöll et al. (2019) and Wintjen et al. (2020).

At the top of the tower (50-m platform), measurements of NO_2 and $NO_{~~2~~}$ were conducted by the NPBW using a chemiluminescence detector (APNA - 360, HORIBA, Tokyo, Japan). The instrument was equipped with a thermal NO_x converter resulting in cross-sensitivity to higher oxidized nitrogen compounds. Measurements of global radiation and atmospheric pressure were also conducted at 50 m. Above the canopy, the concentration gradients of NO_2 and NO were probably not significant. Seok et al. (2013) found highest NO_x concentrations above the canopy but concentration gradients were negligible at this height. Since both measurement heights were above the canopy, no correction was applied to NO_2 and NO concentration measurements. Precipitation was measured at a location in 1 km southwest distance from the tower according to WMO (World Meteorological Organization) guidelines (Jarraud, 2008)~~, and data were quality-checked by the NPBW (Beudert and Breit, 2008, 2010)~~. Wet deposition was collected as bulk and wet-only samples in weekly intervals in close vicinity to the tower using four samplers, three bulk samplers and one wet-only sampler, at an open site. A detailed description of the wet deposition measurements is given as supplemental material A1.

2.3 Flux calculation and post processing

The software package EddyMeas, included in EddySoft (Kolle and Rebmann, 2007), was used to record the data with a time resolution of 10 Hz. Analog signals from CLD, LI-7500, and the sonic anemometer were collected at the interface of the anemometer and joined to a common data stream. Flux determination covered the period from 1 January 2016 to 30 June 2018. Half-hourly fluxes were calculated by the software EddyPro 7.0.4 (LI-COR Biosciences, 2019). For flux calculation a 2-D coordinate rotation of the wind vector was selected (Wilczak et al., 2001), spikes were detected and removed from time series after Vickers and Mahrt (1997), and block averaging was applied. Due to the distance ~~the from inlet of TRANC~~ from the TRANC inlet to the CLD, a time lag between concentration and sonic data was inevitable. The covariance maximization method allows to estimate the time lag via shifting the time series of vertical wind and concentration against each other until the covariance is maximized (Aubinet et al., 2012; Burba, 2013). The time lag was found to be approximately 20 s (see Fig.

S1 of the Supplementary Material). ~~Figures with the notation Sn where n=1...9 can be found in the supplemental material.~~ We instructed EddyPro to compute the time lag after covariance maximization with default setting while using 20 s as default value and set the range from 15 s to 25 s (for details see Wintjen et al., 2020). For correcting flux losses in the high-frequency range we used an empirical method suggested by Wintjen et al. (2020), which uses measured cospectra of sensible heat ($\mathrm{Co}(w,T)$) and $\Sigma\mathrm{N_r}$ flux ($\mathrm{Co}(w,\Sigma\mathrm{N_r})$) and an empirical transfer function. We followed their findings and used ~~bimonthly~~ medians of the damping factors for correcting calculated fluxes since the chemical composition of $\Sigma\mathrm{N_r}$ exhibits seasonal differences (see Fig. 4 and Brümmer et al., 2013). Each damping factor (median) refers to period of two month. On average, the damping factor was 0.78, which corresponds to flux loss of 22% (Wintjen et al., 2020). The authors determined flux loss factors for two different ecosystems, which are different, for example, in the composition of $\Sigma\mathrm{N_r}$. They assumed that the differences in flux losses are also related to the chemical composition of $\Sigma\mathrm{N_r}$. The low-frequency flux loss correction was done with the method of Moncrieff et al. (2004), and the random flux error was calculated after Finkelstein and Sims (2001).

Previous measurements with the same CLD model by Ammann et al. (2012) and Brümmer et al. (2013) revealed that the device is affected by ambient water vapour due to quantum mechanical quenching. Excited NO_2 molecules can reach ground state without emitting a photon by colliding with a H_2O molecule, thereby no photon is detected by the photo cell. It results in a sensitivity reduction of 0.19% per $1\,\mathrm{mmol\,mol^{-1}}$ water vapour increase. Thus, calculated fluxes were corrected after the approach by Ammann et al. (2012) and Brümmer et al. (2013) using the following equation:

$$F_{\mathrm{NO,int}} = -0.0019 \cdot c_{\Sigma\mathrm{N_r}} \cdot F_{\mathrm{H_2O}} \quad (1)$$

The NO interference flux $F_{\mathrm{NO,int}}$ has to be added to every estimated flux value. $c_{\Sigma\mathrm{N_r}}$ is the measured concentration of the CLD and $F_{\mathrm{H_2O}}$ the estimated H_2O flux from the LI-7500 eddy-covariance system. The correction contributed approximately 132 g N ha^{-1} to two years of TRANC flux measurements if the Mean-Diurnal-Variation (MDV) approach was used as gap-filling approach. Half-hourly interference fluxes were between -3 and +0.3 ng N m^{-2} s^{-1}. Their random flux uncertainty ranged between 0.0 and 0.5 ng N m^{-2} s^{-1}. Since we measured H_2O fluxes with an open-path system and used them for correcting $\Sigma\mathrm{N_r}$ fluxes, density corrections following the Webb-Pearman-Leuning correction for H_2O fluxes measured with closed-path systems (Ibrom et al., 2007) were not accounted for. The impact on the correction is likely small, but the determined interference flux correction should be seen as an upper estimate.

After flux calculation, we applied different criteria to identify low-quality fluxes. We removed fluxes, which were outside the predefined flux range of -520 ng N m^{-2} s^{-1} to 420 ng N m^{-2} s^{-1} (I), discarded periods with insufficient turbulence ($u_* < 0.1$ m s^{-1}) (see Zöll et al., 2019) (II), and fluxes with a quality flag of "2" (Mauder and Foken, 2006) (III). In order to avoid uncertainties due to the washout process as it introduces an additional sink below the measurement height leading to a height dependent flux, we applied a precipitation filter on $\Sigma\mathrm{N_r}$ flux measurements (IV). These criteria ensure the quality of the fluxes, but lead to systematic data gaps in flux time series. Flux data with applied u_*-filter were used for investigating the flux pattern of $\Sigma\mathrm{N_r}$. Figures 5, 6, 9, S5, S6, S9, S10, S12, S13, and associated description based on this flux data set. Instrumental performance problems led to further gaps in the time series. Most of them were related to maintaining and repairing of the TRANC and/or CLD, for example, heating and pump issues, broken tubes, empty O_2 gas tanks (O_2 is required for CLD

operation), power failure, or a reduced sensitivity of the CLD. The reduction in sensitivity may be caused by reduced pump performance leading to an increase in sample cell pressure. If pressure in the sampling cell is outside the regular operating range, low pressure conditions needed for the detection of photons emitted by excited NO_2 molecules may not hold. ~~Pump efficiency was controlled at least monthly, and tip seals were replaced if necessary.~~ We checked the pressure in the sample cell of the CLD during each, at least monthly, site visit. If the sample cell pressure was outside the allowed range, tip seals of the pump were replaced. The sensitivity of the CLD could also be reduced by changes in the O_2 supply from gas tanks to ambient, dried box air if O_2 gas tanks were empty. Issues in the air-conditioning system of the box could also affect the sensitivity of the CLD. An influence of aging on the inlet, tubes, and filters may also affect the measurements. In order to minimize an impact on the measurements, half-hourly raw concentrations were carefully checked for irregularities like spikes or drop-outs by visual screening. Considering the time period of ongoing measurements from the beginning of January 2016 till June 2018, the quality flagging resulted in ~~52.2~~58.6% missing data. The loss in flux data is higher than values reported by Brümmer et al. (2013). They reported a flux loss of 24% caused by u_* filtering. In this study, the same u_* threshold caused a flux loss of approximately 15.5%. 32.7% data loss from January 2016 to June 2018 was caused by instrumental performance problems showing that TRANC-CLD system was overall operating moderately stable. For gap-filling we applied the MDV approach to gaps in the ΣN_r flux time series. The window for filling each gap was set to $\pm$5 days. Remaining, long-term gaps were filled by a monthly average of the specific half-hour value estimated from non-gap-filled fluxes (Fig. 6) in order to estimate ΣN_r dry deposition sums from June 2016 to May 2017 and from June 2017 to May 2018. Uncertainties of the gap-filled fluxes are estimated by the standard error of the mean.

Hereafter, we named this MDV approach "original" (OMDV). To examine the impact of the u_*-filter as it may remove preferentially smaller fluxes occurring at low turbulent conditions, we compared dry deposition sums calculated with and without u_*-filter while using OMDV. On both datasets, flux filters (I), (III), and (IV) were applied (see Fig. 11 and associated text). Seasonal and annual ΣN_r dry depositions shown in Table 3 referred to flux data with u_*-filter and were calculated by using OMDV.

In addition to u_*, other micrometeorological parameters may also bias annual dry deposition. Therefore, we examined the impact of temperature, relative humidity, and wind speed on the dry deposition sums of ΣN_r compared to the dry deposition when using OMDV as gap-filling approach. We named this gap-filling approach as "conditional" MDV (CMDV) and applied it to flux data with and without u_*-filter. For CMDV, we considered only fluxes in the time frame of $\pm$5 days, at which temperature agreed within ± 3°C, relative humidity by ± 5%, or wind speed by ± 1.5 m s^{-1}. Remaining, long-term gaps were treated similar to OMDV.

As outlined in Sec. 2.2, measurements of NH_3 were made with a QCL at high temporal resolution. In combination with the sonic anemometer, it gives the opportunity to determine NH_3 fluxes and to further investigate the non-NH_3 component of the ΣN_r flux. However, a calculation of the NH_3 fluxes with the EC method was not possible in this study. No consistent NH_3 time lag was found making flux evaluation impossible. Due to regular pump maintenance, cleaning of the inlet and absorption cell, issues related to the setup of the QCL were unlikely to be the cause. We suppose that the variability in the measured NH_3 concentrations was not sufficiently detectable by the instrument. Significant short-term variability in the ΣN_r

raw concentrations were not found in the NH_3 signal even in spring or summer. Thus, no robust time lag estimation could be applied to the vertical wind component of the sonic anemometer and the NH_3 concentration. Recently, Ferrara et al. (2021) found large uncertainties for low NH_3 fluxes measured with the same QCL model. Cross-covariance functions had a low signal-to noise ratio indicating that most of the fluxes were close to the detection limit.

2.4 Determining deposition velocity ~~and canopy resistance~~ of ΣN_r from measurements

In surface-atmosphere exchange models of N_r species like NO_2, NO, NH_3, HNO_3, or nitrogen aerosols, the flux (F_t) is calculated by multiplying concentrations of a trace gas modeled or measured at a reference height ($\chi_a(z-d)$) with a so-called deposition velocity ($v_d(z-d)$) where z is measurement height and d the zero-plane displacement height (van Zanten et al., 2010). The deposition velocity can be described by an electrical analogy and is defined as the inverse of the sum of three resistances (Wesely, 1989; Erisman and Wyers, 1993). According to its definition a positive v_d indicates deposition, a negative v_d emission. Note that, strictly speaking, for bidirectional exchange v_d needs to be interpreted as an "exchange velocity", i.e. it can technically become negative during emission phases. Equations are the same as for v_d (van Zanten et al., 2010).

$$F_t = -v_d(z-d)\cdot\chi_a(z-d) \quad \text{with } v_d = (R_a(z-d)+R_b+R_{c,\text{eff}})^{-1} \tag{2}$$

R_a is the aerodynamic resistance, R_b is the quasi-laminar boundary layer resistance, and $R_{c,\text{eff}}$ is the ~~(effective)~~ canopy resistance ~~(i.e., including the effects of compensation points for some species)~~. R_a is influenced by turbulent characteristics (Paulson, 1970; Webb, 1970; Garland, 1977) and R_b (Jensen and Hummelshøj, 1995, 1997) depends on surface characteristics and chemical properties of the gas or particle of interest. Both have in common that they are proportional to the inverse of u_*. R_c consists of several parallel connected resistances describing the exchange with the vegetated surface (van Zanten et al., 2010). Further details about the implementation of these resistances in surface-atmosphere models can be found in van Zanten et al. (2010). ~~R_a is adapted from Garland (1977) and R_b based on Jensen and Hummelshøj (1995, 1997). They are influenced by micrometeorological parameters, surface conditions, and chemical properties of the N_r species of interest. R_a is defined as~~

$$R_a(z-d) = \frac{u(z-d)}{u_*^2} - \frac{\Psi_H(\frac{z-d}{L}) - \Psi_M(\frac{z-d}{L})}{u_*}\cdot\kappa \tag{3}$$

~~where u_* is the friction velocity, $u(z-d)$ is the wind speed at the reference height, κ is the von Kàrmàn Constant (≈ 0.41), L is the Obukhov length, and Ψ_H and Ψ_M are the integrated stability corrections for entrained scalars and momentum following Webb (1970) and Paulson (1970), respectively. R_b is given as~~

$$R_b = \frac{\nu_{air}}{D_{cp}}\cdot\left(\frac{c}{LAI^2}\cdot\frac{l\cdot u_*}{\nu_{air}}\right)^{\frac{1}{3}}\cdot\frac{1}{u_*} \tag{4}$$

~~where ν_{air} is the kinematic viscosity of air, D_{cp} is the molecular diffusivity of the N_r species, LAI is the leaf area index, c an empirically determined constant, which is set to 100 according to Jensen and Hummelshøj (1997), and l represents a typical leaf width (Jensen and Hummelshøj, 1995), which is set to 0.01 m. We determined the molecular diffusion coefficient for ΣN_r as~~

the weighted average of the campaign-wise averages of HNO_3, NH_3, NO, and NO_2 multiplied with their individual molecular diffusivities adapted from Massman, W. J. (1998) and J.L. Durham and L. Stockburger (1986). It should be noted that particles are mostly not affected by a boundary-layer resistance compared to gases. However, the analysis of DELTA measurements showed that the mean particle contribution to the ΣN_r concentrations is only 22%. LAI was estimated after the same scheme used for the depostion module DEPAC (DEPosition of Acidifying Components) (Erisman, J. W. and Van Pul, A. and Wyers, P., 1994) (see Appendix B of van Zanten et al., 2010). A linear increase of the LAI was calculated from mid of April to begin of May, a linear decrease from October to begin of November. Values ranged between 4.1 and 4.8. Fig. 1 shows the LAI for measured fractions of spruce and beech forest.

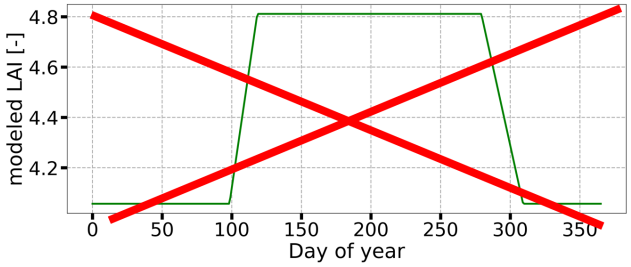

Figure 1. LAI following van Zanten et al. (2010) for measured fractions of coniferous forest (81.1%) and deciduous forest (18.9%) within the flux foot print for a year.

Considering only R_a and R_b, the maximum deposition velocity permitted by micrometeorological conditions is

$$v_{d,max}(z-d) = (R_a(z-d) + R_b)^{-1} \tag{5}$$

Subtracting $v_{d,max}(z-d)$ from measured $v_d(z-d)$, allows to determine an effective canopy resistance ($R_{c,eff}$) for ΣN_r

$$R_{c,eff} = \frac{1}{v_d(z-d)} - \frac{1}{v_{d,max}(z-d)} \tag{6}$$

Commonly, $R_{c,eff}$ consists of different resistances contributing to the uptake capacity of the surface, e.g., a stomatal resistance (R_{stom}), a cuticular resistance (R_w), and a soil resistance (R_{soil}). R_{stom} and R_w describe the exchange through the stomata of plants and with wet leaf surfaces, respectively. Interactions with the soil are merged in R_{soil}.

For N_r species exhibiting a bidirectional exchange pattern like NH_3 (e.g., Farquhar, Graham D. and Firth, Peter M. and Wetselaar, Robbe the existence of a compensation point is assumed. In case of NH_3, the stomatal compensation point is the concentration, at which the gaseous ammonia concentration is in equilibrium with dissolved ammonia in the apoplastic fluid at the reference height. In equilibrium state, the stomatal flux is zero (Farquhar, Graham D. and Firth, Peter M. and Wetselaar, Robbert and Weir, Brian, 198 Consequently, as long as the stomatal concentration is lower than the ambient concentration an uptake of N_r species happens. The cuticular exchange is also bidirectional for NH_3 (Wentworth et al., 2016). Observations by Neirynck, J. and Ceulemans, R. (2008) indicated the existence of a cuticular compensation point (Nemitz, E. and Milford, C. and Sutton, M. A., 2001; Massad, R. S. and Nemitz, at which the gaseous NH_3 concentration is in equilibrium with the solution on the external leaf surfaces.

Hints on NO_2 compensation points were found, for example by Thoene et al. (1996). Breuninger et al. (2013) detected compensation points for NO_2 but compensation point concentrations were not significant. However, the authors found a large uncertainty showing that the determination of compensation points for NO_2 is challenging (I.G. Chaparro-Suarez and F.X. Meixner and J. K

No clear evidence is found on compensation points for HNO_3. The assumption of an ideal uptake seems to be questionable (Tarnay, L. W. and Gertler, A. and Taylor, G. E., 2002). Farmer and Cohen (2008) detected significant emission fluxes of HNO_3 during summer above a spruce forest. HNO_3 emission during summer can be caused by evaporation of NH_4NO_3, which is favored at temperatures above 20°C (Wyers and Duyzer, 1997; Van Oss et al., 1998). The mechanism explaining the HNO_3 emission is still under investigation (Nemitz, E. and Sutton, M. A. and Wyers, G. P. and Jongejan, P. A. C., 2004).

Nitrogen aerosols are likely deposited, and their flux pattern is driven by R_a (Wolff et al., 2010). Soil microbial activities imply a compensation point for soil NO fluxes, which depends on soil temperature, soil water content and N availability (David Fowler and Chris Flechard and Ute Skiba and Mhairi Coyle and J. Neil Cape, 1998; Behrendt, T. and Veres, P. R. and Ashuri, F. an

For the evaluation of v_d and corresponding resistances shown in Sec. 3.2, Eq. (2) to (6) were used.

3 Results

3.1 Concentrations, deposition velocities, and fluxes of ΣN_r during the measurement campaign

Figure 2 shows ambient concentrations of ΣN_r (black), NH_3 (red) and NO_x (blue) as half-hourly averages for the entire measurement campaign. Data gaps were mostly related to instrumental performance problems. No ΣN_r measurements were possible until end of May 2016 due to heating problems of the TRANC. A breakdown of ΣN_r in compounds contributing most to its concentration pattern is shown in Fig. 3, which illustrates a comparison of ΣN_r concentrations with DELTA denuder and NO_x measurements on monthly basis.

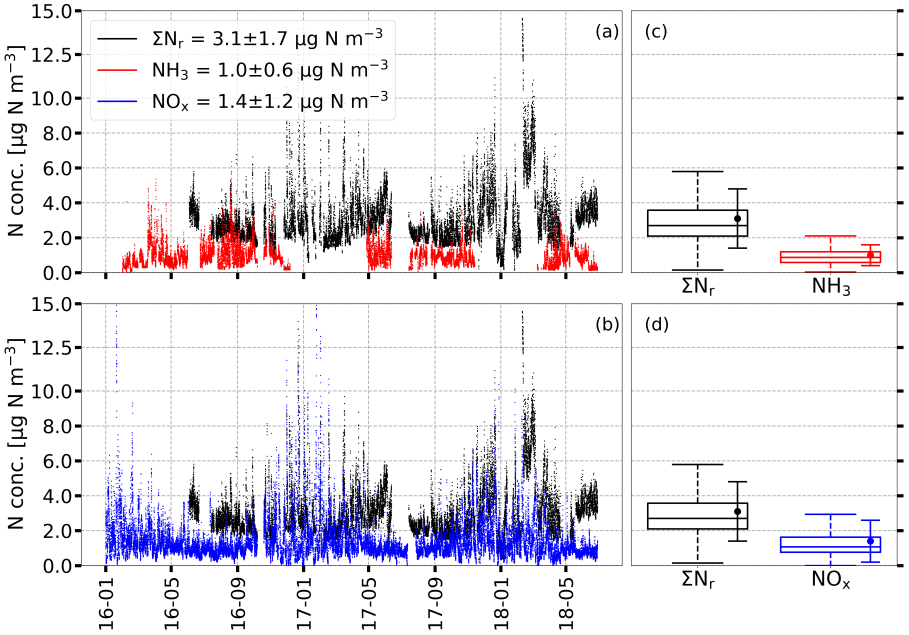

Figure 2. Half-hourly averaged concentrations of ΣN_r (black), NH_3 (red) and NO_x (blue) in µg N m^{-3} from 1 January 2016 to 30 June 2018 displayed in (a) and (b). Box plots (box frame = 25 % to 75 % interquartile range (IQR), bold line = median, whisker = 1.5· IQR) with average values (dots) shown in (c) and (d) refer to the entire campaign. Error bars represent one standard deviation. Y-axis is capped at 15 µg N m^{-3}.

ΣN_r concentrations exhibited highest values during the winter months. For example, values were higher than 10 µg N m^{-3} during January 2017 and February 2018. NO_x showed a relatively high concentration level during winter, too. During spring and summer, NO_x values were ~~mostly~~ lower than 2 µg N m^{-3} and hence, their contribution to ΣN_r decreased. However, ΣN_r values remained around 3 µg N m^{-3} and reached values of up to 6 µg N m^{-3}, which was related to higher NH_3 concentrations during these periods. ΣN_r concentration was 3.1 µg N m^{-3} on average, NH_3 was 1.0 µg N m^{-3}, and NO_x was 1.4 µg N m^{-3} on average with the latter values being in agreement with concentrations reported by Beudert and Breit (2010). Averaged NH_3 concentrations of the QCL agreed well with NH_3 from passive samplers and DELTA measurements (Fig. S2). Overall, the agreement in the annual pattern was good, but a bias between the QCL and the diffusion samplers was found. From passive sampler measurements, an increase in the NH_3 concentration with measurement height could be observed. At 10 m (in the canopy), the lowest NH_3 concentrations were measured. No systematic difference was found between 20 m and 30 m. At 50 m, NH_3 was ~~slightly~~ higher ~~(~~by 0.1 µg N m^{-3}~~)~~ than at 30 m. During winter, the difference in measurement heights diminished. ~~Slightly higher NH_3 concentration were observed at 10 m in winter.~~

The observations made for the seasonal changes of the half-hourly ΣN_r concentrations are also visible for their monthly medians (Fig. S3). Figure S3 shows monthly box plots of the concentrations. In general, median concentrations were ~~almost similar~~ comparable for the entire campaign with slight differences between the years. Medians were between 2 and 3.5 µg N m^{-3}. From July to September, concentrations were slightly higher in 2016 than in 2017. During this period, IQRs and

whiskers were the smallest for the entire year showing less variability in ΣN_r concentrations. In spring and winter, median concentrations were higher, and concentrations covered a wider range compared to the summer month. Figure S4 shows the corresponding diurnal patterns for each month. During the entire day, ΣN_r concentrations ~~were almost stable. Averaged values showed~~ exhibited variations of less than 1 µg N m^{-3}. If concentrations were averaged for each season (not shown), ~~slightly~~ higher concentrations were observed from 9:00 to 15:00 LT and lower values during the night.

Figure 3 shows absolute concentrations of individually measured N_r compounds as stacked bars and ΣN_r from the TRANC from January 2016 to June 2018. TRANC and NO_x measurements were averaged to ~~exposition~~ exposure periods of DELTA measurements. DELTA measurements recorded at an insufficient pump flow were excluded from the analysis. Missing NH_3 values in the DELTA time series were filled by NH_3 data determined from the passive sampler mounted at 30 m. Remaining data gaps in the DELTA time series of NH_3, HNO_3, NH_4^+, and NO_3^- were replaced by monthly averages from other years. ~~The procedure was not applied to the time period covering February 2018 due to the unusually high ΣN_r concentrations.~~

The comparison of the TRANC with DELTA+NO_x revealed ~~slight~~ overestimations by the latter from August 2016 to October 2016 and from January to March 2017. On average, an underestimation by DELTA+NO_x of approximately ~~0.3~~0.41 µg N m^{-3} with a standard deviation of ~~0.7~~0.93 µg N m^{-3} was observed. The median value was about ~~0.35~~0.4 µg N m^{-3}.

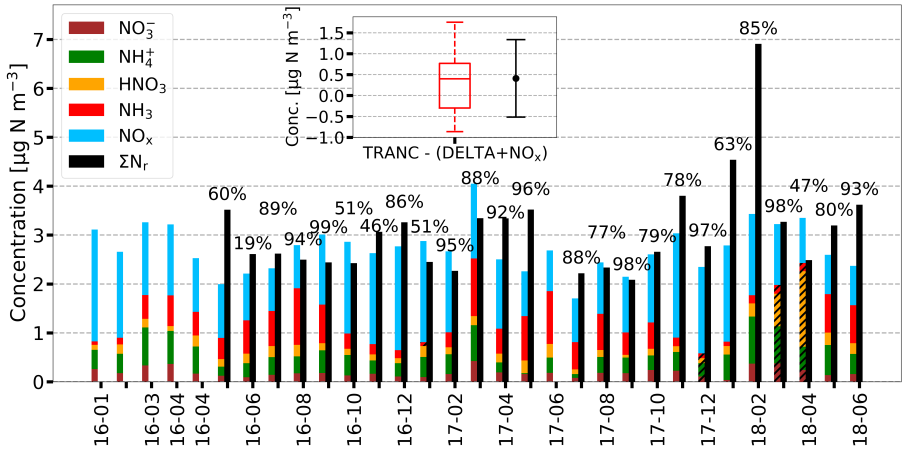

Figure 3. Monthly stacked concentration of TRANC, DELTA, and NO_x in µg N m^{-3} for the entire measurement campaign. Missing NH_3 measurements from the DELTA measurements caused by a low pump flow were filled with passive sampler values from 30 m. This procedure ~~Replacing~~ was done for December 2016 and 2017, ~~January 2017, November 2017,~~ March 2018, and ~~from February to~~ April 2018. Remaining ~~G~~gaps in the time series of ~~the individual components~~ HNO_3, NH_4^+, and NO_3^- were replaced by monthly averages estimated from other years if possible. In case of NH_3, the procedure was applied to January 2017. For the other compounds, the gap-filling was done for December 2017, March 2018, and April 2018. Gap-filled bars are hatched. NO_x and ΣN_r were averaged to the ~~exposition~~ exposure periods of the DELTA samplers.Numbers above the bars the relative coverage of TRANC measurements during each exposure period.

HNO_3, NH_4^+, and NO_3^- concentrations were nearly equal through the entire measurement campaign. Seasonal differences existed mainly for NH_3 and NO_x. We measured average concentrations of 0.5~~6~~5, 0.17, 0.4~~0~~2, 0.19, and 1.40 µg N m^{-3} for

NH_3, HNO_3, NH_4^+, NO_3^-, and NO_x for the entire campaign, respectively. On average, the relative contribution of NH_3, HNO_3, NH_4^+, and NO_3^- to ΣN_r was less than 50% for the entire measurement campaign as visualized by Fig. 4. We further observed a low particle contribution to the ΣN_r concentrations ($\sim$ 22% on average) showing that the ΣN_r concentration pattern was ~~mainly~~ significantly influenced by gaseous N_r compounds.

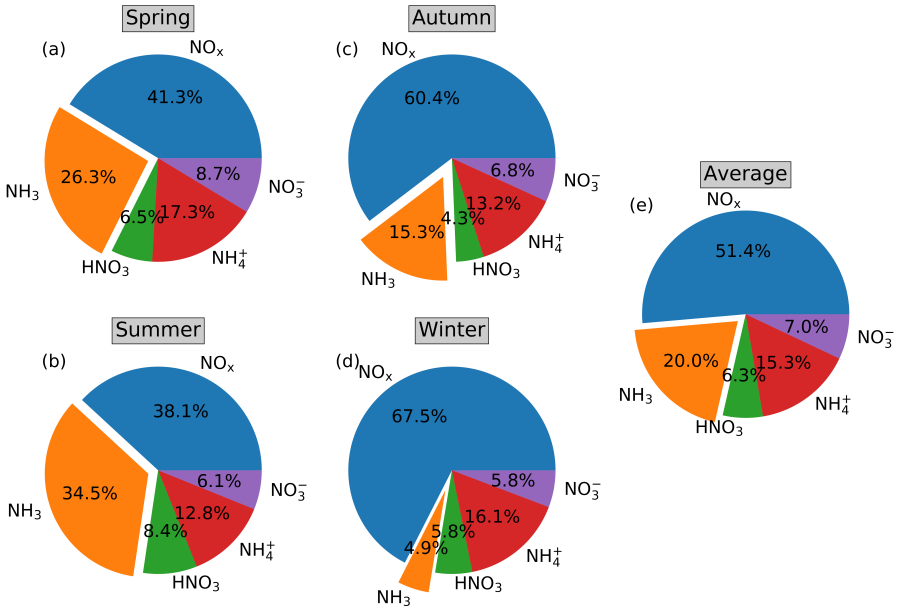

Figure 4. Pie charts showing the relative contribution of concentrations for NO_x, NH_3, NO_3^-, NH_4^+, and HNO_3 to ΣN_r based on DELTA samplers and NO_x measurements for different seasons of the year. NO_x measurements are averaged to ~~exposition~~ exposure periods of the DELTA samplers. (a) to (d) refer to spring, summer, autumn, and winter, respectively. (e) shows the average relative contribution to ΣN_r for the entire measurement period.

In general, NO_x showed the highest contribution to ΣN_r and followed seasonal changes with highest values during winter and lowest values in summer. NH_3 showed also seasonal changes with concentrations lowest in winter and highest values in spring and summer. ~~The~~ Seasonal contributions of HNO_3 varied by less than 2% compared to the average ~~as almost stable~~. ~~A slight increase~~ The highest relative ~~in the~~ contribution of HNO_3 was found for summer.~~As reported by Tang, Y. S. and Flechard, C. R. and D HONO sticks to carbonate coated denuder surfaces, which are designed for collecting HNO_3. Thus, HNO_3 concentrations may be biased.~~ NO_3^- and NH_4^+ exhibited ~~slightly~~ higher~~r~~st values for spring. The excess of NH_4^+ over NO_3^- is obvious. Similar to HNO_3, the seasonal contribution of NO_3^- and NH_4^+ deviated only by $\pm$2% from their averages. Only small seasonal changes in the overall ΣN_r concentration were observed. As seen by Fig. 3, ΣN_r concentrations were ~~mostly~~ between 2 and 4.5 µg N m^{-3} excluding February 2018. We measured 3.3, 2.6, 2.5, and 3..0 µg N m^{-3} with the TRANC system for spring, summer, autumn, and winter, respectively.

Figure 5 shows the non-gapfilled ΣN_r fluxes depicted as box plots on monthly time scale. The convention is as follows: negative fluxes represent deposition, positive fluxes emission.

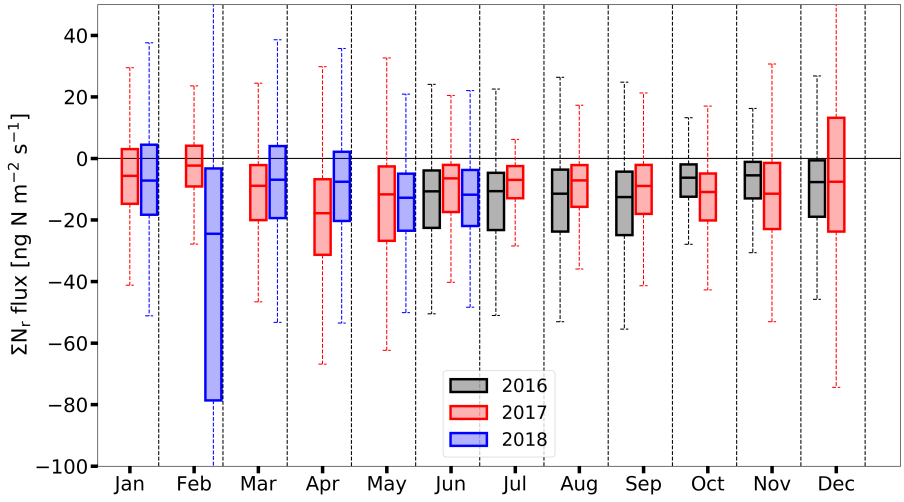

Figure 5. Time series of measured high-quality (flags "0" and "1") ΣN_r fluxes depicted as box plots on monthly basis (box frame = 25% to 75% interquartile ranges (IQR), bold line = median, whisker = 1.5· IQR) in ng N m^{-2} s^{-1}. Colors indicate different years. The whiskers in February 2018 cover the range from -191 to 105 ng N m^{-2} s^{-1}, the upper whisker of December 2017 was at 69 ng N m^{-2} s^{-1}. ~~The displayed range was restricted from -100 to 50 ng N m^{-2} s^{-1}.~~

~~Almost~~ Except for February 2018, all ΣN_r flux medians were between -15 and -5 ng N m^{-2} s^{-1} indicating that ~~mainly~~ deposition of ΣN_r ~~occurred~~ predominated at our measurement site. Quality assured half-hourly fluxes showed 80% deposition and 20% emission fluxes. On half-hourly basis, fluxes were in the range from -516 to 399 ng N m^{-2} s^{-1}. On monthly basis, random flux error medians were between 3 and 6 ng N m^{-2} s^{-1}. According to Langford et al. (2015), limit of detection (LOD) is calculated by multiplying 1.96 with the random flux error (95% confidence limit) .~~The mean random flux error of the non-gapfilled, half-hourly fluxes was 5.9 ng N m^{-2} s^{-1} after Finkelstein and Sims (2001).The flux detection limit was calculated by multiplying 1.96 with the flux error (95% confidence limit) (see Langford et al., 2015). The latter was 11.5 ng N m^{-2} s^{-1}. Both values refer to the entire measurement campaign.~~ The comparison of half-hourly fluxes with their individual LOD revealed that 79% of the measured fluxes were above their detection limits. Deposition fluxes contributed with 84% to fluxes above the LOD. The fraction of emission was estimated to 16%. The relative contribution of emission fluxes to measured fluxes decreased under the consideration of the LOD. It shows that emission fluxes were closer to the flux detection limit of the instrument. ~~Similar values were found by Zöll et al. (2019) at the same site covering a shorter period. In total, 51% of the non gap-filled fluxes were higher than the flux detection limit. It shows that for large parts nitrogen dry deposition was close to detection limit of the used measuring device and that nitrogen exchange happened at a comparatively low level.~~

In general, median deposition was ~~almost~~ on the same level for the entire campaign with ~~slight~~ small seasonal differences. For instance, median deposition was ~~slightly~~ higher during spring and summer than during winter for 2016. However, median

deposition during winter 2017 was ~~similar~~ comparable to median deposition in summer 2017. Median deposition was significantly stronger from June 2016 till September 2016 than for the same period in 2017. IQR and whisker covered a wider range, too. The pattern changed for the time period from October to December. In December 2017, the IQR expanded in the positive range indicating emission events for a significant time period. The largest median deposition with 25 ng N m^{-2} s^{-1} and the widest range in IQR reaching approximately -80 ng N m^{-2} s^{-1} were registered in February 2018 indicating strong deposition phases during that month with sporadic emission events. Such phenomenon~~s~~ were not observed in the years before. In the following month, the deposition was ~~slightly~~ higher from March to April 2017 than for the same period in 2018. Fig. 6 shows averaged daily cycles for every month.

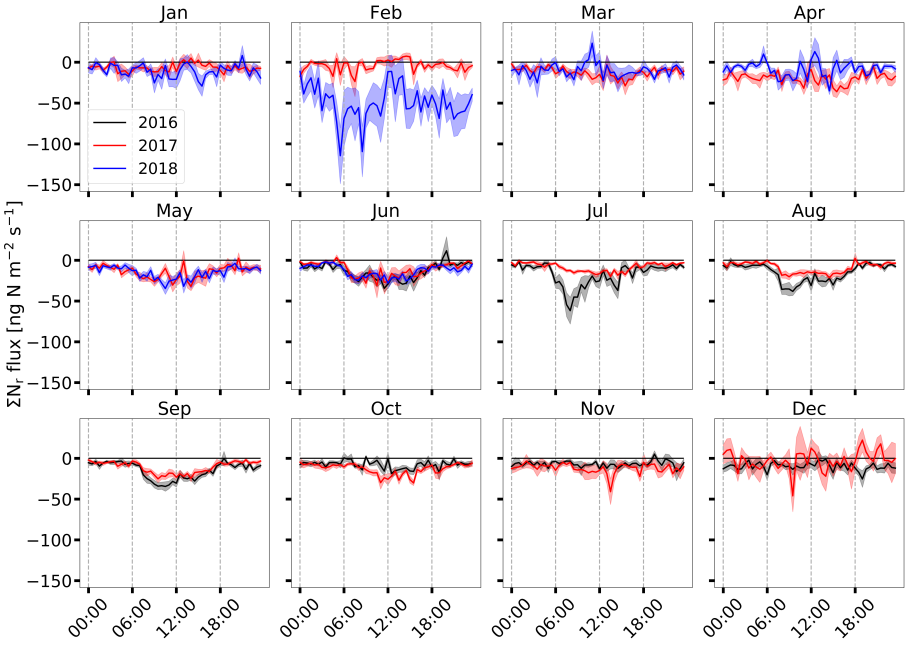

Figure 6. Mean daily cycle for every month of ΣN_r fluxes from June 2016 to June 2018 on half-hourly basis. The shaded area represents the standard error of the mean. Colors indicate different years.

In general, the ΣN_r daily cycle exhibited low deposition or neutral exchange during nighttime/evening and increasing deposition during daytime. Deposition rates were similar during the night for the entire campaign except for February 2018. Maximum deposition was reached between 9:00 and 15:00 LT. Deposition is enhanced from May until September showing fluxes between -40 and -20 ng N m^{-2} s^{-1}. From October to November and from December to February, the daily cycle weakened with ~~almost~~ neutral or ~~slightly~~ small negative fluxes, ~~mostly~~ which were lower than -10 ng N m^{-2} s^{-1}. The daily cycles of the respective same months were ~~mainly similar~~ uniform. However, during certain months, which differ in their micrometeorology and/or in the composition of ΣN_r, differences can be significant. For example, the daily cycle of March and April 2017 was clearly different to daily cycle of March and April 2018. During spring 2017, ~~slight~~ deposition fluxes were found whereas the ΣN_r exchange was close to neutral a year later. The median deposition was also ~~slightly~~ larger in March and April 2017

than in the year after (Fig. 5). In December 2017, the daily cycle was close to the zero line and positive fluxes were observed, although standard errors were relatively large ($\pm$ 11.5 ng N m^{-2} s^{-1} on average). In December 2016, ~~slight~~ small deposition fluxes were observed for the entire daily cycle. The daily cycle of February 2018 showed highest deposition values during the entire day, even the highest values during the measurement campaign. Again, average standard error was relatively large ($\pm$ 19.9 ng N m^{-2} s^{-1}) for February 2018 compared to February 2017.

Figure S5 shows the median v_d ~~to~~ for the corresponding fluxes. Values ranged between 0.2 and 0.5 cm s^{-1} for the entire campaign. In general, median v_d followed closely the seasonality of their corresponding fluxes (Fig. 5). During autumn and winter, v_d remained ~~mostly~~ stable. From May to September, the curve was approximately bell-shaped. Similar to the diurnal fluxes, maximum v_d values were reached between 9:00 and 15:00 LT. During that time, values of v_d were close to 1 cm s^{-1} or even higher (Fig. S6).

3.2 Controlling factors of measured ΣN_r deposition velocities ~~and resistances~~

~~The analysis of v_d and corresponding fluxes show that their diurnal pattern was characterized by lower deposition during the night and highest values around noon, in particular from May to September (Fig. 6 and Fig. S6).~~From May to September, a clear diurnal pattern was found for v_d and their corresponding fluxes (Fig. 6 and Fig. S6). It was characterized by lower deposition during the night and highest values around noon (Fig. S9). During winter, deposition fluxes were close to zero and showed no diurnal variation leading to a constantly low v_d during the day (Fig. S10). Micrometeorological parameters such as global radiation (R_g) (Zöll et al., 2019), temperature and turbulence (Wolff et al., 2010), humidity (Wyers and Erisman, 1998; Milford et al., 2001), ~~and turbulence (Wolff et al., 2010),~~ dry/wet leaf surfaces (Wyers and Erisman, 1998; Wentworth et al., 2016), and concentration of ΣN_r, especially changes in the concentration of the sub components, (Brümmer et al., 2013; Zöll et al., 2016) were reported to control the deposition of ~~N_r compounds~~ ΣN_r.

In order to investigate the ~~effect of micrometeorology and~~ influence of u_* on the ΣN_r exchange, Fig. S7 illustrates the dependency of v_d on u_* for deposition and emission fluxes during day and night. The R_g threshold for day and nighttime fluxes was set to 10 W m^{-2}. For better visibility, we binned data in 0.1 m s^{-1} increments of u_*. Since bins are not equal in size, we added corresponding half-hourly fluxes to the plots. Red dots represent averages of each bin and error bars correspond to their standard error. We found that v_d increased slightly with u_* due to dependency of v_d on R_a and R_b. The latter are proportional to the inverse of u_* suggesting that the increase with u_* should follow a power law. In case of particles, linear relationships between u_* and v_d were found by Gallagher et al. (1997); Lavi et al. (2013); Donateo and Contini (2014). Although uncertainties of the binned averages were large, a relationship between v_d and u_* seems to exist as suggested by the correlations (r), but no clear functional relationship could be identified due to the large scattering of half-hourly v_d.

For visualizing the impact of concentration on v_d (Fig. 7), we plotted ΣN_r concentration against the ratio v_d/u_* in order to reduce the influence of R_a and R_b on v_d. The threshold for R_g was set to 10 W m^{-2}, and we binned data in 0.5 µg N m^{-3} increments of ΣN_r concentration.

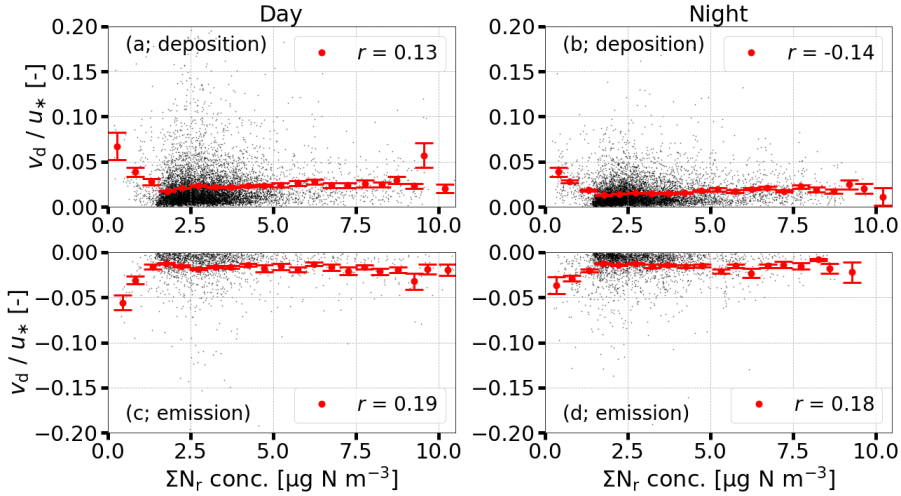

Figure 7. Relationships between measured ΣN_r concentrations and corresponding ratios v_d/u_* separated in emission and deposition during day ((a) and (c)) and night ((b) and (d)) . Half-hourly data is displayed in black, red dots represents averages binned in increments of 0.5 µg N m^{-3}. Error bars indicate the standard error of the averages. The threshold for identifying day and nighttime v_d was set to 10 W m^{-2}. r represents the measure of correlation evaluated for the binned data.

It is obvious that v_d/u_* exhibited no significant dependence on ΣN_r concentration as shown by the low values for r. The ratio appeared to be constant across the (entire) concentration range. It demonstrates that ΣN_r concentration had no significant influence on their v_d. In case of particles, the ratio v_d/u_* depends on Obukov-Length (L) and particle size according to Gallagher et al. (1997) and Lavi et al. (2013). In case of deposition fluxes measured during daytime, we found that the ratio decreased for $-0.2 > L^{-1} < 0$ up to a minimum if L^{-1} reaches zero (neutral stratification) (Fig. S8). This relationship was observed by Gallagher et al. (1997) and Lavi et al. (2013). Although the scattering of half-hourly ratios is large, the decrease of the ratio with increasing L^{-1} as well as the dependence of v_d on u_* demonstrate that v_d had a higher affinity to micrometeorological parameters than to the ΣN_r concentration.

~~and vegetation on deposition, we further determined atmospheric and effective canopy resistances according to the equations given in Sec. 2.4. For visualizing the effect of turbulence on the fluxes, Fig. 8 shows the dependency of the measured fluxes on their concentrations for different u_* classes and global radiation (R_g) higher than 50 W m^{-2}.~~

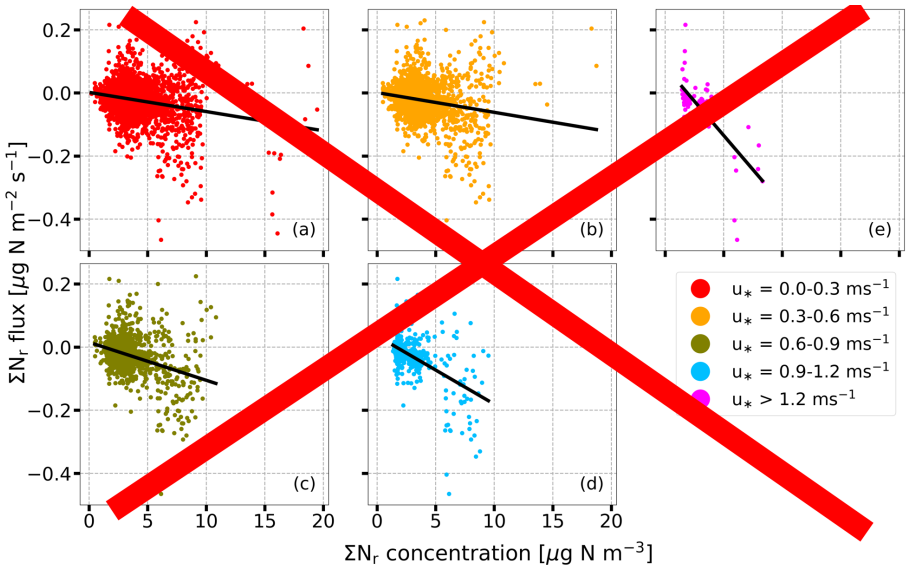

Figure 8. Dependency of measured concentrations on corresponding ΣN_r fluxes shown as scatter plots during daylight ($R_g > 50\,W\,m^{-2}$). Colors indicate different u_* classes. Linear regressions between concentrations and fluxes are made for each u_* class indicated by black lines.

We found a decreasing slope with increasing u_*. The slope corresponds to v_d. Results of the linear regressions, v_d and squared correlations (R^2), are listed in Table 1. In addition, numbers of half-hours used for the regressions are given.

Table 1. Results of linear regressions from Fig. 8 for selected u_* ranges. The slope of the linear function corresponds to v_d, R^2 is the squared correlation of concentrations and fluxes, and n is the number of half-hours used for the regression.

u_* range [m s^{-1}]	v_d [cm s^{-1}]	R^2 [-]	n [-]
0.0–0.3	0.61	0.07	9085
0.3–0.6	0.63	0.05	6124
0.6–0.9	1.20	0.14	2296
0.9–1.2	2.16	0.28	485
$>$ 1.2	4.34	0.51	79

For u_* values lower than 0.6 m s^{-1}, v_d was almost invariant. For u_* values higher than 0.6 m s^{-1} or even higher, an increase in v_d was found. Since R_a (Garland, 1977) and R_b (Jensen and Hummelshøj, 1995, 1997) decrease with increasing u_*, v_d increases. The highest R^2 was determined for u_* higher than 1.2 m s^{-1}. For other u_* ranges, correlations were negligible. However, only 79 half-hourly concentrations and fluxes were available for u_* values higher than 1.2 m s^{-1}. Considering the number of half-hours, atmospheric turbulence had an influence on the deposition of ΣN_r but u_* could not be solely responsible for the observed exchange of ΣN_r.

~~Recently, Zöll et al. (2019) identified R_g as an important controlling factor for the ΣN_r fluxes at the measurement site from July to September. u_* did not emerge as controlling factor as reported by the authors.~~ From the analysis of Figs. 7, S7, and S8, it is impossible to state u_* or L as the controlling variable of the ΣN_r exchange since turbulence, stratification, R_g, sensible heat flux, air temperature, and relative humidity are highly correlated with each other. Figure S~~7~~9 shows the daily cycle of concentration, R_g, u_*, air temperature (T_{air}), and v_d for the period from May to September. During that period, a clear diurnal pattern in v_d was observed with largest values around noon and lowest values during the night. Figure S~~8~~10 is made for the same variables but for December, January, and February. During winter, v_d was almost equal and even lower during the day, which resulted in a lower deposition of ΣN_r during winter. The different shapes of v_d could be induced by micrometerological parameters, which change the composition of available ΣN_r compounds during the day (Seinfeld and Pandis, 2006) and promote photosynthesis.~~were related to plant activity mainly controlled by R_g~~

Within the period ~~of sufficient global radiation inducing~~ of enhanced ΣN_r exchange, in particular from May to September, we investigated the dependency of the ΣN_r deposition velocities ~~and resistances~~ on ~~temperature~~ T_{air}, relative humidity (RH), dry/wet leaf surface, and ΣN_r concentration. We separated half-hourly v_d ~~and $R_{c,eff}$~~ into groups of low and high ~~temperature~~ T_{air}, ~~humidity~~ RH, and concentration according to their median. ~~v_d and $R_{c,eff}$ determined during rain were treated separately.~~ In case of separating v_d ~~and $R_{c,eff}$~~ into groups of dry and wet leaf surfaces, we used the proposed calculation scheme of a leaf wetness boolean (see Sec. 2.2). No significant influence of the different installation heights on leaf surface wetness was found (see Fig. S11 and corresponding description in the supplement). Figure~~s~~ 9 ~~and 10~~ shows the results for v_d ~~and $R_{c,eff}$, respectively~~.

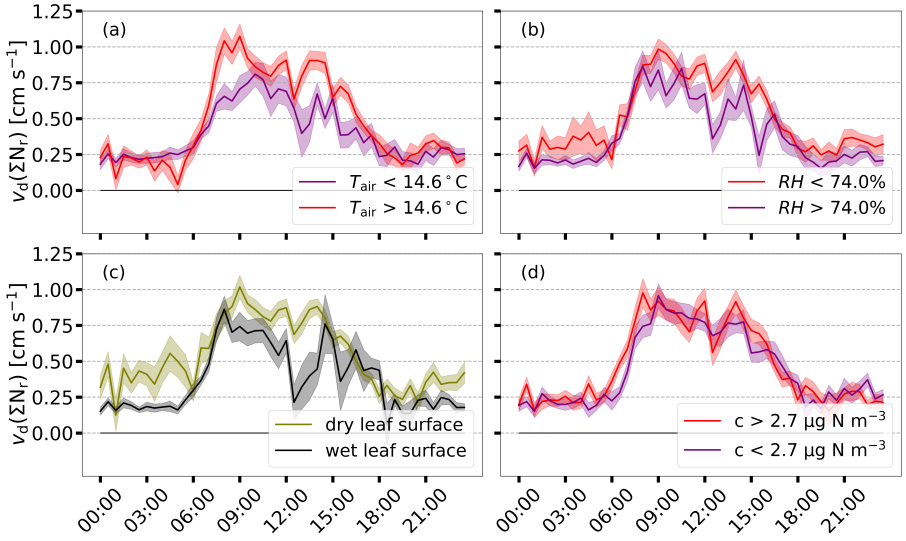

Figure 9. Mean daily cycle from May to September of v_d for low and high temperature (a), relative humidity (b), and concentration (c) ~~separated by precipitation in the conditions "dry" and "wet". Panel (a), (c), and (e) represent the case dry (no precipitation), (b), (d), and (f) the case wet~~. Median values of temperature, humidity, and concentration, which are derived for the same time period, are used as threshold values for separating v_d. In panel (~~g~~d), the mean daily cycle of v_d for dry and wet leaf surfaces is shown. For classifying leaf surfaces as dry or wet, the scheme proposed in Sec. 2.2 is applied. The shaded areas represent the standard error of the mean.

In general, higher air temperatures, less relative humidity, and dry leaf surfaces~~, and dry conditions (no precipitation)~~ were associated with enhanced deposition of ΣN_r, and a clear diurnal pattern was observed for v_d with high values around noon and low, non-zero values in the night ~~during dry conditions~~. During dawn/nighttime, deposition velocities exhibited no significant difference between the applied thresholds. ~~Overall, n~~No difference was found for low and high concentration regimes. ~~In case of precipitation, v_d was reduced during daytime and exhibited a high variability for the entire day. No difference and distinct pattern could be found for low and high temperature, humidity, and concentration regimes during precipitation.~~ During other times of the year, no diurnal pattern was observed ~~during dry conditions~~. In those periods, v_d was almost constant and exhibited lower values during daylight compared to the May to September time frame. Occasionally, negative deposition velocities referring to emission of ΣN_r were recorded during times of lower radiation. ~~Figure 10 is in accordance to Fig. 9 but for $R_{c,eff}$.~~

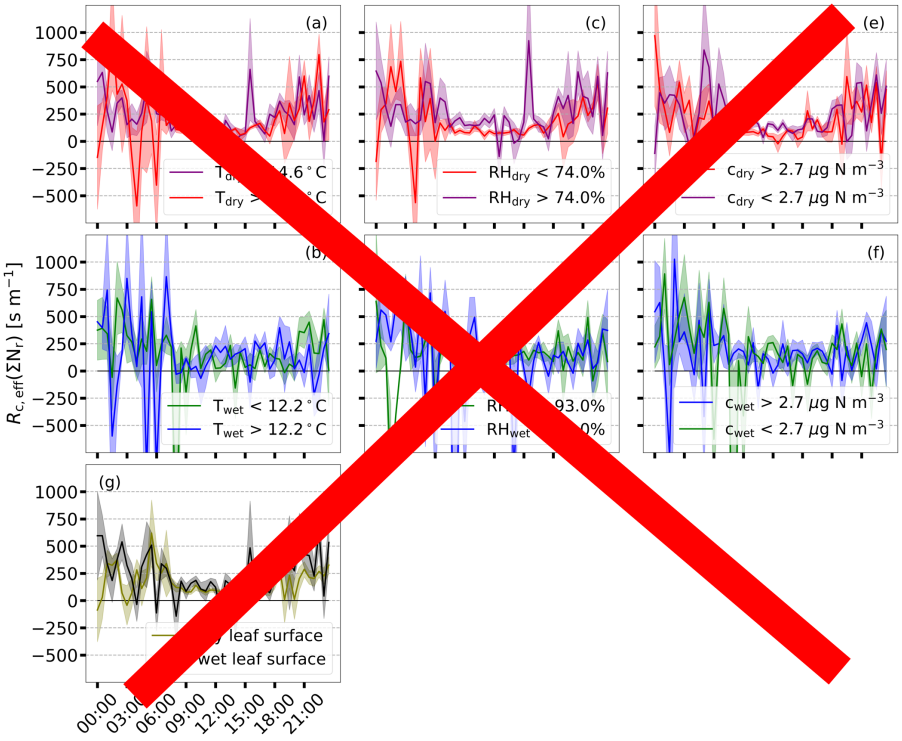

Figure 10. Mean daily cycle from May to September of $R_{c,eff}$ for low and high temperature, relative humidity, and concentration separated by precipitation in the conditions "dry" and "wet". Panel (a), (c), and (e) represent the case dry (no precipitation), (b), (d), and (f) the case wet. Median values of temperature, humidity, and concentration, which are derived for the same time period, are used as threshold values for separating $R_{c,eff}$. In panel (g), the mean daily cycle of $R_{c,eff}$ for dry and wet leaf surfaces is shown. For classifying leaf surfaces as dry or wet, the scheme proposed in Sec. 2.2 is applied. The shaded area represents the standard error of the mean.

$R_{c,eff}$ exhibited lowest values during the day and highest values at night. During nighttime, the variability in $R_{c,eff}$ was enhanced whereas $R_{c,eff}$ was almost stable during daylight. Only slight differences between the applied threshold were found. $R_{c,eff}$ was slightly lower at higher concentrations only for short periods during daylight, for example around noon. In case of relative humidity, $R_{c,eff}$ exhibited slightly lower values for less humid air. Temperature had nearly no effect on $R_{c,eff}$. During precipitation, no difference between the applied thresholds was found. Similar to v_d, $R_{c,eff}$ had a higher variability compared to dry conditions during the day resulting in higher uncertainties. Also phases with negative $R_{c,eff}$ values were observed during rain indicating emission of nitrogen from the canopy.

A similar analysis was made for R_a and R_b. During daylight, values of R_a and R_b were close to zero showing that v_d was mostly driven by the pattern of $R_{c,eff}$. Lower values of R_a and R_b were found for lower air humidity and higher temperature. In case of wet leaf surfaces, R_a and R_b were higher in the morning and evening. If wet leaf surfaces were excluded from the analysis, the differences for v_d and resistances to micrometeorological parameters diminished. Wet leaf surfaces reduced the uptake of ΣN_r at the measurement site. During the night or at lower radiation, R_a and R_b were comparable in magnitude to

~~$R_{c,eff}$. In autumn and winter, $R_{c,eff}$ showed partly negative values and no diurnal pattern. It should be noted that the shapes of the daily cycles of each parameter shown in Fig. 9 and 10 are almost similar for the chosen threshold values and differ only in amplitude.~~

3.3 Sensitivity of ΣN_r dry deposition sums to micrometeorological parameters

We found that ~~higher temperatures, lower relative humidity, and no precipitation~~ preferentially micrometeorological variables enhance deposition velocities and fluxes. The application of data-driven gap-filling methods like MDV (Falge et al., 2001) for estimating dry deposition could lead to biased results if micrometeorological conditions of the certain gap are different to fluxes used for filling the gap. ~~We further applied a u_*-filter, which had removed preferentially smaller fluxes occurring at low turbulent conditions.~~ Therefore, we determined dry deposition budgets with and without u_*-filter and conducted gap-filling with additional ~~restrictions~~ conditions for temperature, relative humidity, and ~~precipitation~~ wind speed.

Figure 11 shows the non gap-filled ΣN_r fluxes depicted as box plots and their cumulative sums with and without a u_*-filter if OMDV is used as gap-filling approach. For details to the implementation of OMDV, we refer to see Sec 2.3. ~~The threshold was set to 0.1 m s^{-1}, and the window for filling each gap was set to $\pm$5 days. Uncertainties of the gap-filled fluxes were estimated by the standard error of the mean. The total uncertainties were calculated as the sum of the standard errors.~~

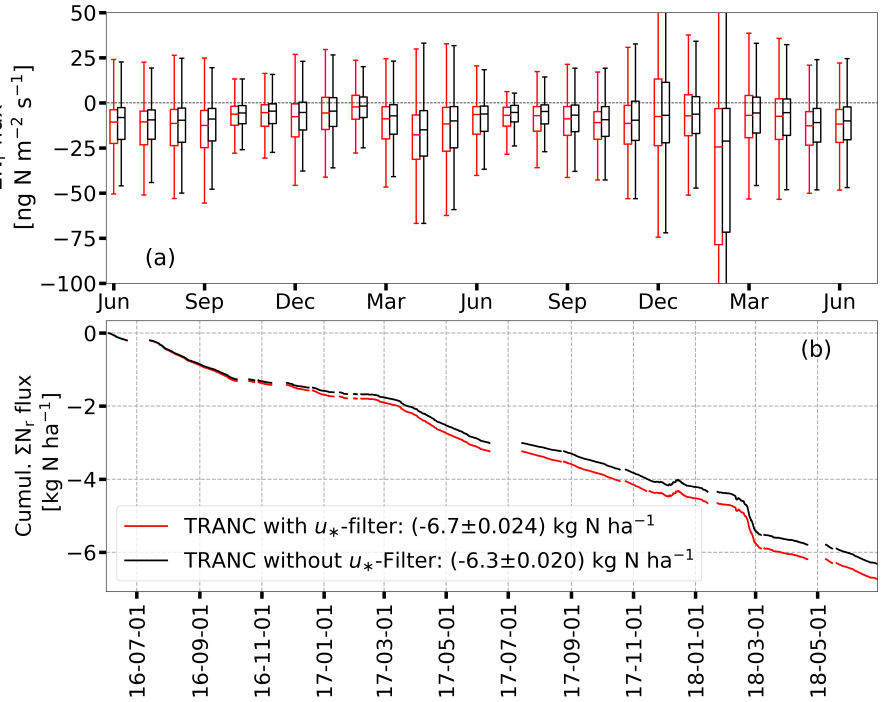

Figure 11. Panel (a) shows the non-gap filled ΣN_r fluxes depicted as box plots with (red) and without (black) u_*-filter in ng N m^{-2} s^{-1} (box frame = 25% to 75% interquartile ranges (IQR), bold line = median, whisker = 1.5· IQR). The threshold for u_* was set to 0.1 m s^{-1}. In panel (b), the cumulative dry deposition of ΣN_r is plotted for both cases in kg N ha^{-1}. For determining the cumulative curves, OMDV was used as gap-filling method, and gaps were filled with fluxes being in a range of ±5 days. Remaining gaps were not filled. In the legend of panel (b), cumulative ΣN_r deposition and the total uncertainty of the gap-filled fluxes according to Eq. (7) (Pastorello et al., 2020) are shown.

The difference in dry deposition was approximately 400 g N ha^{-1} after 2 years and ~~is within the uncertainty range of the estimated dry depositions~~ corresponds to 6% of the cumulative sum with u_*-filter. Panel (a) of Fig. 11 shows that median depositions of the ΣN_r fluxes with u_*-filter were ~~almost~~ equal to or larger than the median depositions without u_*-filter. ~~Figure 8 indicates that we measured large and small fluxes below 0.1 m s^{-1}.~~ Thus, the applied u_* threshold removed not only small fluxes resulting in a consistent bias between the median depositions. The contribution of the water vapor correction (Eq. 1) to the estimated dry deposition was very low. ΣN_r interference fluxes were between -3 and -0.3 ng N $m^{-2}s^{-1}$. The uncertainty ranged between 0.0 and 0.5 ng N $m^{-2}s^{-1}$. Considering two years of TRANC flux measurements with OMDV as gap-filling approach, the correction contributed with 1321 g ha^{-1} to the estimated dry deposition of 6.67 kg ha^{-1}.

~~We further investigated the impact of temperature, humidity, and precipitation on the dry deposition sums of ΣN_r compared to the dry deposition without restrictions when using MDV as gap-filling approach since we found differences in the diurnal patterns of ΣN_r for micrometeorological parameters. Therefore, we considered only fluxes in the time frame of ±5 days, at which temperature varied by ±3°C, humidity by ±5%, or precipitation was recorded. Remaining long-term gaps (see panel (b) of Fig. 11) were filled by a monthly average of the respective half-hourly value estimated from non-gap-filled fluxes (Fig. 6).~~

~~Those averages were also calculated for low and high humidity and temperature regimes separated by their monthly median. The calculations were made with and without the application of a u_*-filter. Figure 12 shows the annual dry deposition of the measurement years from the beginning of June to end of May.~~ In order to evaluate the influence of micrometeorological variables such as temperature (T), RH, and wind speed (wsp) on annual ΣN_r dry deposition, we compared the deposition estimates of OMDV with CMDV in regard to the measurement years from the beginning of June to end of May (Fig. 12). Details about the implementation of CMDV are given in Sec. 2.3.

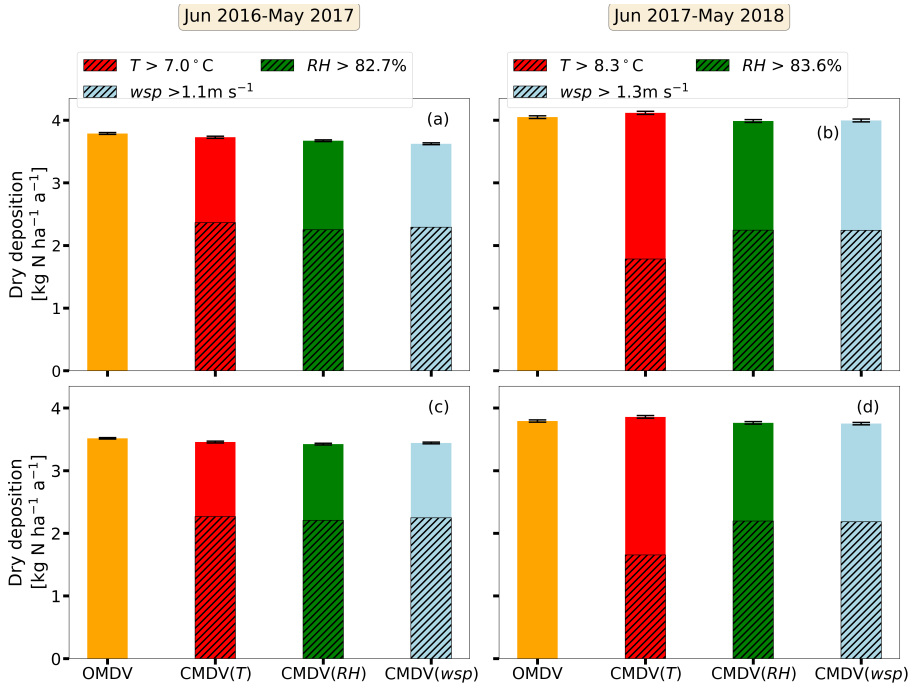

Figure 12. Annual ΣN_r dry deposition depicted as bar graphs from June to May in kg N ha^{-1} a^{-1}. For the orange bar, short-term gaps were filled with the OMDV approach while using only fluxes in the time frame of ± 5 days. In case of the red, green, and blue bar, the CMDV approach is applied for temperature (T), relative humidity (RH), and wind speed (wsp). Fluxes used for CMDV ~~gap-filling~~ have to additionally ~~fulfilled criteria~~ be in a range for ~~temperature~~ T (± 3°C), ~~humidity~~ RH ($\pm 5\%$), or ~~precipitation (wet or dry)~~ wsp (± 1.5 ms^{-1}). For OMDV and CMDV, ~~R~~remaining gaps were replaced by monthly averages estimated for each half-hour calculated from the non-gap-filled fluxes. ~~For the meteorological cases, monthly medians were used to determine those averages for low and high humidity and temperature regimes.~~ (a) and (b) were made for fluxes with u_*-filter, (c) and (d) without it. The hatched area of the bars represent the dry deposition for ~~temperature~~ T, ~~and relative humidity~~ RH ~~values~~, and wsp values higher than the annual median shown in the legend~~and for wet conditions~~.Error bars correspond to the root sum squared errors of the gap-filled fluxes (see Eq. (7)).

No significant difference could be found between the dry depositions sums and their cumulative uncertainties related to gap-filling for both measurement years. Consequently, the applied selection criteria did not lead to biased sums compared to the dry deposition calculated with OMDV ~~determined without restrictions for meteorological parameters. Warm, drier conditions~~

exhibited a higher contribution to the annual dry deposition, in particular for the first measurement year. During rain, dry deposition was less than 500 g N ha^{-1} per 12-month period. The relative contribution to dry deposition related to temperatures, relative humidity, and wind speeds above their respective medians was at 60% and at 55% in the first and second measurement year, respectively. As shown before, a difference in the application of a u_*-filter exists but is within the uncertainty range. Dry deposition was higher in 2017/2018, which was related to the large deposition fluxes observed in February 2018. In total, we estimated 3.8±0.8 kg N ha^{-1} a^{-1} and 4.10±1.1 kg N ha^{-1} a^{-1} with the OMDV approach (orange bar) and u_*-filter for 2016/2017 and 2017/2018, respectively.

Wet deposition was estimated from measurements of bulk and wet-only samplers. Table 2 3 shows estimated ΣN_r dry depositions, the deposition estimates of NH_4^+-N, NO_3^--N, dissolved organic nitrogen (DON), and the resulting total nitrogen from wet deposition (TWD) for all seasons and both measurement years. Please note that the sum of all seasons corresponds to the sum of both measurement years.

Table 2. Annual sums of NH_4^+-N, NO_3^--N, dissolved organic nitrogen (DON), and the resulting total wet depostion (TWD) from wet deposition samplers (bulk and wet-only). ∅ represents the average and *s* the standard deviation.

Sampler type	year	NH_4^+-N [kg ha^{-1}]	NO_3^- [kg ha^{-1}],	DON [kg ha^{-1}]	TWD [kg ha^{-1}]
Bulk	2016	3.8	3.4	1.5	8.7
	2017	3.4	3.4	0.7	7.5
	2018	2.8	2.7	0.7	6.2
	∅	3.3	3.2	1.0	7.5
	s	0.5	0.4	0.5	1.3
Wet-only	2016	4.0	3.6	0.9	8.5
	2017	3.4	3.6	0.5	7.5
	2018	2.9	2.6	0.6	6.1
	∅	3.4	3.3	0.7	7.4
	s	0.6	0.6	0.2	1.2

Differences between deposition estimates from bulk and wet-only samplers were not significant, and deposition estimates of NH_4^+-N and NO_3^--N were almost equal. Results from both sampling systems have in common that wet deposition of NH_4^+ and NO_3^- decreased from 2016 to 2018. In 2018, TWD was possibly lower due to the decreased amount of precipitation. Annual precipitation was approximately 200 mm lower in 2018 compared to 2017. In comparison to the results from dry deposition, wet deposition was about a factor two higher than dry deposition. Mean TWDs of wet-only samplers were 8.0 kg N ha^{-1} and 6.8 kg N ha^{-1} for the timeframe 2016/2017 and 2017/2018, respectively.

Table 3. Annual and seasonal sums of dry deposition estimates (DD) and NH_4^+-N, NO_3^--N, dissolved organic nitrogen (DON), and the resulting total wet depostion (TWD) from wet deposition samplers (bulk (BD) and wet-only (WD)) in kg N ha^{-1} $period^{-1}$.

Time	DD [kg N ha^{-1} $period^{-1}$]	WD [kg N ha^{-1} $period^{-1}$]				BD [kg N ha^{-1} $period^{-1}$]			
		NO_3^--N	NH_4^+-N	DON	TWD	NO_3^--N	NH_4^+-N	DON	TWD
Winter	2.0	1.5	0.9	0.4	2.8	1.7	1.3	0.5	3.5
Spring	2.2	1.8	2.3	0.1	4.2	1.9	2.4	0.1	4.4
Summer	2.0	1.9	2.6	0.2	4.7	1.6	2.2	0.6	4.4
Autumn	1.7	1.5	1.4	0.6	3.5	1.4	1.4	0.6	3.4
June 16 – May 17	3.8	3.8	4.2	0.4	8.4	3.5	4.2	1.0	8.7
June 17 – May 18	4.0	2.9	3.1	0.9	6.9	3.0	3.1	0.9	7.0

Small seasonal and annual differences in dry deposition were determined (approx. 200 g N ha^{-1} $period^{-1}$). Total seasonal and annual uncertainties related to gap-filling (Eq. (7)) were between 7 and 21 g N ha^{-1} $period^{-1}$. Dry deposition contributed approximately one third to total deposition except for winter (Fig. S12). In the second year, contribution of dry deposition was higher than in the first year. Higher fractions of dry deposition were related to the large dry deposition occurring in late February 2018. Thus, dry deposition and its uncertainty were remarkably high during winter. Total wet deposition (TWD) was highest in spring and summer. During those periods, NH_4^+-N contributed most to TWD, which was probably related to high NH_3 concentrations. Interseasonal differences for NO_3^--N were found but were lower compared to changes in NH_4^+-N. DON deposition was lowest and was between 0.1 and 0.6 kg N ha^{-1} a^{-1}. Overall, differences in TWD for both sampler types were less than 300 g N ha^{-1} a^{-1} except for winter. ~~In total, we got a total nitrogen deposition of~~ Total wet + dry deposition was equivalent to ~~11.8~~12.2 kg N ha^{-1} a^{-1} for 2016/2017 and 10.9 kg N ha^{-1} a^{-1} for 2017/2018.

4 Discussion

4.1 Interpretation of measured concentrations ~~, deposition velocities,~~ and fluxes

Measured half-hourly ΣN_r concentrations were low relative to sites exposed to agricultural activities or urban environments. On average, we measured 5.5 ppb (3.1 µg N m^{-3}) ΣN_r, 1.8 ppb (1.0 µg N m^{-3}) NH_3, and 2.5 ppb (1.4 µg N m^{-3}) NO_x. Wintjen et al. (2020) determined an average ΣN_r concentration level of 21 ppb (12 µg N m^{-3}) for a seminatural peatland, Brümmer et al. (2013) measured between 7 and 23 ppb (4 and 13 µg N m^{-3}) as monthly averages above a cropland site, and Ammann et al. (2012) measured half-hourly ΣN_r concentrations ranging from less than 1 ppb to 350 ppb (0.6 to 201 µg N m^{-3}) for a grassland site. Only for certain time periods, ΣN_r concentrations reached significantly higher values. During winter, NO_x increased due to emission from heating with fossil fuels and from combustion processes, for example through traffic and power plants. A

generally lower mixing height, which is often observed during winter, also leads to higher ground-level concentrations of air pollutants. In spring and autumn, higher ΣN_r concentrations can be attributed to NH_3 emission from the application of fertilizer and livestock farming in the surrounding environment (Beudert and Breit, 2010). NH_3 emissions from livestock farming in rural districts around the NPBW are approximately half of the emissions compared to rural districts located in the ~~Donau~~Danube-Inn valley (Beudert and Breit, 2010)~~, who~~. The authors measured concentrations of NO_2 (2.1-4.8 ppb (1.2-2.8 µg N m^{-3})), NO (0.4-1.6 ppb (0.2-0.9 µg N m^{-3})) and NH_3 (1.4 ppb (0.8 µg N m^{-3})) at the same site. Those values for NO_2 and NO refer to 1992 until the end of 2008, NH_3 was measured from mid of 2003 to 2005. The low concentration level and seasonal variability of the ΣN_r compounds, in particular NH_3 and NO_2, are in agreement with Beudert and Breit (2010). Low ~~C~~concentration values of NH_3 and NO_x are ~~expectable~~ reasonable for a site, which is some kilometers away from anthropogenic emission sources. Studies like Wyers and Erisman (1998); Horii et al. (2004); Wolff et al. (2010) conducted measurements of NH_3 and NO_2 above remote (mixed) forests and reported similar concentrations for those gases.

Our measurements further indicated that NO_x made the highest contribution to the measured ΣN_r concentrations. At the measurement height, the contribution of NO to NO_x was negligible. Median contribution of NO to NO_x concentrations was approximately 10% at 50 m. NO exhibits higher concentrations and fluxes close to the forest floor as shown by Rummel et al. (2002). Even if soil NO was converted to NO_2 it could still contribute to the measured ΣN_r flux except for the fraction that is removed by the canopy. As mentioned in Sec. 2.2, NO_2 concentrations had been measured at 50 m. Seok et al. (2013) reported marginal differences in NO_2 concentrations above the canopy at a remote site. Above the canopy, height differences in NO_2 concentrations were probably not relevant for the measurement site. The NO_x analyzer was equipped with a thermal converter and likely cross-sensitive to other NO_y compounds. However, measured concentrations of HNO_3 or NO_3^- were comparatively low as seen in Fig. 3. Thus, their influence on NO_x measurements appeared to be small. In the context of height differences, we found no systematic difference between NH_3 concentrations within the canopy and just above the canopy. Only for short time periods, for example in summer 2016 and 2017, differences in passive samplers were found indicating a small NH_3 flux. Considering the LOD of IVL passive samplers for NH_3 of 0.4 µg N m^{-3} determined by Dämmgen et al. (2010), shows that passive sampler measurements were conducted close to their LOD. It suggests that the uncertainty of the passive samplers was too large to resolve flux gradients. Still, NH_3 had a strong presence in the ΣN_r concentration within the growing period of the plants, in particular during spring and summer. DELTA measurements further suggested that gaseous N_r influenced the ΣN_r concentration pattern at most.

The increase in the relative contributions of HNO_3 from spring to summer compared to the decrease of NH_4^+ and NO_3^- (Fig. 4) can be related to the evaporation of NH_4NO_3 (Wyers and Duyzer, 1997; Van Oss et al., 1998; Schaap et al., 2002). However, the findings of Tang et al. (2015) and Tang et al. (2021) revealed that HNO_3 concentrations measured by the DELTA system using carbonate coated denuders may be significantly overestimated (45% on average) since HONO sticks also at those prepared surfaces. Thus, the measured HNO_3 concentrations should be seen as an upper estimate. Due to the reaction of NH_3 with HNO_3 and sulphuric acid particulate NH_4^+ is formed, available as NH_4NO_3 or $(NH_4)_2SO_4$. These aerosols are mainly in the fine mode and assigned with diameters less than 2.5 µm ($PM_{2.5}$) (Kundu et al., 2010; Putaud et al., 2010; Schwarz et al., 2016). Since the DELTA cut-off size is approximately 4.5 µm (Tang et al., 2015), fine accumulated particles could be adequately

detected. Coarse mode NO_3^- aerosols like sodium nitrate ($NaNO_3$) are formed in the presence of sea salt (Na^+ and Cl^-) or other geological minerals or biological particles like pollen (Lee et al., 2008; Putaud et al., 2010). Generally, concentrations of Na^+, Ca^{2+}, and Mg^{2+} were close to zero during the entire campaign. On average, we measured 0.08 µg m^{-3} for Na^+ and 0.01 µg m^{-3} for Ca^{2+} and Mg^{2+}. Although these concentrations were close to and lower than the LOD of DELTA (Tang et al., 2021) and partly underestimated by the filters of the DELTA system due to the cut-off size of approximately 4.5 µm, it illustrates that coarse mode nitrate levels are not expected to be significant at the measurement site. As noted in Sec. 2.2, cellulose filters were used for collecting NO_3^- and SO_4^{2-}. According to Tang et al. (2015), cellulose filters underestimate NO_3^- and SO_4^{2-} ions, sulphate by 11% and nitrate by 37%. However, Schaap et al. (2004) found that cellulose filter are appropriate for capturing NO_3^-. Inside of the TRANC, high temperatures (≥870°C) probably led to a chemical decomposition of coarse aerosols (Yuvaraj et al., 2003). Marx et al. (2012) found that the TRANC is able to convert $NaNO_3$. Thus, we assume that the TRANC's cut-off size was higher resulting in a higher sensitivity to aerosols in the coarse mode. Still, we observed a clear excess of NH_4^+ over NO_3^-. Presumably, the contribution of NO_3^- aerosols to TRANC measurements was not significant. In addition, higher oxidized compounds like N_2O_5 or peroxy acteyl nitrates could not be collected by DELTA, but probably converted by the TRANC. Issues in the temperature stability or CO supply leading to instabilities in the conversion efficiency of the TRANC may be responsible for disagreements to the collection efficiency of the denuders. A key uncertainty was the data coverage of the TRANC, which was 78% on average during the exposure periods. In total, the comparison of the total N concentrations shows that the TRANC can adequately measure ΣN_r concentration.

In general, a comparison of ΣN_r concentrations and fluxes to other studies is difficult due to the measurement of the total nitrogen. Most studies, which have been published so far, focused only on a single or a few compounds of ΣN_r and are limited to selected sites and time periods of a few days or months. Only a few studies had been focusing on ΣN_r flux measurements using the EC method (see Ammann et al., 2012; Brümmer et al., 2013; Zöll et al., 2019; Wintjen et al., 2020). Brümmer et al. (2013) measured ΣN_r exchange above an agricultural land. During unmanaged phases, fluxes were between -20 ng N m^{-2} s^{-1} and 20 ng N m^{-2} s^{-1}. Apart from management events, fluxes above the arable field site were ~~closer to neutral conditions~~ closer to zero compared to our unmanaged forest site, which is ~~mainly characterized~~ dominated by deposition fluxes and is therefore a larger sink for reactive nitrogen. Ammann et al. (2012) measured ΣN_r fluxes above a managed grassland. In the growing season, ~~mostly~~ deposition fluxes of -40 ng N m^{-2} s^{-1} were measured. The authors reported ~~slightly~~ increased deposition due to weak NO emission during that ~~phase~~ period. Similar to Brümmer et al. (2013), the flux pattern observed by Ammann et al. (2012) is influenced by fertilizer application and thus, varying contributions of N_r compounds, for instance by bidirectionally exchanged NH_3 leading to both net emission and deposition phases of ΣN_r. ~~Flux detection limit is almost equal to Zöll et al. (2019) but slightly higher than upper flux detection limits determined by Ammann et al. (2012) and Brümmer et al. (2013) for the same model.~~ Despite the low signal-to-noise ratio of emission fluxes and data coverage of 50% from June 2016 to June 2018 at the measurement site, we were able to investigate the exchange pattern of ΣN_r and could estimate reliable dry deposition sums. To our knowledge, flux measurements of ΣN_r above mixed forests have not been carried out so far. We found that the flux magnitude and diurnal flux pattern were similar to observations reported for individual N_r species above forests, e.g. NH_3 (Wyers and Erisman, 1998; Hansen et al., 2013, 2015), NO_2 (Horii et al., 2004; Geddes and Murphy, 2014), HNO_3 (Munger

et al., 1996; Horii et al., 2006), and total ammonium (tot-NH_4^+) and total nitrate (tot-NO_3^-) (Wolff et al., 2010). As seen by the flux values and measurements of individual compounds, deposition prevails in the reported flux pattern, which corresponds to our measurements.

However, under certain circumstances regarding micrometeorology or the availability of ΣN_r compounds large deposition or emission fluxes can be observed. In February 2018, remarkably high ΣN_r concentrations and depositions were measured. ~~Unfortunately, we had no DELTA measurements for February 2018, which could provide insights in the ambient concentrations of individual N_r species, but we found that SO_2 concentrations were unusually high (daily means up to 5.5 µg m^{-3}). During the entire campaign, we measured 1.0 µg m^{-3} SO_2 on average. SO_2 concentrations were slightly correlated with ΣN_r concentrations during the deposition period in February 2018. For the period of enhanced ΣN_r concentrations, a correlation of 0.29 was determined. Since reactions involving SO_2 and N_r species happen at different timescales, and ΣN_r consists of several, chemically different compounds, low correlations are reasonable. SO_2 is rapidly converted to H_2SO_4. The latter is neutralized by NH_3 resulting in the formation of ammonium sulfate $(NH_4)_2SO_4$, a secondary inorganic aerosol. In the presence of HNO_3, NH_4NO_3 is formed by the reaction with NH_3. However, the formation of $(NH_4)_2SO_4$ is favored over the neutralization of HNO_3 at low NH_3 concentrations (Seinfeld and Pandis, 2006; Squizzato, S. and Masiol, M. and Brunelli, A. and Pistollat~~

~~Passive sampler measurements showed a low NH_3 concentration level in February 2018.~~

~~If the $[NH_4^+]/[SO_2^{-4}]$ molar ratio is lower than two (Squizzato, S. and Masiol, M. and Brunelli, A. and Pistollato, S. and Tarabotti, E. and~~ ~~the aqueous or solid phase of $(NH_4)_2SO_4$ is prevailed aerosol form. At higher ratios, most of the sulfate is expended, and NH_3 is available for the neutralization of HNO_3. The existence of the solid phases depends highly on humidity, temperature, and the concentration of the constituents (Bok Haeng Baek and Viney P. Aneja and Quansong Tong, 2004; Seinfeld and Pandis, 2006; Squizzato, S~~ ~~The concentration of NH_3 needed for the formation of solid $(NH_4)_2SO_4$ is higher than values measured at our site, but the threshold depends on micrometeorology, for example, it reduces towards lower humidity levels (Seinfeld and Pandis, 2006). Presumably, not only $(NH_4)_2SO_4$ contributes to ΣN_r during February 2018 but compounds formed at lower ratios, e.g., ammonium bisulfate.~~

During the exposure period of the DELTA samplers, we found 0.96, 0.17, 0.37, 0.27, and 1.70 µg N m^{-3} for NH_4^+, NH_3, NO_3^-, HNO_3, and NO_x, respectively. The aerosol concentrations were exceptionally large in February 2018, which have affected these averages considerably. Averaged NH_4^+ concentration during winter excluding February 2018 was only 0.38 µg N m^{-3} in comparison to 0.96 µg N m^{-3} for February 2018. The concentration in this month results in a NH_4^+ concentration 2.5 times higher than the average. Also, SO_2 was much larger concentrations (1.54 µg N m^{-3}) in this month compared to the other winter month (0.37 µg N m^{-3}). Figure 13 shows the relative contributions of each N_r compound for February 2018 compared to averaged fractions during winter excluding February 2018.

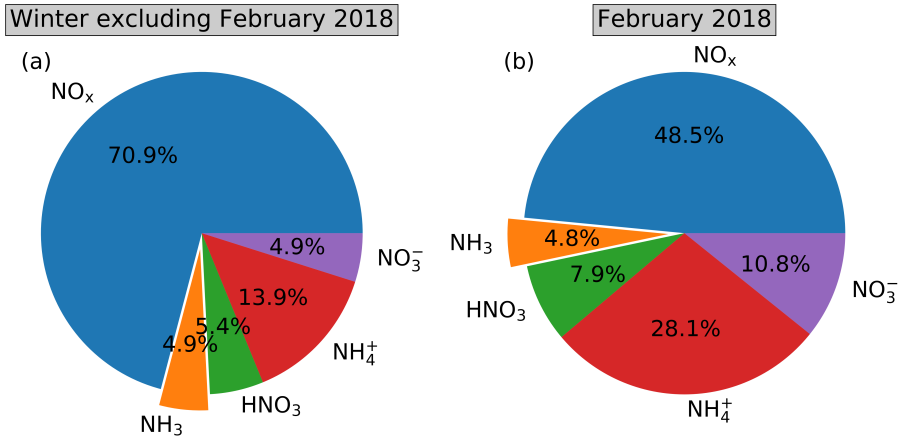

Figure 13. Relative contribution of concentrations for NO_x, NH_3, HNO_3, NO_3^-, and NH_4^+ to ΣN_r estimated from DELTA and NO_x measurements for winter and separately for February 2018. NO_x measurements are averaged to exposure periods of the DELTA samplers.

During February 2018, NH_4^+ made a significant contribution to the ΣN_r concentration. The measured NH_4^+ value is an integrated value over approximately one month. Thus, daily contributions of NH_4^+ could have been even higher. Earlier studies by e.g. Wolff et al. (2010) report events with large aerosol deposition. During their campaign, wind speeds were relatively high. Largest aerosol deposition occurred during dry conditions, e.g. low *RH*, no rain, and high visibility. Figure S13 shows micrometeorological parameters, deposition velocities, and gap-filled ΣN_r fluxes from the 12 February to 6 March. Large deposition fluxes were accompanied by high wsp and u_* values, high R_g indicating high visibility, and low *RH*. The observed conditions are typical for cold air streams with high aerosol loads coming from North east and led to a reduction in turbulent resistances resulting in a high v_d, which is allowed by turbulence. Hence, at low concentrations of NH_4^+ significant aerosol deposition is possible if R_a and the surface resistance are reduced. In conclusion, NH_4^+ aerosols, ammonium (bi)sulfate and nitrate, were most responsible for the large ΣN_r deposition due to their excess over NO_3^-. Since we had no high-resolution flux measurements of any ΣN_r compound, we have no evidence which aerosol predominated the ΣN_r flux.

In December 2017, large emission fluxes were measured. Compared to 2016, significant difference in temperature and snowdepth were observed. Figure 14 shows recorded temperature, snow fall, concentrations, and estimated fluxes of ΣN_r from 6 December to 15 December for 2016 and 2017. Here, ± 3 days were chosen for filling the gaps in order to keep the short-term variability of the fluxes.

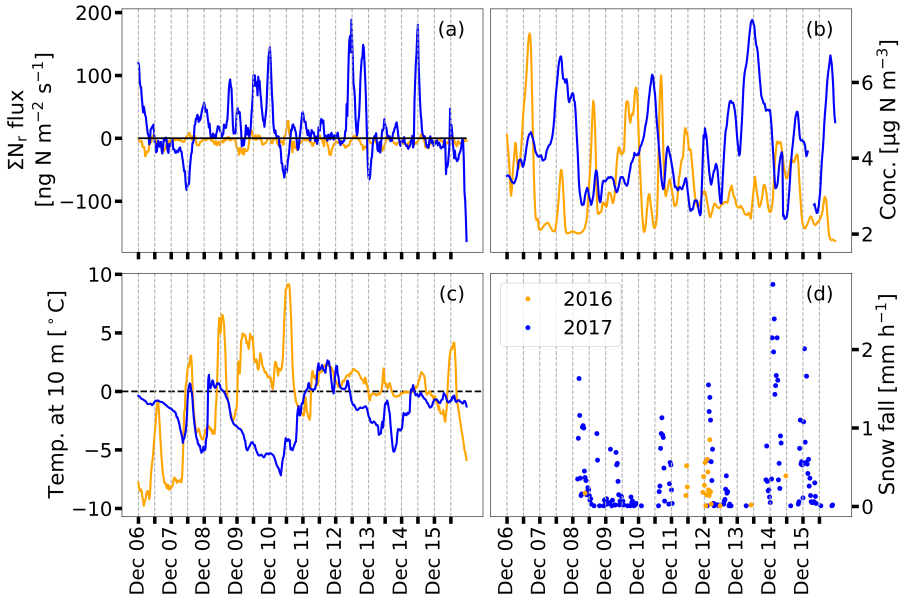

Figure 14. ΣN_r gap-filled fluxes (a), ΣN_r concentrations (b), air temperature at 10 m height above ground (c), and snow fall (d) from 6 December to 15 December for 2016 (~~green~~orange) and 2017 (~~red~~blue). Gaps are filled with the OMDV approach with fluxes being in a range of ± 3 days. Fluxes and concentrations of ΣN_r were smoothed with a 3-h-running mean for better visualization.

In 2017, we observed substantial snow fall and a slower varying temperature compared to 2016 leading to significant snow depths compared to 2016. On the 1st of December, 1 cm and 20 cm snow depth were measured in the fetch of the tower for 2016 and 2017, respectively. Two weeks later, snow depth increased to 5 cm and 60 cm, respectively. In addition, temperatures ~~were mostly higher than~~ alternated around 0°C with minimum and maximum values close to ±10°C in December 2016. In 2017, temperatures were ~~mostly~~ below 0°C and only for one day above 0°C, and global radiation was ~~mostly~~ below 100 W m^{-2}.

~~Hansen et al. (2013) reported a change in the NH_3 flux pattern from deposition to emission due to the senescing of fallen leaves.~~ The decomposition of litter ~~leading to NH_3 emissions~~ from the forest ground could be responsible for the observed emission fluxes of ΣN_r although the decomposition rate of litter is reduced at lower temperatures. However, the snow pack could act as an insulator and inhibited soil frost penetration. Therefore, decomposition of litter could have been ~~happened~~ occurring under the snow pack. Kreyling et al. (2013) compared different snow treatments and their effect on decomposition. The authors observed nearly no soil frost penetration under snow insulation. The annual cellulose decomposition was greatly reduced for the snow removal treatment ($\sim 46\%$). An increasing mass loss rate was found under a deeper snow pack (Saccone et al., 2013) depending on the type and age of litter (Bokhorst et al., 2013). Due to a small snow depth in 2016, soil frost penetration had a higher potential to reduce the decomposition rate. ~~In addition, temperatures were mostly above the freezing point leading to partial melting of the snow layer, which probably inhibited the release of hygroscopic N_r species such as NH_3. Thus, emission of nitrogen from the soil or the decomposition of leaves was probably reduced compared to 2017. The deeper~~

snow layer promoted microbial activity, and the generally lower temperatures and radiation inhibited a melting of the upper snow layers. Thus, leakage of N_r species like NH_3 could have happened in December 2017.

NO seems to be less responsible for the observed emission pattern following the findings of Medinets et al. (2016). They measured soil NO, N_2O, and CO_2 fluxes at a spruce forest during the 'cold' season (daily average temperature $< 3°C$). They found that NO fluxes were positively correlated to air and soil temperature. Snow cover was not identified as a determining factor for the NO fluxes by the authors, since NO efflux during snow cover and snow free periods were similar. However, the reported snow depth was only 4.6 cm on average. Soil frost penetration could have happened in the topsoil and lowered the NO emissions leading to lower correlation between NO and snow cover. As stated by the authors, different results had been published about the origin of NO emissions from snow covered soils (see Medinets et al., 2016, and references therein). An influence of NO either emitted from the snow pack or the soil cannot be fully excluded. A correlation of the measured fluxes with temperature was not found. This could be related to a time-shift between emission and dropping temperature. It has also to be considered that we measure approximately 30 m above the forest soil, and not only NO contributes ΣN_r. In addition, NO emitted from the forest floor can be converted to NO_2 (Rummel et al., 2002). Thus, low correlations were of ΣN_r fluxes to micrometerological parameters were expected.

Our measurements further indicated that NO_x had the highest contribution to the measured ΣN_r concentrations. At the measurement height, the contribution of NO to NO_x was probably negligible. Median contribution of NO to NO_x is approximately 10% at 50 m. NO exhibits higher concentrations and fluxes close to the forest floor as shown by Rummel et al. (2002). Even if soil NO was converted to NO_2 it could still contribute to the measured ΣN_r flux except for the fraction that is removed by the canopy. NH_3 had strong presence in the ΣN_r concentration within the growing period of the plants, in particular during spring and summer. DELTA results revealed that gaseous N_r species have a high potential to influence the exchange pattern of ΣN_r. The slight increase in HNO_3 and decrease of NH_4^+ can be related to the evaporation of NH_4NO_3 (Wyers and Duyzer, 1997; Van Oss et al., 1998). However, the findings of Tang, Y. S. and Flechard, C. R. and Dämmgen, U. and Vidic, S. revealed that HNO_3 concentrations measured by the DELTA system using carbonate coated denuders may be significantly overestimated (45% on average) since HONO sticks also at those prepared surfaces. Thus, the HNO_3 contributions should be seen as an upper estimate. The comparison of the total N concentrations shows that the TRANC can adequately measure ΣN_r concentration. Obviously, not all components of ΣN_r were included in this comparison, for example, higher oxidized components like N_2O_5 could not be considered.As mentioned in Sec. 2.2, NO_2 had been measured at 50 m. However, Seok et al. (2013) found only slight differences in NO_2 concentrations above the canopy at a remote site. Thus, height differences in NO_2 are likely insignificant. Issues in the temperature stability or CO supply resulting in instabilities in the conversion efficiency of the TRANC, or a reduced sensitivity of the CLD could lead to differences to DELTA+NO_x. DELTA measurements report concentrations integrated over long time periods. Concentration peaks could not be collected sufficiently by the coated surfaces. The latter are exposed to environmental influences like temperature and moisture, and their sensitivity may reduce over time.

As shown in Fig. S5, median v_d of ΣN_r were low compared to deposition velocities determined for NH_3 or HNO_3 above other forests. Values range between 1.1 and 2.2 cm s^{-1} for NH_3 (see Schrader and Brümmer, 2014, and references therein) and between 2 and 8 cm s^{-1} for HNO_3 (Pryor and Klemm, 2004; Horii et al., 2006; Farmer and Cohen, 2008). v_d values reported

~~for NO_2 are closer to v_d of ΣN_r. In the literature, v_d is between 0.015 and 0.51 cm s^{-1} for NO_2 (e.g., Rondon et al., 1993; Horii et al., 2004; For tot-NH_4^+ and tot-NO_3^-, mean v_d of 3.4 cm s^{-1} and 4.2 cm s^{-1} were determined by Wolff et al. (2010), respectively. Since the analysis of the different N_r species contributing to the ΣN_r concentrations states NO_2 as the dominant compound, a similarity of v_d for ΣN_r to deposition velocities of NO_2 can be excepted. It further implicates a lower contribution of NH_3 than NO_2 to the measured flux.~~

4.2 Influence of micrometeorology and nitrogen concentrations on deposition and emission

4.2.1 ~~Influence of R_g on ΣN_r exchange~~

Figure S~~7~~9 and S~~8~~10 show~~ed~~ that the ~~shape~~ variability of v_d and other micrometeorological variables were highly correlated with each other. Thus, we could not examine the mechanistic micrometeorological driver of the ΣN_r flux. The dependencies on u_* or L could also be related to effects of sensible heat flux, R_g or T_{air}. Surely, micrometeorological parameters such as R_g and T_{air} promote photosynthesis of plants (Jarvis, 1976), i.e. lower the stomatal resistance, which is essential for the stomatal uptake of ΣN_r compounds such as NO_2 (e.g., Thoene et al., 1996) and NH_3 (e.g., Wyers and Erisman, 1998). The analysis revealed that deposition velocities were independent of the ΣN_r concentration. Consequently, ΣN_r concentration did not emerge as a driver of its deposition velocities at our measurement site. Still, the impact of increasing concentration on nitrogen (deposition) fluxes is well documented, for example, by Ammann et al. (2012) and Brümmer et al. (2013) for ΣN_r above grassland and arable land, respectively, by Horii et al. (2006) for NO_y and Horii et al. (2004) for NO_x above a mixed forest, and by Zöll et al. (2016) for NH_3 above a seminatural peatland.

Since we had no possibility to determine the actual contribution of the individual compounds to the ΣN_r flux, comparing micrometeorological dependencies of v_d to observations made for individual compounds is not possible. In case of NH_3, surface wetness was identified as a controlling factor for the NH_3 uptake in previous studies (Wyers and Erisman, 1998; Milford et al., 2001; Wentworth et al., 2016). For total ammonium and total nitrate (tot-NH_4^+ and tot-NO_3^-, respectively), Wolff et al. (2010) found that tot-NO_3^- exchange was almost neutral and emission was observed for tot-NH_4^+ during rain or fog. Highest deposition was observed during sunny days. For the actual compound mix at our measurement site, high temperatures ($>$ 14.6°C), low relative humidity ($<$ 74.0%), and dry leaf surfaces, were found to enhance the surface uptake of ΣN_r from May to September. Since the actual composition of the ΣN_r flux is not known, no arguments about an agreement or disagreement to the cited publications can be made.

We further found that the ΣN_r concentration did not change significantly through the year. The difference between lowest and highest seasonal concentration means was only 0.8 µg N m^{-3}. However, DELTA measurements demonstrated that the contribution of individually compounds do show a seasonal cycle. Since the ΣN_r compounds differentiate in their v_d, the observed seasonality in the dry deposition flux is related to the availability of ΣN_r compounds. For example, in spring and summer, NH_3 had probably the largest contribution on the ΣN_r flux. Elevated NH_3 concentrations were likely caused by emissions from agricultural management in the surrounding region (Ge et al., 2020). The concentration of NH_3 was still lower than NO_2, but the v_d of NH_3 is significantly higher than NO_2 for woodland. Deposition velocities of NH_3 range between 1.1

and 2.2 cm s^{-1} for NH_3 (see Schrader and Brümmer, 2014, and references therein), and values between 0.015 and 0.51 cm s^{-1} were reported for NO_2 (e.g., Rondon et al., 1993; Horii et al., 2004; Breuninger et al., 2013; Delaria et al., 2018, 2020). Still, variations in the composition of ΣN_r may correlate with micrometerological parameters. For example, the formation of HNO_3 is correlated to R_g. The solar radiation responsible for the stomatal opening also promotes the formation hydroxyl radicals, which react with NO_x (Seinfeld and Pandis, 2006). T_{air} influences the diurnal pattern of NH_4NO_3, which may also volatilize close to the surface due to the depletion of its precursors and in acase the temperature gradient is large enough (Wyers and Duyzer, 1997; Van Oss et al., 1998). Thus, some NH_4^+ and NO_3^- aerosols may be converted to NH_3 and HNO_3, which can deposit faster than aerosols. For tot-NH_4^+ and tot-NO_3^-, mean v_d of 3.4 cm s^{-1} and 4.2 cm s^{-1} were determined by Wolff et al. (2010). In case of HNO_3, mean values between 2 and 8 cm s^{-1} were published by Pryor and Klemm (2004); Horii et al. (2006); Farmer and Cohen (2008).

In conclusion, variability in micrometeorological controls such as R_g, T_{air}, u_*, or RH in combination with changes in ambient concentration levels of the ΣN_r compounds explain the observed variation in the ΣN_r flux pattern. Definitely, ΣN_r concentration had no influence on its deposition velocities.

~~is strongly correlated to R_g. Global radiation had been identified as an important 'driver' for the ΣN_r exchange, recently verified by an artificial neural network approach conducted by Zöll et al. (2019). The word 'driver' is a paraphrase of the expression 'controlling input variable' (Moffat, Antje M. and Beckstein, Clemes and Churkina, Galina and Mund, Martina and Heimann, M Drivers are identified by their correlation with the flux. As a remark, correlations could also be influenced by other parameters, which have not or could not considered by Zöll et al. (2019), for example chemical interactions of components contributing to ΣN_r.~~

~~As shown by Zöll et al. (2019), ΣN_r and CO_2 fluxes exhibited a similar daily cycle and showed a strong dependence on R_g during summer. The latter controls the opening of the stomata (Jarvis, 1976), i.e. lowers the stomatal resistance. Thus, photosynthesis controlling the CO_2 exchange through stomatal pathway appears to be the mechanism for controlling the ΣN_r exchange as compounds like NO_2 (Thoene et al., 1996) or NH_3 (Wyers and Erisman, 1998) are taken up by the stomatal pathway, too. However, ΣN_r compounds are not willingly absorbed by the plants as seen by the light response curves of Zöll et al. (2019, Fig. 5). The light response curve of ΣN_r has a reversal instead of a saturation point as observed for CO_2 (Zöll et al., 2019). Consequently, a second mechanism, the stomatal compensation point firstly proposed by Farquhar, Graham D. and Firth, likely controls the uptake of the ΣN_r compounds. Basically, if the stomatal concentration is lower than the ambient concentration, deposition is observed. Thus, both parameters, the stomatal resistance and the stomatal compensation point, which are regulated by R_g and concentration, respectively, affect the uptake of ΣN_r. As further shown by Zöll et al. (2019), other parameters like u_* were not identified as important drivers for ΣN_r. Photochemistry and stomatal control appear to be more important than turbulent mixing. Radiation changes the composition of ΣN_r due to the formation of O_3. In addition, R_g had an influence on u_* as seen by their similar shapes in daily cycle (Fig. S7 and S8). The low correlations of ΣN_r fluxes to concentration for most of the selected u_* ranges show that atmospheric turbulence had a generally low influence on nitrogen deposition at the measurement site. Thus, u_* adds almost no additional information to the ΣN_r exchange and was not identified as important controlling factor for the ΣN_r exchange from July to September by Zöll et al. (2019). Similar conclusions can be drawn for~~

temperature and relative humidity. They are also affected by light/energy input into the ecosystem and follow a similar diurnal pattern. It shows that R_g contains most of the information for the explanation of the ΣN_r fluxes.

It has to be noted that the study was conducted for ΣN_r at the same natural, unmanaged site from July to September. Micrometeorological parameters were controlled by natural processes. The low response to micrometeorological parameters may also related to other processes influencing the composition of ΣN_r, to opposing effects on N_r species, or effects happened on a shorter time scale such as molecular interactions between the ΣN_r compounds. R_g was not identified as primary controlling factor for NH_3 by Milford et al. (2001). Milford et al. (2001) measured NH_3 fluxes above moorland, which has a generally higher humidity level than our measurement site. They concluded that NH_3 exchange is mostly driven by canopy temperature, wetness, and ambient concentrations. Radiation was not identified as primary controlling factor by the authors. They found higher deposition of NH_3 through the cuticular than through the stomatal pathway. However, Zöll et al. (2019) found only minor improvements in their driver analysis if water vapor pressure deficit was considered as secondary driver. Additionally, we found that v_d was reduced for high ambient humidity and wet leaf surfaces. Since we measured NH_3 indirectly by the TRANC and above an ecosystem characterized by lower humidity than a peatland, R_g favoring the exchange through the stomatal pathway appears to be more important for ΣN_r at the measurement site.

4.2.2 Influence of N_r species on measured v_d

Zöll et al. (2019) further identified ΣN_r concentration as secondary driver for the ΣN_r deposition. The impact of increasing concentration on nitrogen (deposition) fluxes is well documented, for example, by Ammann et al. (2012) and Brümmer et al. (2013) for ΣN_r, by Horii et al. (2006) for NO_y, Horii et al. (2004) for NO_x, and by Zöll et al. (2016) for NH_3. We measured almost the same ΣN_r concentration for each season. Consequently, it was not only the change in the overall ΣN_r concentration that influences v_d. The changes in the contribution of the components of ΣN_r had a higher influence on v_d of ΣN_r than the overall concentration.

The higher nitrogen deposition in April 2017 (Fig. 5) compared to April 2018 was mainly related to gaps in flux time series. In 2018, we had no flux measurements from mid of April to the beginning of May. During that time, foliage began in 2018 providing uptake of ΣN_r compounds. Increased plant activity was caused by continously, high radiation values during daylight ($> 400\,W\,m^{-2}$) leading to higher temperatures in April 2018 ($\sim 11.0°C$) than in April 2017 ($\sim 6.0°C$). We further observed high NH_3 concentrations measured by passive samplers and the DELTA system for the same time. Elevated NH_3 concentrations were likely caused by emissions from agricultural management in the surrounding region. In 2017, leaf emergence began in early May. Thus, measured N deposition would have been higher in April 2018 than a year before presumably related to a lower stomatal resistance in 2018. Almost equal patterns of v_d and $R_{c,eff}$ were determined for May 2017 and 2018. The conditions for uptake of ΣN_r by the canopy were comparable. Consequently, the different contributions in NH_3 and conditions in radiation and temperature strongly affected v_d and $R_{c,eff}$ and therewith the deposition of ΣN_r.

In the summer of 2016 and 2017, differences in the ΣN_r median concentration were lower than 1 ppb. No remarkable differences in micrometeorology were found between summer 2016 and 2017. Figure 3 revealed that the contribution of components to ΣN_r differed between the investigated time periods. From July to September 2017, the mean NH_3 concentration

was about 0.3 µg N m^{-3} lower than a year before. HNO_3, NH_4^+, and NO_3^- were remarkably low in July 2017 compared to July 2016. In conclusion, the deviations in the median deposition were not related to differences in the ΣN_r concentration. The differences in the composition of ΣN_r affected v_d, in particular the canopy compensation point, more and therewith the uptake of ΣN_r.

However, we found that higher ΣN_r concentrations led to lower $R_{c,eff}$ during no precipitation around noon, which could be related to an increased energy input or/and to an increased contribution of nitrogen compounds like NH_3 to ΣN_r. Since the impact of concentration on $R_{c,eff}$ was comparatively low, it was superimposed by slight differences induced by R_a and R_b. Thus, ΣN_r concentration had almost no measurable net effect on v_d. Since we had measured the ΣN_r exchange in a low nitrogen environment, the influence of the stomatal compensation point on the uptake of N_r species may be reduced. Zöll et al. (2019) calculated a light response curve of ΣN_r for the same site. The increase in deposition got lower for R_g between 300 and 500 W m^{-2} and reached a reversal point around 600 W m^{-2}. We found slight differences in $R_{c,eff}$ for the concentration threshold around noon, at times with the highest radiation. It shows that a stomatal compensation point exists but its influence is limited by the low, ambient nitrogen concentrations and radiation.

4.2.3 Seasonal changes in ΣN_r uptake capacity

Within the period of high incident radiation, in particular from May to September, a distinct diurnal pattern for v_d was observed, and no precipitation, high temperatures (> 14.6°C), low relative humidity ($< 74.0\%$), and dry leaf surfaces, were found to enhance the surface uptake, presumably through the stomatal pathway, of nitrogen during daylight. The observed differences in v_d for relative humidity and temperature were mostly related to R_a and R_b. $R_{c,eff}$ showed only a slight response to lower air humidity. Responses to the chosen temperature threshold and to dry leaf surfaces were not found.

During the rest of the year, no diurnal pattern was found under dry conditions (no precipitation) since stomata were likely closed, or requirements for stomatal deposition were not fulfilled (stomatal compensation point). Since we still observed a low, non-zero v_d but also short phases of ΣN_r emission during seasons with lower radiation, cuticular, soil, and turbulent driven processes were likely to be responsible for the ΣN_r exchange. In periods of reduced plant activity, for instance in winter and autumn, the uptake through the stomatal pathway was greatly reduced or even inhibited due to reduced radiation or leaf area surfaces. Besides stomatal deposition, cuticular deposition is also an important pathway for ΣN_r compounds, which likely deposit on wet surfaces such as NH_3, HNO_3 or NH_4^+.

However, v_d was lower under wet conditions. Presumably, requirements for cuticular deposition were not fully met. Measurements of ΣN_r were conducted several kilometers away from nearby sources, and thus hydrophilic ΣN_r components could be washed out before air masses reached the site. We showed that the contribution and concentrations of N_r species, which can deposit on wet leaf surfaces, was comparatively low at the measurement site. Furthermore, those species were only indirectly measured, and wet leaf surfaces could be already saturated with water soluble N_r species leading to a high cuticular compensation point. These issues may reduce the cuticular contribution to exchange processes with the canopy. Presumably, cuticular deposition was probably not as important as stomatal deposition during the timeframe of high incident radiation, in particular from May to

September. Stomatal deposition seems to be more important than other in-canopy uptake processes for the ecosystem in close proximity to the measurement site for those month.

The statement holds for the estimated fractions of N_r species found for this ecosystem. Ecosystems which are exposed to enhanced concentrations of NH_3 or nitrogen aerosols may differ in their uptake capacities. Wyers and Erisman (1998) measured highest NH_3 deposition if the canopy has a high water storage level (CWS) (> 2 mm). The deposition efficiency was reduced if CWS was higher than 0.25 mm but lower than 2 mm. By comparing different measurement years, they found differences in the deposition efficiency even if the canopy was saturated with water. They attributed the effect to the solubility of NH_3 in the water film. If canopy gets drier, evaporation of water occurs and the concentration of NH_3 increases in the water film. The cuticular resistance increases and deposition of NH_3 is reduced. Even emission of NH_3 was observed by Wyers and Erisman (1998), especially during the day when the canopy was dry, and NH_3 exchange was bidirectional. They showed that stomatal resistance was higher than canopy resistance. The authors identified cuticular deposition as more important for NH_3 as stomatal deposition. They measured an average NH_3 concentration of 5.2 µg m^{-3}. We measured 0.65 µg m^{-3} on average and found that the contribution of NH_3 to ΣN_r was comparatively low at the measurement site. If contribution of NH_3 or other soluble N_r species to ΣN_r is comparatively low, cuticular deposition is most likely reduced under wet conditions. The authors proposed that even under low ambient humidity leaf surfaces can exhibit high humidity due to the accumulation of particles. In case of conifer needles, Burkhardt, J. and Peters, K. and Crossley, A. (1995) showed that particles deposit close to their stomata. Most of them are hygroscopic. Therewith, cuticular deposition seems to be possible even under low ambient humidity. However, our measurement site was several kilometers away from potential (anthropogenic) emission sources. Concentrations of NO_3^-, NH_4^+, sulphur dioxide (SO_2), and NO_x were comparatively low at the site, in particular during summer. Thus, stomatal deposition appears to be more important for ΣN_r under high temperatures, low relative humidity, and no precipitation. This conclusion is valid for months with sufficient light/energy input leading to an increased plant activity, i.e. from May to September. Within the other seasons, aerosol concentrations originating from natural or anthropogenic emission sources are probably higher resulting in a higher particle density on leaf surfaces promoting cuticular deposition.

Wolff et al. (2010) observed high deposition of tot-NH_4^+ and tot-NO_3^- during sunny days. During rain or fog, tot-NO_3^- exchange was almost neutral and emission was observed for tot-NH_4^+. They measured median concentration of 0.57, 0.12, 0.76, and 0.45 µg m^{-3} for NH_3, HNO_3, NH_4^+, and NO_3^-, respectively. For the September months, we measured average concentrations of 0.76, 0.46, 0.50, and 0.78 µg m^{-3} for NH_3, HNO_3, NH_4^+, and NO_3^-, respectively. Measured tot-NO_3^- and tot-NH_4^+ of Wolff et al. (2010) exhibited a higher particle than gaseous contribution. At our measurement site, the gaseous contribution was higher than the values reported by Wolff et al. (2010). Median deposition velocities of tot-NO_3^- and tot-NH_4^+ were higher than values measured for ΣN_r at our site, and they found that deposition was mainly driven by aerodynamic resistance rather than by surface resistance, in particular during periods of high radiation. It shows that changes in the contribution of N_r species to ΣN_r lead to different deposition pathways.

4.3 Uncertainties in dry deposition estimates

Fluxes determined with the ~~eddy-covariance~~EC method are exposed to systematic and random errors. Systematic errors are related to the design of the measurement setup and the instruments, data processing steps including calibration, tilt correction, detrending, and corrections due to low and high-frequency attenuation (Wintjen et al., 2020), and advection fluxes originating preferentially from non-homogeneous surfaces. Uncertainties from the measurement setup were likely caused by an insufficient pump performance, issues in temperature stability of the TRANC and CLD, sensitivity loss of the CLD, and problems in the O_2 and CO supply. Therefore, regular maintenance and continuous observation of instrument performance parameters such as TRANC temperature and flow rate were made. With manual screening of measured half-hours and the recording of these parameters, low-quality half-hours could be effectively excluded from analysis. A basic assumption for the EC method is that the terrain needs to be flat, and the canopy height and density should be uniform (Burba, 2013). These site criteria are not perfectly fulfilled at our measurement site. The site is located in a low mountain range and tree density is rather sparse south of the flux tower. Such diverse terrain characteristics could lead to unwanted turbulent fluctuations (non-stationarity of time series), which introduce noise in the cross-covariance function.

Random errors are ~~mostly~~ related to turbulence sampling errors (Finkelstein and Sims, 2001; Hollinger and Richardson, 2005; Loescher et al., 2006). An inadequate sample size results in an incomplete sampling of large-scale eddies, which compromises the cross-covariance of the vertical wind and the scalar of interest. The method of Finkelstein and Sims (2001) allows to quantify the random error of the measured fluxes ($F_{\mathrm{unc,meas}}$). In order to determine the effect of the random flux error on the estimated dry deposition sums, we used the method proposed by Pastorello et al. (2020):

$$F_{\mathrm{unc,cum_i}} = \sqrt{\Sigma_i^n (F_{\mathrm{unc,meas_i}})^2} \tag{7}$$

Using Eq. (7), we determined an uncertainty of ~~11~~9 g N ha^{-1} a^{-1} for 2016/2017 and 21 g N ha^{-1} a^{-1} for 2017/2018 due to insufficient sampling of turbulent motion. The uncertainty related to u_* filtering is difficult to quantify since common approaches for estimating u_* thresholds, i.e. Moving Point Threshold (Reichstein et al., 2005) or Change Point ~~Dectection~~ Detection (Barr et al., 2013), are designed for CO_2. Applying these threshold detection algorithms to N_r species is not suggested since their exchange patterns are characterized by a higher variability for different time scales. The chosen u_* threshold of 0.1 cm s^{-1} should be interpreted as minimal filter to exclude periods of insufficient turbulence (for details see Zöll et al., 2019, Sec. 2.4). In combination with the MDV approach as gap-filling method, the applied threshold may lead to biased dry deposition sums. As seen in Fig. 11, the difference between dry deposition sums was within the error range of the dry deposition sum. Presumably, not only small fluxes were removed from the analysis by the u_*-filter.~~Figure 8 shows that large fluxes were observed at low turbulent conditions.~~ We further showed that the contribution of the water vapor correction was negligible. Brümmer et al. (2013) and Ammann et al. (2012) reported a low contribution of the correction to their observed TRANC fluxes.

The uncertainty related to gap-filling of a certain half-hour was determined by the standard error of the averaged flux, and their annual and seasonal uncertainties were determined by Eq. (7). Both random errors, the random uncertainty of Finkelstein and Sims (2001) and the uncertainty due to the MDV approach, are negligible. Presumably, systematic errors affected

the TRANC measurements at most. However, estimating a total systematic uncertainty is not possible since the contribution of individual systematic errors is not known and their quantification is difficult. ~~We calculated the uncertainties for the annual sums as standard error of the averaged flux, which is appropriate in case of the MDV method.~~Regarding the gap-filling technique, ~~W~~we showed that the results when applying the MDV method were independent of the applied micrometeorological ~~temperature, humidity, and precipitation~~ criteria. The differences in v_d to micrometeorology were observed for a limited time period of the year. During other months, we found no influence of micrometeorological parameters such as temperature, humidity, and ~~precipitation~~ wet/dry leaf surfaces on diurnal pattern of the ΣN_r fluxes. Thus, the dry deposition sums ~~were almost equal~~ exhibited no significant differences for the applied micrometeorological criteria. The difference between the estimated dry depositions for the measurements was likely related to the large deposition occurring in February 2018. ~~Presumably, the difference would have been even higher if flux measurements during the foliage period were available. It highlights the important role of radiation and the contribution of nitrogen compounds to the ΣN_r exchange at measurement site.~~

Using the MDV approach is recommended for gaps spanning over not more than a few days. Using statistical gap-filling approaches such as ~~LUT~~ look-up tables, ~~NLR~~ non-linear regression, or MDV (Falge et al., 2001) for longer gaps, is not suggested. Statistical methods like MDV assume a periodic variability with high auto-correlation of fluxes. This assumption is ~~mostly~~ valid for CO_2, which ha~~ve~~s a distinctive daily cycle. Reactive gases ~~mostly~~ do not exhibit a clearly predictable flux pattern. Their flux variability depends on micrometeorological conditions and their chemical and physical properties sometimes leading to instationarities in data time series. Gap-filling methods based on inferential modeling or artificial neural networks may be a further valuable option, especially for long-term gaps - if models would be available. Monthly averages estimated for each half-hour do not account for short-term deposition or emission events. Since 80% of measured half-hourly fluxes were deposition fluxes ~~we measured mostly ΣN_r deposition~~ at the measurement site, the applied gap-filling method for long-term gaps is somewhat justified. ~~Also, biases due to the usage of statistical methods can be eliminated, for example, the shown effect of the u_*-filter on MDV. However, exchange patterns of every N_r species, at least the most important ones such as NO, NO_2, HNO_3, NH_3, NH_4^+, and NO_3^- have to be accurately modeled. In case of NH_3, stomatal and cuticular exchange is well documented (see references in Sec. 2.4). Investigations on other nitrogen compounds are still needed. As mentioned in Sec. 2.4, there are significant uncertainties in compensation points of NO_2 and HNO_3.~~

The results of wet deposition have shown that dry deposition contributes approximately one third to the total deposition, which is comparable to previous nitrogen deposition estimates obtained by canopy budget models ~~results of canopy outflow measurements conducted~~ at the same site (Beudert and Breit, 2014). The comparison of TRANC measurements with ~~canopy outflow~~ nitrogen throughfall measurements will be shown the second part of this study. ~~Wet deposition results from both sampler types were almost similar. It shows that deposition of sedimenting organic and inorganic particles is not relevant at the site.~~ As shown in Table 1, differences between bulk and wet-only deposition were negligible. Small differences between TWD from wet-only and bulk measurements were related to the sedimentation of inorganic and organic dust particles or to dry deposition of NH_3 and HNO_3 (Staelens et al., 2005). The effects were not relevant for the annual nitrogen deposition at the measurement site. Estimated total N depositions were in the range of critical loads for *Picea abies* and *Fagus sylvatica* reaching from 10 to 15 kg N ha^{-1} a^{-1} and 10 to 20 kg N ha^{-1} a^{-1}, respectively (Bobbink and Hettelingh, 2011). Since the

forest stand consists to approximately 80% of Norway spruce in the footprint and the surrounding forest stand is predominated by Norway spruce, the critical load for the forest stand is probably closer to the values of *Picea abies*. It suggests that the forest is currently not in a critical state in relation atmospheric N input.

5 Conclusions

Our study is the first one presenting 2.5 years of flux measurements of total reactive atmospheric nitrogen (ΣN_r) measured with a custom-built converter called Total Reative Atmospheric nitrogen converter (TRANC) coupled to fast-response chemiluminescence detector (CLD) above a protected mixed forest.

A comparison of monthly averaged ΣN_r concentrations from the TRANC and DELTA (DEnuder for Long-Term Atmospheric sampling) and chemiluminescence measurements of ~~nitrogen monoxide~~ nitric oxide (NO) and nitrogen dioxide (NO_2) ~~measurements~~ showed a reasonable agreement in their seasonal patterns. On average, concentrations by the TRANC-CLD system were ~~slightly~~ higher by ~~(~~$\sim$ ~~0.3~~0.41 µg N m^{-3} ~~)~~ showing that the TRANC-CLD system can adequately measure ΣN_r concentrations. Differences could be related to higher oxidized nitrogen compounds, which are not detected by the DELTA system, an insufficient data coverage of TRANC measurements during the exposure periods, the presumably lower aerosol cut-off size of DELTA ~~to a degrading of the denuder surfaces due to enviromental influences~~, issues in the conversion efficiency of the TRANC, etc.. Only nitrogen oxides (NO_x) and ammonia (NH_3) showed distinct seasonal changes in their concentrations whereas ΣN_r concentration remained stable through the year. NO_x exhibited highest concentrations during winter, NH_3 during spring and summer. In total, the sum of both gases had a mean contribution of 7~~2~~1.0% to the ΣN_r concentrations highlighting their importance for the observed ΣN_r exchange pattern.

~~We observed mostly deposition~~ ~~d~~During 2.5 years of flux measurements~~.~~, ~~M~~median deposition ranged from -15 to -5 ng N m^{-2} s^{-1}. Deposition velocities followed the diurnal pattern of the fluxes, and median values ranged between 0.2 and 0.5 cm s^{-1}. Highest deposition was observed during the timeframe of high incident radiation, in particular from May to September. Our findings suggest that seasonal changes in the concentrations of the ΣN_r compounds, ~~and~~ global radiation(R_g), and micrometerological controls correlated with R_g were most likely responsible for the observed pattern of v_d. ~~Within periods of high incident radiation, e.g. f~~From May to September, deposition velocity (v_d) was elevated in presence of dry leaf surfaces, at a low humidity level, and at higher temperatures. No relationship between ΣN_r concentration and corresponding deposition velocities was found. These findings are exclusively related to the composition of the ΣN_r flux at the measurement site. Comparing results to other sites is challenging due to a different mixture of compounds in the ΣN_r flux. Still, a comparison of modeled and measured deposition velocities of ΣN_r the latter determined by inferential modeling with regard to micrometeorological controls could hint on deficits in deposition modeling. ~~, and during no precipitation. Calculated effective canopy resistance ($R_{c,eff}$) was slightly lower at lower humidity and higher concentrations of ΣN_r. Aerodynamic and boundary-layer resistances showed no significant contribution to v_d implicating a low influence of turbulent processes on the ΣN_r exchange during those times. During rain, v_d was greatly reduced or even negative resulting in emission of ΣN_r. During the year, uptake pathways for ΣN_r changed depending on the presence of individual ΣN_r compounds and micrometeorological conditions.~~

~~Stomatal deposition seemed to be prevailing mostly from May to September. During the rest of the year, cuticular, soil, or turbulent processes appeared to be most responsible for the ΣN_r exchange.~~

From June 2016 to May 2017 and June 2017 to May 2018, we estimated dry deposition sums of 3.8~~$\pm$0.8 kg N ha^{-1}~~ and 4.~~10$\pm$1.13~~ kg N ha^{-1} a^{-1}, respectively. No significant influence of micrometeorological parameters on estimated dry depositions sums was found. ~~Influences of temperature, humidity, friction velocity, or precipitation were in the uncertainty ranges of the estimated dry depositions sums.~~ Using ~~other~~ gap-filling approaches based on inferential modeling ~~or artificial neural networks~~ for long-term gaps, is an ~~valuable~~ option which we investigate in the companion paper. ~~Also, biases related to the usage friction velocity thresholds, which potentially removes lower fluxes from the analysis and therefore affects data-driven gap-filling methods, will be avoided. Mean total wet deposition were 8.0 kg N ha^{-1} and 6.8 kg N ha^{-1} for the timeframes 2016/2017 and 2017/2018, respectively. The reduction in wet deposition was most likely related to the reduced precipitation in 2018.~~ In the first and second measurement year, we determined ~~11.8~~12.2 ~~kg N ha^{-1}~~ and 10.9 kg N ha^{-1} a^{-1} as total nitrogen deposition, respectively. A review of published critical loads show that estimated total deposition were at the lower end of the critical load range.

The data set presented in this study provides an unique opportunity for a comparison to deposition models. In the second part of this paper, a comparison of the acquired dataset to the performance of deposition models will be made. Modeled exchange dynamics will be discussed in regard to their biophysical controlling factors. Annual N budgets from measurements, modeling approaches using in-situ and modeled input parameters, and canopy outflow measurements will be shown.

Code and data availability. All data are available upon request from the first author of this study (pascal.wintjen@thuenen.de). Also, Python 3.7 code for flux data analysis can be requested from the first author.

Author contributions. PW, FS, and CB conceived the study. PW wrote the manuscript, carried out the measurements at the forest site, and conducted flux data analysis and interpretation. FS evaluated meteorological measurements. FS and MS provided insights in interpreting deposition velocities ~~and resistances~~. BB performed the wet deposition analysis. CB installed the flux tower equipment and gave scientific advise to the overall data analysis and interpretation. All authors discussed the results and FS, MS, BB, and CB contributed to the manuscript.

Competing interests. The authors declare that they have no conflict of interest.

Acknowledgements. Funding by the German Environment Agency (UBA) (project FORESTFLUX, support code FKZ 3715512110) and by the German Federal Ministry of Education and Research (BMBF) within the framework of the Junior Research Group NITROSPHERE (support code FKZ 01LN1308A) is greatly acknowledged. We thank Undine Zöll for scientific and logistical help, Jeremy Rüffer and Jean-Pierre Delorme for excellent technical support, Ute Tambor, Andrea Niemeyer, and Dr. Daniel Ziehe for conducting laboratory analyses of

denuder and filter samples, and the Bavarian Forest Nationalpark (NPBW) Administration, namely Wilhelm Breit and Ludwig Höcker for technical and logistical support at the measurement site.

References

Ammann, C., Wolff, V., Marx, O., Brümmer, C., and Neftel, A.: Measuring the biosphere-atmosphere exchange of total reactive nitrogen by eddy covariance, Biogeosciences, 9, 4247–4261, https://doi.org/10.5194/bg-9-4247-2012, http://www.biogeosciences.net/9/4247/2012/, 2012.

Aubinet, M., Vesala, T., and Papale, D., eds.: Eddy Covariance: A Practical Guide to Measurement and Data Analysis, Springer Science+Business Media B.V. 2012, Dordrecht, The Netherlands, 2012.

Barr, A., Richardson, A., Hollinger, D., Papale, D., Arain, M., Black, T., Bohrer, G., Dragoni, D., Fischer, M., Gu, L., Law, B., Margolis, H., McCaughey, J., Munger, J., Oechel, W., and Schaeffer, K.: Use of change-point detection for friction–velocity threshold evaluation in eddy-covariance studies, Agricultural and Forest Meteorology, 171-172, 31–45, https://doi.org/https://doi.org/10.1016/j.agrformet.2012.11.023, https://www.sciencedirect.com/science/article/pii/S0168192312003607, 2013.

Beudert, B. and Breit, W.: Integrated Monitoring Programm an der Meßstelle Forellenbach im Nationalpark Bayerischer Wald, Untersuchungen zu Prozessen und Räumen der Hochwasserbildung im Forellenbachgebiets, Förderkennzeichen 351 01 012. Nationalparkverwaltung Bayerischer Wald, Sachgebiet IV, techreport, Umweltbundesamt, http://docplayer.org/80741933-Integrated-monitoring-programm-an-der-messstelle-forellenbach-im-nationalpark-bayerischer-wald.html, 2008.

Beudert, B. and Breit, W.: Integrated Monitoring Programm an der Meßstelle Forellenbach im Nationalpark Bayerischer Wald, Untersuchungen zum Stickstoffeintrag und zum wassergebundenen Stickstoffhaushalt des Forellenbachgebiets, Förderkennzeichen 351 01 012. Nationalparkverwaltung Bayerischer Wald, Sachgebiet IV, techinal report, Umweltbundesamt, Dessau-Roßlau, Germany, http://www.umweltbundesamt.de/sites/default/files/medien/370/dokumente/ece_im_forellenbach_berichtsjahr_2009.pdf, 2010.

Beudert, B. and Breit, W.: Kronenraumbilanzen zur Abschätzung der Stickstoffgesamtdeposition in Waldökosysteme des Nationalparks Bayerischer Wald, techninal report, Umweltbundesamt, Dessau-Roßlau, Germany, https://www.umweltbundesamt.de/sites/default/files/medien/370/dokumente/kronenraumbilanzen_stickstoffgesamtdeposition_nationalpark_bayerisches_wald_-_berichtsjahr_2013_im_forellenbach.pdf, 2014.

Beudert, B., Bernsteinová, J., Premier, J., and Bässler, C.: Natural disturbance by bark beetle offsets climate change effects on streamflow in headwater catchments of the Bohemian Forest, Silva Gabreta, 24, 21–45, https://www.npsumava.cz/wp-content/uploads/2019/06/2_sg_24_beudertetal.pdf, 2018.

Bokhorst, S., Metcalfe, D. B., and Wardle, D. A.: Reduction in snow depth negatively affects decomposers but impact on decomposition rates is substrate dependent, Soil Biology and Biochemistry, 62, 157–164, https://doi.org/j.soilbio.2013.03.016, https://www.sciencedirect.com/science/article/pii/S0038071713001041, 2013.

Breuninger, C., Meixner, F. X., and Kesselmeier, J.: Field investigations of nitrogen dioxide (NO_2) exchange between plants and the atmosphere, Atmospheric Chemistry and Physics, 13, 773–790, https://doi.org/10.5194/acp-13-773-2013, https://acp.copernicus.org/articles/13/773/2013/, 2013.

Brümmer, C., Marx, O., Kutsch, W., Ammann, C., Wolff, V., Flechard, C. R., and Freibauer, A.: Fluxes of total reactive atmospheric nitrogen (ΣN_r) using eddy covariance above arable land, Tellus B: Chemical and Physical Meteorology, 65, 19 770, https://doi.org/10.3402/tellusb.v65i0.19770, https://doi.org/10.3402/tellusb.v65i0.19770, 2013.

Burba, G.: Eddy Covariance Method for Scientific, Industrial, Agricultural and Regulatory Applications: A Field Book on Measuring Ecosystem Gas Exchange and Areal Emission Rates, LI-COR Biosciences, Lincoln, Nebraska, USA, 2013.

Civerolo, K. L. and Dickerson, R. R.: Nitric oxide soil emissions from tilled and untilled cornfields, Agricultural and Forest Meteorology, 90, 307–311, https://doi.org/10.1016/S0168-1923(98)00056-2, http://www.sciencedirect.com/science/article/pii/S0168192398000562, 1998.

Aubinet, M., Grelle, A., Ibrom, A., Rannik, U., Moncrieff, J., Foken, T., Kowalski, A. S., Martin, P. H., Berbigier, P., Bernhofer, C., Clement, R., Elbers, J., Granier, A., Grünwald, T., Morgenstern, K., Pilegaard, K., Rebmann, C., Snijders, W., Valentini, R., and Vesala, T.: Estimates of the Annual Net Carbon and Water Exchange of Forests: The EUROFLUX Methodology, vol. 30 of *Advances in Ecological Research*, pp. 113–175, Academic Press, https://doi.org/10.1016/S0065-2504(08)60018-5, http://www.sciencedirect.com/science/article/pii/S0065250408600185, 1999.

Heiskanen, J., Brümmer, C., Buchmann, N., Calfapietra, C., Chen, H., Gielen, B., Gkritzalis, T., Hammer, S., Hartman, S., Herbst, M., Janssens, I., Jordan, A., Juurola, E., Karstens, U., Kasurinen, V., Kruijt, B., Lankreijer, H., Levin, I., Linderson, M.-L., Loustau, D., Merbold, L., Lund Myhre, C., Papale, D., Pavelka, M., Pilegaard, K., Ramonet, M., Rebmann, C., Rinne, J., Rivier, L., Saltikoff, E., Sanders, R., Steinbacher, M., Steinhoff, T., Watson, A., Vermeulen, A., Vesala, T., Vítková, G., and Kutsch, W.: The Integrated Carbon Observation System in Europe, Bulletin of the American Meteorological Society, pp. 1 – 54, https://doi.org/10.1175/BAMS-D-19-0364.1, https://journals.ametsoc.org/view/journals/bams/aop/BAMS-D-19-0364.1/BAMS-D-19-0364.1.xml, 2021.

Lee, T., Yu, X.-Y., Ayres, B., Kreidenweis, S. M., Malm, W. C., and Collett, J. L.: Observations of fine and coarse particle nitrate at several rural locations in the United States, Atmospheric Environment, 42, 2720–2732, https://doi.org/10.1016/j.atmosenv.2007.05.016, https://www.sciencedirect.com/science/article/pii/S1352231007004621, vienna Visibility Conference 2006, 2008.

Moncrieff, J. B., Massheder, J. M., deBruin, H., Elbers, J., Friborg, T., Heusinkveld, B., Kabat, P., Scott, S., Soegaard, H., and Verhoef, A.: A system to measure surface fluxes of momentum, sensible heat, water vapour and carbon dioxide, Journal of Hydrology, 188, 589–611, https://doi.org/10.1016/S0022-1694(96)03194-0, http://www.sciencedirect.com/science/article/pii/S0022169496031940, 1997.

Putaud, J.-P., Van Dingenen, R., Alastuey, A., Bauer, H., Birmili, W., Cyrys, J., Flentje, H., Fuzzi, S., Gehrig, R., Hansson, H., Harrison, R., Herrmann, H., Hitzenberger, R., Hüglin, C., Jones, A., Kasper-Giebl, A., Kiss, G., Kousa, A., Kuhlbusch, T., Löschau, G., Maenhaut, W., Molnar, A., Moreno, T., Pekkanen, J., Perrino, C., Pitz, M., Puxbaum, H., Querol, X., Rodriguez, S., Salma, I., Schwarz, J., Smolik, J., Schneider, J., Spindler, G., ten Brink, H., Tursic, J., Viana, M., Wiedensohler, A., and Raes, F.: A European aerosol phenomenology – 3: Physical and chemical characteristics of particulate matter from 60 rural, urban, and kerbside sites across Europe, Atmospheric Environment, 44, 1308–1320, https://doi.org/https://doi.org/10.1016/j.atmosenv.2009.12.011, https://www.sciencedirect.com/science/article/pii/S1352231009010358, 2010.

Schaap, M., Müller, K., and ten Brink, H.: Constructing the European aerosol nitrate concentration field from quality analysed data, Atmospheric Environment, 36, 1323–1335, https://doi.org/https://doi.org/10.1016/S1352-2310(01)00556-8, https://www.sciencedirect.com/science/article/pii/S1352231001005568, 2002.

Schaap, M., Spindler, G., Schulz, M., Acker, K., Maenhaut, W., Berner, A., Wieprecht, W., Streit, N., Müller, K., Brüggemann, E., Chi, X., Putaud, J.-P., Hitzenberger, R., Puxbaum, H., Baltensperger, U., and ten Brink, H.: Artefacts in the sampling of nitrate studied in the "INTERCOMP" campaigns of EUROTRAC-AEROSOL, Atmospheric Environment, 38, 6487–6496, https://doi.org/https://doi.org/10.1016/j.atmosenv.2004.08.026, https://www.sciencedirect.com/science/article/pii/S135223100400771X, contains Special Issue section on Measuring the composition of Particulate Matter in the EU, 2004.

Baldocchi, D., Falge, E., Gu, L., Olson, R., Hollinger, D., Running, S., Anthoni, P., Bernhofer, C., Davis, K., Evans, R., Fuentes, J., Goldstein, A., Katul, G., Law, B., Lee, X., Malhi, Y., Meyers, T., Munger, W., Oechel, W., Paw, K. T., Pilegaard, K., Schmid, H. P., Valentini, R., Verma, S., Vesala, T., Wilson, K., and Wofsy, S.: FLUXNET: A New Tool to Study the Temporal and Spatial Variability of Ecosys-

tem–Scale Carbon Dioxide, Water Vapor, and Energy Flux Densities, Bulletin of the American Meteorological Society, 82, 2415–2434, https://doi.org/10.1175/1520-0477(2001)082<2415:Fantts>2.3.Co;2, 2001.

Baldocchi, D. D.: Assessing the eddy covariance technique for evaluating carbon dioxide exchange rates of ecosystems: past, present and future, Global Change Biology, 9, 479–492, https://doi.org/10.1046/j.1365-2486.2003.00629.x, https://onlinelibrary.wiley.com/doi/pdf/10.1046/j.1365-2486.2003.00629.x, 2003.

Bobbink, R. and Hettelingh, J.-P.: Review and revision of empirical critical loads and dose-response relationships, Tech. Rep. RIVM report 680359002, National Institute for Public Health and the Environment (RIVM), https://www.rivm.nl/bibliotheek/rapporten/680359002.pdf, last access: 31 October 2021, 2011.

Donateo, A. and Contini, D.: Correlation of Dry Deposition Velocity and Friction Velocity over Different Surfaces for PM2.5 and Particle Number Concentrations, Advances in Meteorology, 2014, 1–12, https://doi.org/10.1155/2014/760393, https://doi.org/10.1155/2014/760393, 2014.

Erisman, J. W., Mennen, M. G., Fowler, D., Flechard, C. R., Spindler, G., Grüner, A., Duyzer, J. H., Ruigrok, W., and Wyers, G. P.: Towards development of a deposition monitoring network for air pollution in Europe, resreport Report no. 722108015, RIVM, the Netherlands, https://rivm.openrepository.com/bitstream/handle/10029/10432/722108015.pdf;jsessionid=532211C11FE7D0487F070927B24AE8ED?sequence=1, last access: 31 October 2021, 1996.

Gallagher, M., Beswick, K., Duyzer, J., Westrate, H., Choularton, T., and Hummelshøj, P.: Measurements of aerosol fluxes to speulder forest using a micrometeorological technique, Atmospheric Environment, 31, 359–373, https://doi.org/https://doi.org/10.1016/S1352-2310(96)00057-X, https://www.sciencedirect.com/science/article/pii/S135223109600057X, 1997.

Ge, X., Schaap, M., Kranenburg, R., Segers, A., Reinds, G. J., Kros, H., and de Vries, W.: Modeling atmospheric ammonia using agricultural emissions with improved spatial variability and temporal dynamics, Atmospheric Chemistry and Physics, 20, 16 055–16 087, https://doi.org/10.5194/acp-20-16055-2020, https://acp.copernicus.org/articles/20/16055/2020/, 2020.

Ibrom, A., Dellwick, E., Flyvbjerg, H., Jensen, N. O., and Pilegaard, K.: Strong low-pass filtering effects on water vapour flux measurements with closed-path eddy correlation systems, Agricultural and Forest Meteorology, 147, 140–156, https://doi.org/10.1016/j.agrformet.2007.07.007, http://www.sciencedirect.com/science/article/pii/S0168192307001888, 2007.

Kundu, S., Kawamura, K., and Lee, M.: Seasonal variation of the concentrations of nitrogenous species and their nitrogen isotopic ratios in aerosols at Gosan, Jeju Island: Implications for atmospheric processing and source changes of aerosols, Journal of Geophysical Research: Atmospheres, 115, https://doi.org/10.1029/2009JD013323, https://agupubs.onlinelibrary.wiley.com/doi/abs/10.1029/2009JD013323, 2010.

Lavi, A., Farmer, D., Segre, E., Moise, T., Rotenberg, E., Jimenez, J. L., and Rudich, Y.: Fluxes of Fine Particles Over a Semi-Arid Pine Forest: Possible Effects of a Complex Terrain, Aerosol Science and Technology, 47, 906–915, https://doi.org/10.1080/02786826.2013.800940, https://doi.org/10.1080/02786826.2013.800940, 2013.

Lenshow, D. H. and Raupach, M. R.: The attenuation of fluctuations in scalar concentrations through sampling tubes, Journal of Geophysical Research, 96, 15 259–15 268, https://doi.org/10.1029/91JD01437, https://agupubs.onlinelibrary.wiley.com/doi/abs/10.1029/91JD01437, 1991.

Massman, W. J.: The attenuation of concentration fluctuations in turbulent flow through a tube, Journal of Geophysical Research, 96, 15 269–15 274, https://doi.org/10.1029/91JD01514, https://agupubs.onlinelibrary.wiley.com/doi/abs/10.1029/91JD01514, 1991.

Munger, J. W., Fan, S.-M., Bakwin, P. S., Goulden, M. L., Goldstein, A. H., Colman, A. S., and Wofsy, S. C.: Regional budgets for nitrogen oxides from continental sources: Variations of rates for oxidation and deposition with season and distance from source regions, Journal of

Geophysical Research: Atmospheres, 103, 8355–8368, https://doi.org/https://doi.org/10.1029/98JD00168, https://agupubs.onlinelibrary.wiley.com/doi/abs/10.1029/98JD00168, 1998.

Neirynck, J., Kowalski, A. S., Carrara, A., Genouw, G., Berghmans, P., and Ceulemans, R.: Fluxes of oxidised and reduced nitrogen above a mixed coniferous forest exposed to various nitrogen emission sources, Environmental Pollution, 149, 31–43, https://doi.org/10.1016/j.envpol.2006.12.029, https://www.ncbi.nlm.nih.gov/pubmed/17337104, 2007.

Schwarz, J., Cusack, M., Karban, J., Chalupníčková, E., Havránek, V., Smolík, J., and Ždímal, V.: PM2.5 chemical composition at a rural background site in Central Europe, including correlation and air mass back trajectory analysis, Atmospheric Research, 176-177, 108–120, https://doi.org/https://doi.org/10.1016/j.atmosres.2016.02.017, https://www.sciencedirect.com/science/article/pii/S0169809516300345, 2016.

Staelens, J., De Schrijver, A., Van Avermaet, P., Genouw, G., and Verhoest, N.: A comparison of bulk and wet-only deposition at two adjacent sites in Melle (Belgium), Atmospheric Environment, 39, 7 – 15, https://doi.org/https://doi.org/10.1016/j.atmosenv.2004.09.055, https://www.sciencedirect.com/science/article/pii/S135223100400946X, 2005.

Tang, Y. S., Cape, J. N., Braban, C. F., Twigg, M. M., Poskitt, J., Jones, M. R., Rowland, P., Bentley, P., Hockenhull, K., Woods, C., Leaver, D., Simmons, I., van Dijk, N., Nemitz, E., and Sutton, M. A.: Development of a new model DELTA sampler and assessment of potential sampling artefacts in the UKEAP AGANet DELTA system: summary and technical report, Tech. rep., London, https://uk-air.defra.gov.uk/library/reports?report_id=861, last access: 31 October 2021, 2015.

Tang, Y. S., Flechard, C. R., Dämmgen, U., Vidic, S., Djuricic, V., Mitosinkova, M., Uggerud, H. T., Sanz, M. J., Simmons, I., Dragosits, U., Nemitz, E., Twigg, M., van Dijk, N., Fauvel, Y., Sanz, F., Ferm, M., Perrino, C., Catrambone, M., Leaver, D., Braban, C. F., Cape, J. N., Heal, M. R., and Sutton, M. A.: Pan-European rural monitoring network shows dominance of NH_3 gas and NH_4NO_3 aerosol in inorganic atmospheric pollution load, Atmospheric Chemistry and Physics, 21, 875–914, https://doi.org/10.5194/acp-21-875-2021, https://acp.copernicus.org/articles/21/875/2021/, 2021.

Yuvaraj, S., Fan-Yuan, L., Tsong-Huei, C., and Chuin-Tih, Y.: Thermal Decomposition of Metal Nitrates in Air and Hydrogen Environments, The Journal of Physical Chemistry B, 107, 1044–1047, https://doi.org/10.1021/jp026961c, 2003.

~~A. Remde and F. Slemr and R. Conrad~~: ~~Microbial production and uptake of nitric oxide in soil~~, ~~FEMS Microbiology Letters~~, ~~62~~, ~~221–230~~, https://doi.org/~~https://doi.org/10.1016/0378-1097(89)90246-2~~, https://www.sciencedirect.com/science/article/pii/0378109789902462, 1989.

~~Alberto Rondón and Lennart Granat~~: ~~Studies on the dry deposition of NO2 to coniferous species at low NO2 concentrations~~, ~~Tellus B: Chemical and Physical Meteorology~~, ~~46~~, ~~339–352~~, https://doi.org/~~10.3402/tellusb.v46i5.15809~~, https://doi.org/10.3402/tellusb.v46i5.15809, 1994.

~~Behrendt, T. and Veres, P. R. and Ashuri, F. and Song, G. and Flanz, M. and Mamtimin, B. and Bruse, M. and Williams, J. and Meixner, F. X.~~: ~~Characterisation of NO production and consumption: new insights by an improved laboratory dynamic chamber technique~~, ~~Biogeosciences~~, ~~11~~, ~~5463–5492~~, https://doi.org/~~10.5194/bg-11-5463-2014~~, https://bg.copernicus.org/articles/11/5463/2014/, 2014.

~~Bok Haeng Baek and Viney P. Aneja and Quansong Tong~~: ~~Chemical coupling between ammonia, acid gases, and fine particles~~, ~~Environmental Pollution~~, ~~129~~, ~~89–98~~, https://doi.org/~~https://doi.org/10.1016/j.envpol.2003.09.022~~, https://www.sciencedirect.com/science/article/pii/S0269749103003816, 2004.

~~Burkhardt, J. and Peters, K. and Crossley, A.~~: ~~The presence of structural surface waxes on coniferous needles affects the pattern of dry deposition of fine particles~~, ~~Journal of Experimental Botany~~ , ~~46~~, ~~823–831~~, 1995.

David Fowler and Chris Flechard and Ute Skiba and Mhairi Coyle and J. Neil Cape: The Atmospheric Budget of Oxidized Nitrogen and Its Role in Ozone Formation and Deposition, The New Phytologist, 139, 11–23, http://www.jstor.org/stable/2588244, 1998.

Erisman, J. W. and Van Pul, A. and Wyers, P.: Parametrization of surface resistance for the quantification of atmospheric deposition of acidifying pollutants and ozone, Atmospheric Environment, 28, 2595–2607, https://doi.org/10.1016/1352-2310(94)90433-2, http://www.sciencedirect.com/science/article/pii/1352231094904332, 1994.

Farquhar, Graham D. and Firth, Peter M. and Wetselaar, Robbert and Weir, Brian: On the Gaseous Exchange of Ammonia between Leaves and the Environment: Determination of the Ammonia Compensation Point, Plant Physiology, 66, 710–714, https://doi.org/10.1104/pp.66.4.710, http://www.plantphysiol.org/content/66/4/710, 1980.

Flechard, C. R. and Fowler, D. and Sutton, M. A. and Cape, J. N.: A dynamic chemical model of bi-directional ammonia exchange between semi-natural vegetation and the atmosphere, Quarterly Journal of the Royal Meteorological Society, 125, 2611–2641, https://doi.org/10.1002/qj.49712555914, https://rmets.onlinelibrary.wiley.com/doi/abs/10.1002/qj.49712555914, 1999.

Gessler, Arthur and Rienks, Michael and Rennenberg, Heinz: NH3 and NO2 fluxes between beech trees and the atmosphere – correlation with climatic and physiological parameters, New Phytologist, 147, 539–560, https://doi.org/10.1046/j.1469-8137.2000.00712.x, http://doi.wiley.com/10.1046/j.1469-8137.2000.00712.x, 2000.

Gessler, Arthur and Rienks, Michael and Rennenberg, Heinz: Stomatal uptake and cuticular adsorption contribute to dry deposition of NH_3 and NO_2 to needles of adult spruce (Picea abies) trees, New Phytologist, 156, 179–194, https://doi.org/10.1046/j.1469-8137.2002.00509.x, https://nph.onlinelibrary.wiley.com/doi/abs/10.1046/j.1469-8137.2002.00509.x, 2002.

I.G. Chaparro-Suarez and F.X. Meixner and J. Kesselmeier: Nitrogen dioxide (NO2) uptake by vegetation controlled by atmospheric concentrations and plant stomatal aperture, Atmospheric Environment, 45, 5742–5750, https://doi.org/10.1016/j.atmosenv.2011.07.021, https://www.sciencedirect.com/science/article/pii/S1352231011007461, 2011.

J.L. Durham and L. Stockburger: Nitric acid-air diffusion coefficient: Experimental determination, Atmospheric Environment (1967), 20, 559–563, https://doi.org/0004-6981(86)90098-3, https://www.sciencedirect.com/science/article/pii/0004698186900983, 1986.

Ludwig, Jörg and Meixner, Franz and Vogel, Bernhard and Förstner, Jochen: Soil-air exchange of nitric oxide: An overview of processes, environmental factors, and modeling studies, Biogeochemistry, 52, 225–257, https://doi.org/10.1023/A:1006424330555, 2001.

Massad, R. S. and Nemitz, E. and Sutton, M. A.: Review and parameterisation of bi-directional ammonia exchange between vegetation and the atmosphere, Atmospheric Chemistry and Physics, 10, 10 359–10 386, https://doi.org/10.5194/acp-10-10359-2010, https://www.atmos-chem-phys.net/10/10359/2010/, 2010.

Massman, W. J.: A review of the molecular diffusivities of H2O, CO2, CH4, CO, O3, SO2, NH3, N2O, NO, and NO2 in air, O2 and N2 near STP, Atmospheric Environment, 32, 1111–1127, https://doi.org/10.1016/s1352-2310(97)00391-9, 1998.

Moffat, Antje M. and Beckstein, Clemes and Churkina, Galina and Mund, Martina and Heimann, Martin: Characterization of ecosystem responses to climatic controls using artificial neural networks, Global Change Biology, 16, 2737–2749, https://doi.org/j.1365-2486.2010.02171.x, https://onlinelibrary.wiley.com/doi/abs/10.1111/j.1365-2486.2010.02171.x, 2010.

Neirynck, J. and Ceulemans, R.: Bidirectional ammonia exchange above a mixed coniferous forest, NEnvironmental Pollution, N154, N424–38, https://doi.org/N10.1016/j.envpol.2007.11.030, https://www.ncbi.nlm.nih.gov/pubmed/18258346, 2008.

Nemitz, E. and Milford, C. and Sutton, M. A.: A two-layer canopy compensation point model for describing bi-directional biosphere-atmosphere exchange of ammonia, Quarterly Journal of the Royal Meteorological Society, 127, 815–833, https://doi.org/10.1002/qj.49712757306, https://rmets.onlinelibrary.wiley.com/doi/abs/10.1002/qj.49712757306, 2001.

Nemitz, E. and Sutton, M. A. and Schjoerring, J. K. and Husted, S. and Wyers, G. P.: Resistance modelling of ammonia exchange over oilseed rape, Agricultural and Forest Meteorology, 105, 405–425, https://doi.org/10.1016/S0168-1923(00)00206-9, http://www.sciencedirect.com/science/article/pii/S0168192300002069, 2000.

Nemitz, E. and Sutton, M. A. and Wyers, G. P. and Jongejan, P. A. C.: Gas-particle interactions above a Dutch heathland: I. Surface exchange fluxes of NH_3, SO_2, HNO_3 and HCl, Atmospheric Chemistry and Physics, 4, 989–1005, https://doi.org/10.5194/acp-4-989-2004, https://www.atmos-chem-phys.net/4/989/2004/, 2004.

Remde, Armin and Conrad, Ralf: Role of nitrification and denitrification for NO metabolism in soil, Biogeochemistry, 12, 189–205, https://doi.org/110.1007/BF00002607, https://doi.org/10.1007/BF00002607, 1993.

Schindlbacher, A. and Zechmeister-Boltenstern, S. and Butterbach-Bahl, K.: Effects of soil moisture and temperature on NO, NO2, and N2O emissions from European forest soils, Journal of Geophysical Research-Atmospheres, 109, 1–12, https://doi.org/10.1029/2004jd004590, https://agupubs.onlinelibrary.wiley.com/doi/abs/10.1029/2004JD004590, 2004.

Schrader, F. and Brümmer, C. and Flechard, C. R. and Wichink Kruit, R. J. and van Zanten, M. C. and Zöll, U. and Hensen, A. and Erisman, J. W.: Non-stomatal exchange in ammonia dry deposition models: comparison of two state-of-the-art approaches, Atmospheric Chemistry and Physics, 16, 13 417–13 430, https://doi.org/10.5194/acp-16-13417-2016, https://www.atmos-chem-phys.net/16/13417/2016/, 2016.

Sparks, J. P. and Monson, R. K. and Sparks, K. L. and Lerdau, M.: Leaf uptake of nitrogen dioxide (NO2) in a tropical wet forest: implications for tropospheric chemistry, Oecologia, 127, 214–221, https://doi.org/10.1007/s004420000594, https://www.ncbi.nlm.nih.gov/pubmed/24577652, 2001.

Squizzato, S. and Masiol, M. and Brunelli, A. and Pistollato, S. and Tarabotti, E. and Rampazzo, G. and Pavoni, B.: Factors determining the formation of secondary inorganic aerosol: a case study in the Po Valley (Italy), Atmospheric Chemistry and Physics, 13, 1927–1939, https://doi.org/10.5194/acp-13-1927-2013, https://acp.copernicus.org/articles/13/1927/2013/, 2013.

Sutton, M. A. and Asman, W. A. H. and Schjorring, J. K.: Dry Deposition of Reduced Nitrogen, Tellus Series B-Chemical and Physical Meteorology, 46, 255–273, https://doi.org/10.1034/j.1600-0889.1994.t01-2-00002.x, https://onlinelibrary.wiley.com/doi/abs/10.1034/j.1600-0889.1994.t01-2-00002.x, 1994.

Sutton, M. A. and Burkhardt, J. K. and Guerin, D. and Nemitz, E. and Fowler, D.: Development of resistance models to describe measurements of bi-directional ammonia surface–atmosphere exchange, Atmospheric Environment, 32, 473–480, https://doi.org/10.1016/s1352-2310(97)00164-7, http://www.sciencedirect.com/science/article/pii/S1352231097001647http://linkinghub.elsevier.com/retrieve/pii/S1352231097001647, 1998.

Sutton, M. A and Schjorring, J. K. and Wyers, G. P. and Duyzer, J. H. and Ineson, P. and Powlson, D. S.: Plant—atmosphere exchange of ammonia, Philosophical Transactions of the Royal Society of London. Series A: Physical and Engineering Sciences, 351, 261–278, https://doi.org/10.1098/rsta.1995.0033, http://rsta.royalsocietypublishing.org/cgi/doi/10.1098/rsta.1995.0033, 1995.

Tang, Y. S. and Flechard, C. R. and Dämmgen, U. and Vidic, S. and Djuricic, V. and Mitosinkova, M. and Uggerud, H. T. and Sanz, M. J. and Simmons, I. and Dragosits, U. and Nemitz, E. and Twigg, M. and van Dijk, N. and Fauvel, Y. and Sanz-Sanchez, F. and Ferm, M. and Perrino, C. and Catrambone, M. and Leaver, D. and Braban, C. F. and Cape, J. N. and Heal, M. R. and Sutton, M. A.: Pan-European rural atmospheric monitoring network shows dominance of NH_3 gas and NH_4NO_3 aerosol in inorganic pollution load, Atmospheric Chemistry and Physics Discussions, 2020, 1–61, https://doi.org/10.5194/acp-2020-275, https://acp.copernicus.org/preprints/acp-2020-275/, 2020.

Tarnay, L. W. and Gertler, A. and Taylor, G. E.: The use of inferential models for estimating nitric acid vapor deposition to semi-arid coniferous forests, Atmospheric Environment, 36, 3277–3287, https://doi.org/10.1016/S1352-2310(02)00303-5, http://www.sciencedirect.com/science/article/pii/S1352231002003035, 2002.

Teklemmariam, Thomas and Sparks, Jed: Leaf fluxes of NO and NO2 in four herbaceous plant species: The role of ascorbic acid, Atmospheric Environment, 40, 2235–2244, https://doi.org/10.1016/j.atmosenv.2005.12.010, 2006.

Thoene, Barbara and Schröder, Peter and Papen, Hans and Egger, Alfred and Rennenberg, Heinz: Absorption of atmospheric NO2 by spruce (Picea abies L. Karst.) trees, New Phytologist, 117, 575–585, https://doi.org/https://doi.org/10.1111/j.1469-8137.1991.tb00962.x, https://nph.onlinelibrary.wiley.com/doi/abs/10.1111/j.1469-8137.1991.tb00962.x, 1991.

Wichink Kruit, R. J. and Aben, J. and de Vries, W. and Sauter, F. and van der Swaluw, E. and van Zanten, M. C. and van Pul, W. A. J.: Modelling trends in ammonia in the Netherlands over the period 1990–2014, Atmospheric Environment, 154, 20–30, https://doi.org/10.1016/j.atmosenv.2017.01.031, https://www.sciencedirect.com/science/article/pii/S1352231017300316, 2017.

Wichink Kruit, R. J. and van Pul, W. A. J. and Sauter, F. J. and van den Broek, M. and Nemitz, E. and Sutton, M. A. and Krol, M. and Holtslag, A. A. M.: Modeling the surface–atmosphere exchange of ammonia, Atmospheric Environment, 44, 945–957, https://doi.org/10.1016/j.atmosenv.2009.11.049, http://www.sciencedirect.com/science/article/pii/S1352231009010346, 2010.

Dämmgen, U., Thöni, L., Lumpp, R., Gilke, K., Seitler, E., and Bullinger, M.: Feldexperiment zum Methodenvergleich von Ammoniak- und Ammonium-Konzentrationsmessungen in der Umgebungsluft, 2005 bis 2008 in Braunschweig, vol. 337 of *Landbauforschung : Sonderheft*, Johann Heinrich von Thünen-Institut, Braunschweig, https://www.openagrar.de/receive/timport_mods_00006160, jahresberichtskategorie: 10-M4;10-3, 2010.

Delany, A. C., Fitzjarrald, D. R., Lenschow, D. H., Pearson, R., Wendel, G. J., and Woodrufl, B.: Direct measurements of nitrogen oxides and ozone fluxes over grassland, Journal of Atmospheric Chemistry, 4, 429–444, https://doi.org/10.1007/BF00053844, https://doi.org/10.1007/BF00053844, 1986.

Delaria, E. R., Vieira, M., Cremieux, J., and Cohen, R. C.: Measurements of NO and NO_2 exchange between the atmosphere and *Quercus agrifolia*, Atmospheric Chemistry and Physics, 18, 14 161–14 173, https://doi.org/10.5194/acp-18-14161-2018, https://www.atmos-chem-phys.net/18/14161/2018/, 2018.

Delaria, E. R., Place, B. K., Liu, A. X., and Cohen, R. C.: Laboratory measurements of stomatal NO_2 deposition to native California trees and the role of forests in the NO_x cycle, Atmospheric Chemistry and Physics, 20, 14 023–14 041, https://doi.org/10.5194/acp-20-14023-2020, https://acp.copernicus.org/articles/20/14023/2020/, 2020.

Erisman, J. W. and Wyers, G. P.: Continuous measurements of surface exchange of SO_2 and NH_3; Implications for their possible interaction in the deposition process, Atmospheric Environment. Part A. General Topics, 27, 1937–1949, https://doi.org/10.1016/0960-1686(93)90266-2, http://linkinghub.elsevier.com/retrieve/pii/0960168693902662, 1993.

Erisman, J. W., Galloway, J. N., Seitzinger, S., Bleeker, A., Dise, N. B., Petrescu, A. M., Leach, A. M., and de Vries, W.: Consequences of human modification of the global nitrogen cycle, Philosophical Transactions of the Royal Society London B: Biological Sciences, 368, 20130 116, https://doi.org/10.1098/rstb.2013.0116, https://royalsocietypublishing.org/doi/abs/10.1098/rstb.2013.0116, 2013.

Eugster, W. and Hesterberg, R.: Transfer resistances of NO_2 determined from eddy correlation flux measurements over a litter meadow at a rural site on the swiss plateau, Atmospheric Environment, 30, 307–311, https://doi.org/10.1016/1352-2310(95)00418-1, http://www.sciencedirect.com/science/article/pii/1352231095004181, 1996.

Falge, E., Baldocchi, D., Olson, R., Anthoni, P., Aubinet, M., Bernhofer, C., Burba, G., Ceulemans, R., Clement, R., Dolman, H., Granier, A., Gross, P., Grünwald, T., Hollinger, D., Jensen, N.-O., Katul, G., Keronen, P., Kowalski, A., Lai, C. T., Law, B. E., Meyers, T., Moncrieff, J., Moors, E., Munger, J., Pilegaard, K., Üllar Rannik, Rebmann, C., Suyker, A., Tenhunen, J., Tu, K., Verma, S., Vesala, T., Wilson, K., and Wofsy, S.: Gap filling strategies for defensible annual sums of net ecosystem exchange, Agricultural and Forest Meteorology, 107, 43–69, https://doi.org/10.1016/S0168-1923(00)00225-2, http://www.sciencedirect.com/science/article/pii/S0168192300002252, 2001.

Famulari, D., Fowler, D., Hargreaves, K., Milford, C., Nemitz, E., Sutton, M. A., and Weston, K.: Measuring Eddy Covariance Fluxes of Ammonia Using Tunable Diode Laser Absorption Spectroscopy, Water, Air, & Soil Pollution: Focus, 4, 151–158, https://doi.org/10.1007/s11267-004-3025-1, http://link.springer.com/10.1007/s11267-004-3025-1, 2004.

Farmer, D. K. and Cohen, R. C.: Observations of HNO_3, Σ AN, Σ PN and NO_2 fluxes: evidence for rapid HO_x chemistry within a pine forest canopy, Atmospheric Chemistry and Physics, 8, 3899–3917, https://doi.org/10.5194/acp-8-3899-2008, https://www.atmos-chem-phys.net/8/3899/2008/, 2008.

Farmer, D. K., Wooldridge, P. J., and Cohen, R. C.: Application of thermal-dissociation laser induced fluorescence (TD-LIF) to measurement of HNO_3, Σ alkyl nitrates, Σ peroxy nitrates, and NO_2 fluxes using eddy covariance, Atmospheric Chemistry and Physics, 6, 3471–3486, https://doi.org/10.5194/acp-6-3471-2006, https://www.atmos-chem-phys.net/6/3471/2006/, 2006.

Farmer, D. K., Kimmel, J. R., Phillips, G., Docherty, K. S., Worsnop, D. R., Sueper, D., Nemitz, E., and Jimenez, J. L.: Eddy covariance measurements with high-resolution time-of-flight aerosol mass spectrometry: a new approach to chemically resolved aerosol fluxes, Atmospheric Measurement Techniques, 4, 1275–1289, https://doi.org/10.5194/amt-4-1275-2011, https://www.atmos-meas-tech.net/4/1275/2011/, 2011.

Ferm, M.: A Sensitive Diffusional Sampler, Report L91-172, Swedish Environmental Research Institute, Gothenburg, 1991.

Ferrara, R. M., Loubet, B., Di Tommasi, P., Bertolini, T., Magliulo, V., Cellier, P., Eugster, W., and Rana, G.: Eddy covariance measurement of ammonia fluxes: Comparison of high frequency correction methodologies, Agricultural and Forest Meteorology, 158-159, 30–42, https://doi.org/10.1016/j.agrformet.2012.02.001, https://doi.org/10.1016/j.agrformet.2012.02.001, 2012.

Ferrara, R. M., Di Tommasi, P., Famulari, D., and Rana, G.: Limitations of an Eddy-Covariance System in Measuring Low Ammonia Fluxes, Boundary-Layer Meteorology, https://doi.org/10.1007/s10546-021-00612-6, https://doi.org/10.1007/s10546-021-00612-6, 2021.

Finkelstein, P. L. and Sims, P. F.: Sampling error in eddy correlation flux measurements, Journal of Geophysical Research: Atmospheres, 106, 3503–3509, https://doi.org/10.1029/2000JD900731, https://agupubs.onlinelibrary.wiley.com/doi/abs/10.1029/2000JD900731, 2001.

Flechard, C. R., Nemitz, E., Smith, R. I., Fowler, D., Vermeulen, A. T., Bleeker, A., Erisman, J. W., Simpson, D., Zhang, L., Tang, Y. S., and Sutton, M. A.: Dry deposition of reactive nitrogen to European ecosystems: a comparison of inferential models across the NitroEurope network, Atmospheric Chemistry and Physics, 11, 2703–2728, https://doi.org/10.5194/acp-11-2703-2011, 2011.

Flechard, C. R., Massad, R. S., Loubet, B., Personne, E., Simpson, D., Bash, J. O., Cooter, E. J., Nemitz, E., and Sutton, M. A.: Advances in understanding, models and parameterizations of biosphere-atmosphere ammonia exchange, Biogeosciences, 10, 5183–5225, https://doi.org/10.5194/bg-10-5183-2013, https://www.biogeosciences.net/10/5183/2013/, 2013.

Flechard, C. R., Ibrom, A., Skiba, U. M., de Vries, W., van Oijen, M., Cameron, D. R., Dise, N. B., Korhonen, J. F. J., Buchmann, N., Legout, A., Simpson, D., Sanz, M. J., Aubinet, M., Loustau, D., Montagnani, L., Neirynck, J., Janssens, I. A., Pihlatie, M., Kiese, R., Siemens, J., Francez, A.-J., Augustin, J., Varlagin, A., Olejnik, J., Juszczak, R., Aurela, M., Berveiller, D., Chojnicki, B. H., Dämmgen, U., Delpierre, N., Djuricic, V., Drewer, J., Dufrêne, E., Eugster, W., Fauvel, Y., Fowler, D., Frumau, A., Granier, A., Gross, P., Hamon, Y., Helfter, C., Hensen, A., Horváth, L., Kitzler, B., Kruijt, B., Kutsch, W. L., Lobo-do Vale, R., Lohila, A., Longdoz, B., Marek, M. V., Matteucci, G., Mitosinkova, M., Moreaux, V., Neftel, A., Ourcival, J.-M., Pilegaard, K., Pita, G., Sanz, F., Schjoerring, J. K., Sebastià, M.-T., Tang, Y. S., Uggerud, H., Urbaniak, M., van Dijk, N., Vesala, T., Vidic, S., Vincke, C., Weidinger, T., Zechmeister-Boltenstern, S., Butterbach-Bahl, K., Nemitz, E., and Sutton, M. A.: Carbon–nitrogen interactions in European forests and semi-natural vegetation – Part 1: Fluxes and budgets of carbon, nitrogen and greenhouse gases from ecosystem monitoring and modelling, Biogeosciences, 17, 1583–1620, https://doi.org/10.5194/bg-17-1583-2020, https://www.biogeosciences.net/17/1583/2020/, 2020.

Galloway, J. N., Aber, J. D., Erisman, J. W., Seitzinger, S. P., Howarth, R. W., Cowling, E. B., and Cosby, B. J.: The Nitrogen Cascade, BioScience, 53, 341–356, https://doi.org/10.1641/0006-3568(2003)053[0341:TNC]2.0.CO;2, https://doi.org/10.1641/0006-3568(2003)053[0341:TNC]2.0.CO;2, 2003.

Garland, J. A.: The Dry Deposition of Sulphur Dioxide to Land and Water Surfaces, Proceedings of the Royal Society A: Mathematical, Physical and Engineering Sciences, 354, 245–268, https://doi.org/10.1098/rspa.1977.0066, https://royalsocietypublishing.org/doi/abs/10.1098/rspa.1977.0066, 1977.

Geddes, J. A. and Murphy, J. G.: Observations of reactive nitrogen oxide fluxes by eddy covariance above two midlatitude North American mixed hardwood forests, Atmospheric Chemistry and Physics, 14, 2939–2957, https://doi.org/10.5194/acp-14-2939-2014, https://acp.copernicus.org/articles/14/2939/2014/, 2014.

Hansen, K., Sorensen, L. L., Hertel, O., Geels, C., Skjoth, C. A., Jensen, B., and Boegh, E.: Ammonia emissions from deciduous forest after leaf fall, Biogeosciences, 10, 4577–4589, https://doi.org/10.5194/bg-10-4577-2013, https://bg.copernicus.org/articles/10/4577/2013/, 2013.

Hansen, K., Pryor, S. C., Boegh, E., Hornsby, K. E., Jensen, B., and Sorensen, L. L.: Background concentrations and fluxes of atmospheric ammonia over a deciduous forest, Agricultural and Forest Meteorology, 214-215, 380–392, https://doi.org/10.1016/j.agrformet.2015.09.004, http://www.sciencedirect.com/science/article/pii/S0168192315007091, 2015.

Högberg, P.: Nitrogen impacts on forest carbon, Nature, 447, 781–782, https://doi.org/10.1038/447781a, https://doi.org/10.1038/447781a, 2007.

Hollinger, D. Y. and Richardson, A. D.: Uncertainty in eddy covariance measurements and its application to physiological models, Tree Physiology, 25, 873–85, https://www.ncbi.nlm.nih.gov/pubmed/15870055, 2005.

Horii, C. V., Munger, J. W., Wofsy, S. C., Zahniser, M., Nelson, D., and McManus, J. B.: Fluxes of nitrogen oxides over a temperate deciduous forest, Journal of Geophysical Research: Atmospheres, 109, https://doi.org/10.1029/2003JD004326, https://agupubs.onlinelibrary.wiley.com/doi/abs/10.1029/2003JD004326, 2004.

Horii, C. V., Munger, J. W., Wofsy, S. C., Zahniser, M., Nelson, D., and McManus, J. B.: Atmospheric reactive nitrogen concentration and flux budgets at a Northeastern US forest site, Agricultural and Forest Meteorology, 136, 159–174, https://doi.org/10.1016/j.agrformet.2006.03.005, http://www.sciencedirect.com/science/article/pii/S0168192306000888, 2006.

Hurkuck, M., Brümmer, C., Mohr, K., Grünhage, L., Flessa, H., and Kutsch, W. L.: Determination of atmospheric nitrogen deposition to a semi-natural peat bog site in an intensively managed agricultural landscape, Atmospheric Environment, 97, 296–309, https://doi.org/10.1016/j.atmosenv.2014.08.034, http://www.sciencedirect.com/science/article/pii/S1352231014006281, 2014.

Jarraud, M.: Guide to meteorological instruments and methods of observation (WMO-No. 8), World Meteorological Organization, Geneva, Switzerland, 2008.

Jarvis, P. G.: The Interpretation of the Variations in Leaf Water Potential and Stomatal Conductance Found in Canopies in the Field, Philosophical Transactions of the Royal Society B: Biological Sciences, 273, 593–610, https://doi.org/10.1098/rstb.1976.0035, http://rstb.royalsocietypublishing.org/cgi/doi/10.1098/rstb.1976.0035, 1976.

Jensen, N. and Hummelshøj, P.: Derivation of canopy resistance for water vapor fluxes over a spruce forest, using a new technique for the viscous sublayer resistance (correction to vol. 73, p. 339, 1995), Agricultural and Forest Meteorology, 85, 289, https://doi.org/10.1016/S0168-1923(97)00024-5, http://www.sciencedirect.com/science/article/pii/S0168192397000245, 1997.

Jensen, N. O. and Hummelshøj, P.: Derivation of canopy resistance for water-vapor fluxes over a spruce forest, using a new technique for the viscous sublayer resistance, Agricultural and Forest Meteorology, 73, 339–352, https://doi.org/10.1016/0168-1923(94)05083-I, http://www.sciencedirect.com/science/article/pii/016819239405083I, 1995.

Kolle, O. and Rebmann, C.: EddySoft Documentation of a Software Package to Acquire and Process Eddy Covariance Data, techreport, MPI-BGC, https://repository.publisso.de/resource/frl:4414276-1/data, 2007.

Kreyling, J., Haei, M., and Laudon, H.: Snow removal reduces annual cellulose decomposition in a riparian boreal forest, Canadian Journal of Soil Science, 93, 427 – 433, https://doi.org/10.1139/CJSS2012-025, https://doi.org/10.1139/CJSS2012-025, 2013.

Krupa, S. V.: Effects of atmospheric ammonia (NH_3) on terrestrial vegetation: a review, Environmental Pollution, 124, 179–221, https://doi.org/10.1016/S0269-7491(02)00434-7, http://www.sciencedirect.com/science/article/pii/S0269749102004347, 2003.

Langford, B., Acton, W., Ammann, C., Valach, A., and Nemitz, E.: Eddy-covariance data with low signal-to-noise ratio: time-lag determination, uncertainties and limit of detection, Atmospheric Measurement Techniques, 8, 4197–4213, https://doi.org/10.5194/amt-8-4197-2015, https://www.atmos-meas-tech.net/8/4197/2015/, 2015.

Li, Y., Aneja, V. P., Arya, S. P., Rickman, J., Brittig, J., Roelle, P., and Kim, D. S.: Nitric oxide emission from intensively managed agricultural soil in North Carolina, Journal of Geophysical Research: Atmospheres, 104, 26 115–26 123, https://doi.org/10.1029/1999JD900336, https://agupubs.onlinelibrary.wiley.com/doi/abs/10.1029/1999JD900336, 1997.

Loescher, H. W., Law, B. E., Mahrt, L., Hollinger, D. Y., Campbell, J., and Wofsy, S. C.: Uncertainties in, and interpretation of, carbon flux estimates using the eddy covariance technique, Journal of Geophysical Research: Atmospheres, 111, https://doi.org/https://doi.org/10.1029/2005JD006932, https://agupubs.onlinelibrary.wiley.com/doi/abs/10.1029/2005JD006932, 2006.

LTER: Long Term Ecological Research (LTER) network, https://deims.org/993ed2fc-1cb0-4810-a619-8bcf78b6ecee, last access: ~~17 June 2020~~ 31 October 2021, 2020.

Magnani, F., Mencuccini, M., Borghetti, M., Berbigier, P., Berninger, F., Delzon, S., Grelle, A., Hari, P., Jarvis, P. G., Kolari, P., Kowalski, A. S., Lankreijer, H., Law, B. E., Lindroth, A., Loustau, D., Manca, G., Moncrieff, J. B., Rayment, M., Tedeschi, V., Valentini, R., and Grace, J.: The human footprint in the carbon cycle of temperate and boreal forests, Nature, 447, 848–50, https://doi.org/10.1038/nature05847, https://www.ncbi.nlm.nih.gov/pubmed/17568744, 2007.

Marx, O., Brümmer, C., Ammann, C., Wolff, V., and Freibauer, A.: TRANC – a novel fast-response converter to measure total reactive atmospheric nitrogen, Atmospheric Measurement Techniques, 5, 1045–1057, https://doi.org/10.5194/amt-5-1045-2012, http://www.atmos-meas-tech.net/5/1045/2012/, 2012.

Mauder, M. and Foken, T.: Impact of post-field data processing on eddy covariance flux estimates and energy balance closure, Meteorologische Zeitschrift, 15, 597–609, https://doi.org/10.1127/0941-2948/2006/0167, 2006.

Medinets, S., Gasche, R., Skiba, U., Schindlbacher, A., Kiese, R., and Butterbach-Bahl, K.: Cold season soil NO fluxes from a temperate forest: drivers and contribution to annual budgets, Environmental Research Letters, 11, 114 012, https://doi.org/10.1088/1748-9326/11/11/114012, https://doi.org/10.1088/1748-9326/11/11/114012, 2016.

Milford, C., Hargreaves, K. J., Sutton, M. A., Loubet, B., and Cellier, P.: Fluxes of NH_3 and CO_2 over upland moorland in the vicinity of agricultural land, Journal of Geophysical Research: Atmospheres, 106, 24 169–24 181, https://doi.org/10.1029/2001jd900082, http://doi.wiley.com/10.1029/2001JD900082, 2001.

Min, K.-E., Pusede, S. E., Browne, E. C., LaFranchi, B. W., Wooldridge, P. J., and Cohen, R. C.: Eddy covariance fluxes and vertical concentration gradient measurements of NO and NO_2 over a ponderosa pine ecosystem: observational evidence for within-

canopy chemical removal of NO_x, Atmospheric Chemistry and Physics, 14, 5495–5512, https://doi.org/10.5194/acp-14-5495-2014, http://www.atmos-chem-phys.net/14/5495/2014/, 2014.

Moffat, A. M., Papale, D., Reichstein, M., Hollinger, D. Y., Richardson, A. D., Barr, A. G., Beckstein, C., Braswell, B. H., Churkina, G., Desai, A. R., Falge, E., Gove, J. H., Heimann, M., Hui, D. F., Jarvis, A. J., Kattge, J., Noormets, A., and Stauch, V. J.: Comprehensive comparison of gap-filling techniques for eddy covariance net carbon fluxes, Agricultural and Forest Meteorology, 147, 209–232, https://doi.org/10.1016/j.agrformet.2007.08.011, https://doi.org/10.1016/j.agrformet.2007.08.011, 2007.

Moncrieff, J., Clement, R., Finnigan, J., and Meyers, T.: Averaging, Detrending, and Filtering of Eddy Covariance Time Series, pp. 7–31, Kluwer Academic, Dordrecht, https://doi.org/10.1007/1-4020-2265-4_2, https://doi.org/10.1007/1-4020-2265-4_2, 2004.

Moravek, A., Singh, S., Pattey, E., Pelletier, L., and Murphy, J. G.: Measurements and quality control of ammonia eddy covariance fluxes: A new strategy for high frequency attenuation correction, Atmospheric Measurement Techniques, 12, 6059–6078, https://doi.org/10.5194/amt-12-6059-2019, https://www.atmos-meas-tech.net/12/6059/2019/, 2019.

Munger, J. W., Wofsy, S. C., Bakwin, P. S., Fan, S. M., Goulden, M. L., Daube, B. C., Goldstein, A. H., Moore, K. E., and Fitzjarrald, D. R.: Atmospheric deposition of reactive nitrogen oxides and ozone in a temperate deciduous forest and a subarctic woodland: 1. Measurements and mechanisms, Journal of Geophysical Research-Atmospheres, 101, 12 639–12 657, https://doi.org/10.1029/96JD00230, https://agupubs.onlinelibrary.wiley.com/doi/abs/10.1029/96JD00230, 1996.

Nemitz, E., Jimenez, J. L., Huffman, J. A., Ulbrich, I. M., Canagaratna, M. R., Worsnop, D. R., and Guenther, A. B.: An Eddy-Covariance System for the Measurement of Surface/Atmosphere Exchange Fluxes of Submicron Aerosol Chemical Species—First Application Above an Urban Areas, Aerosol Science and Technology, 42, 636–657, https://doi.org/10.1080/02786820802227352, https://doi.org/10.1080/02786820802227352, 2008.

Pastorello, G., Trotta, C., and Canfora, E. e. a.: The FLUXNET2015 dataset and the ONEFlux processing pipeline for eddy covariance data, Scientific Data, 7, 225, https://doi.org/10.1038/s41597-020-0534-3, https://doi.org/10.1038/s41597-020-0534-3, 2020.

Paulson, C. A.: The Mathematical Representation of Wind Speed and Temperature Profiles in the Unstable Atmospheric Surface Layer, Journal of Applied Meteorology, 9, 857–861, https://doi.org/10.1175/1520-0450(1970)009<0857:Tmrows>2.0.Co;2, 1970.

Peake, E. and Legge, A. H.: Evaluation of methods used to collect air quality data at remote and rural sites in Alberta, Canada, in: Proc. 1987 EPA/APCA Symposium on Measurements of Toxic and Related Air Pollutants, APCA, 1987.

Peake, M.: A Preliminary Report on the Design and Testing of the KAPS (Kananaskis Atmospheric Pollutant Sampler) for the Collection of Acidic and Basic Gases and Fine Particles, Document 0012e/July 8/85. Typskript University Calgary, 1985.

Pryor, S. and Klemm, O.: Experimentally derived estimates of nitric acid dry deposition velocity and viscous sub-layer resistance at a conifer forest, Atmospheric Environment, 38, 2769–2777, https://doi.org/10.1016/j.atmosenv.2004.02.038, https://www.sciencedirect.com/science/article/pii/S1352231004002158, 2004.

Reichstein, M., Falge, E., Baldocchi, D., Papale, D., Aubinet, M., Berbigier, P., Bernhofer, C., Buchmann, N., Gilmanov, T., Granier, A., Grünwald, T., Havránková, K., Ilvesniemi, H., Janous, D., Knohl, A., Laurila, T., Lohila, A., Loustau, D., Matteucci, G., Meyers, T., Miglietta, F., Ourcival, J.-M., Pumpanen, J., Rambal, S., Rotenberg, E., Sanz, M., Tenhunen, J., Seufert, G., Vaccari, F., Vesala, T., Yakir, D., and Valentini, R.: On the separation of net ecosystem exchange into assimilation and ecosystem respiration: review and improved algorithm, Global Change Biology, 11, 1424–1439, https://doi.org/10.1111/j.1365-2486.2005.001002.x, https://onlinelibrary.wiley.com/doi/abs/10.1111/j.1365-2486.2005.001002.x, 2005.

Rondon, A., Johansson, C., and Granat, L.: Dry Deposition of Nitrogen-Dioxide and Ozone to Coniferous Forests, Journal of Geophysical Research-Atmospheres, 98, 5159–5172, https://doi.org/10.1029/92jd02335, 1993.

Rummel, U., Ammann, C., Gut, A., Meixner, F. X., and Andreae, M. O.: Eddy covariance measurements of nitric oxide flux within an Amazonian rain forest, Journal of Geophysical Research-Atmospheres, 107, LBA 17–1–LBA 17–9, https://doi.org/10.1029/2001JD000520, https://doi.org/10.1029/2001JD000520, 2002.

Saccone, P., Morin, S., Baptist, F., Bonneville, J.-M., Colace, M.-P., Domine, F., Faure, M., Geremia, R., Lochet, J., Poly, F., Lavorel, S., and Clèment, J.-C.: The effects of snowpack properties and plant strategies on litter decomposition during winter in subalpine meadows, Plant and Soil, 363, 215–229, https://doi.org/10.1007/s11104-012-1307-3, https://doi.org/10.1007/s11104-012-1307-3, 2013.

Schrader, F. and Brümmer, C.: Land Use Specific Ammonia Deposition Velocities: a Review of Recent Studies (2004–2013), Water, Air, and Soil Pollution, 225, 2114, https://doi.org/10.1007/s11270-014-2114-7, https://doi.org/10.1007/s11270-014-2114-7, 2014.

Seinfeld, J. H. and Pandis, S. N.: Atmospheric Chemistry and Physics – From Air Pollution to Climate Change, John Wiley & Sons, New York, USA, 2 edn., 2006.

Seok, B., Helmig, D., Ganzeveld, L., Williams, M. W., and Vogel, C. S.: Dynamics of nitrogen oxides and ozone above and within a mixed hardwood forest in northern Michigan, Atmospheric Chemistry and Physics, 13, 7301–7320, https://doi.org/10.5194/acp-13-7301-2013, https://acp.copernicus.org/articles/13/7301/2013/, 2013.

Stella, P., Kortner, M., Ammann, C., Foken, T., Meixner, F. X., and Trebs, I.: Measurements of nitrogen oxides and ozone fluxes by eddy covariance at a meadow: evidence for an internal leaf resistance to NO_2, Biogeosciences, 10, 5997–6017, https://doi.org/10.5194/bg-10-5997-2013, http://www.biogeosciences.net/10/5997/2013/, 2013.

Sutton, M. A., Tang, Y. S., Miners, B., and Fowler, D.: A New Diffusion Denuder System for Long-Term, Regional Monitoring of Atmospheric Ammonia and Ammonium, Water, Air and Soil Pollution: Focus, 1, 145–156, https://doi.org/10.1023/a:1013138601753, https://doi.org/10.1023/A:1013138601753, 2001.

Sutton, M. A., Simpson, D., Levy, P. E., Smith, R. I., Reis, S., van Oijen, M., and de Vries, W.: Uncertainties in the relationship between atmospheric nitrogen deposition and forest carbon sequestration, Global Change Biology, 14, 2057–2063, https://doi.org/10.1111/j.1365-2486.2008.01636.x, https://onlinelibrary.wiley.com/doi/abs/10.1111/j.1365-2486.2008.01636.x, 2008.

Sutton, M. A., Howard, C. M., Erisman, J. W., Billen, G., Bleeker, A., Grennfelt, P., van Grinsven, H., and Grizzetti, B., eds.: The European Nitrogen Assessment: sources, effects and policy perspectives, Cambridge University Press, Cambridge, UK, 2011.

Sutton, M. A., Reis, S., Riddick, S. N., Dragosits, U., Nemitz, E., Theobald, M. R., Tang, Y. S., Braban, C. F., Vieno, M., Dore, A. J., Mitchell, R. F., Wanless, S., Daunt, F., Fowler, D., Blackall, T. D., Milford, C., Flechard, C. R., Loubet, B., Massad, R., Cellier, P., Personne, E., Coheur, P. F., Clarisse, L., Van Damme, M., Ngadi, Y., Clerbaux, C., Skjoth, C. A., Geels, C., Hertel, O., Wichink Kruit, R. J., Pinder, R. W., Bash, J. O., Walker, J. T., Simpson, D., Horvath, L., Misselbrook, T. H., Bleeker, A., Dentener, F., and de Vries, W.: Towards a climate-dependent paradigm of ammonia emission and deposition, Philosophical Transactions of the Royal Society of London. Series B.: Biological Sciences, 368, 20130 166, https://doi.org/10.1098/rstb.2013.0166, https://www.ncbi.nlm.nih.gov/pubmed/23713128, 2013.

Tang, Y. S., Simmons, I., van Dijk, N., Di Marco, C., Nemitz, E., Dämmgen, U., Gilke, K., Djuricic, V., Vidic, S., Gliha, Z., Borovecki, D., Mitosinkova, M., Hanssen, J. E., Uggerud, T. H., Sanz, M. J., Sanz, P., Chorda, J. V., Flechard, C. R., Fauvel, Y., Ferm, M., Perrino, C., and Sutton, M. A.: European scale application of atmospheric reactive nitrogen measurements in a low-cost approach to infer dry deposition fluxes, Agriculture, Ecosystems and Environment, 133, 183–195, https://doi.org/10.1016/j.agee.2009.04.027, http://www.sciencedirect.com/science/article/pii/S0167880909001388, 2009.

Thoene, B., Rennenberg, H., and Weber, P.: Absorption of atmospheric NO_2 by spruce (Picea abies) trees, New Phytologist, 134, 257–266, https://doi.org/j.1469-8137.1996.tb04630.x, https://nph.onlinelibrary.wiley.com/doi/abs/10.1111/j.1469-8137.1996.tb04630.x, 1996.

UNECE: International Cooperative Program on Integrated Monitoring of Air pollution Effects on Ecosystems (ICP IM) within the framework of the Geneva Convention on Long-Range Transboundary, http://www.unece.org/env/lrtap/, last access: ~~17 June 2020~~ 31 October 2021, 2020.

Van Oss, R., Duyzer, J., and Wyers, P.: The influence of gas-to-particle conversion on measurements of ammonia exchange over forest, Atmospheric Environment, 32, 465 – 471, https://doi.org/10.1016/S1352-2310(97)00280-X, http://www.sciencedirect.com/science/article/pii/S135223109700280X, 1998.

van Zanten, M. C., Sauter, F. J., Wichink Kruit, R. J., van Jaarsveld, J. A., and van Pul, W. A. J.: Description of the DEPAC module; Dry deposition modeling with DEPAC_GCN2010, Tech. rep., RIVM, Bilthoven, NL, 2010.

Vickers, D. and Mahrt, L.: Quality Control and Flux Sampling Problems for Tower and Aircraft Data, Journal of Atmospheric and Oceanic Technology, 14, 512–526, https://doi.org/10.1175/1520-0426(1997)014<0512:QCAFSP>2.0.CO;2, http://doi.org/10.1175/1520-0426(1997)014<0512:QCAFSP>2.0.CO;2, 1997.

Webb, E. K.: Profile relationships: The log-linear range, and extension to strong stability, Quarterly Journal of the Royal Meteorological Society, 96, 67–90, https://doi.org/10.1002/qj.49709640708, https://rmets.onlinelibrary.wiley.com/doi/abs/10.1002/qj.49709640708, 1970.

Wentworth, G. R., Murphy, J. G., Benedict, K. B., Bangs, E. J., and Collett Jr, J. L.: The role of dew as a nighttime reservoir and morning source for atmospheric ammonia, Atmospheric Chemistry and Physics Discussions, 16, 1–36, https://doi.org/10.5194/acp-2016-169, http://www.atmos-chem-phys-discuss.net/acp-2016-169/, 2016.

Wesely, M. L.: Parameterization of Surface Resistances to Gaseous Dry Deposition in Regional-Scale Numerical-Models, Atmospheric Environment, 23, 1293–1304, https://doi.org/Doi 10.1016/0004-6981(89)90153-4, http://www.sciencedirect.com/science/article/pii/0004698189901534, 1989.

Whitehead, J. D., Twigg, M., Famulari, D., Nemitz, E., Sutton, M. A., Gallagher, M. W., and Fowler, D.: Evaluation of laser absorption spectroscopic techniques for eddy covariance flux measurements of ammonia, Environ Sci Technol, 42, 2041–6, https://doi.org/10.1021/es071596u, https://www.ncbi.nlm.nih.gov/pubmed/18409634, 2008.

Wilczak, J. M., Oncley, S. P., and Stage, S. A.: Sonic Anemometer Tilt Correction Algorithms, Boundary-Layer Meteorology, 99, 127–150, https://doi.org/10.1023/A:1018966204465, https://doi.org/10.1023/A:1018966204465, 2001.

Wintjen, P., Ammann, C., Schrader, F., and Brümmer, C.: Correcting high-frequency losses of reactive nitrogen flux measurements, Atmospheric Measurement Techniques, 13, 2923–2948, https://doi.org/10.5194/amt-13-2923-2020, https://www.atmos-meas-tech.net/13/2923/2020/, 2020.

Wolff, V., Trebs, I., Foken, T., and Meixner, F. X.: Exchange of reactive nitrogen compounds: concentrations and fluxes of total ammonium and total nitrate above a spruce canopy, Biogeosciences, 7, 1729–1744, https://doi.org/10.5194/bg-7-1729-2010, https://www.biogeosciences.net/7/1729/2010/, 2010.

Wyers, G. and Duyzer, J.: Micrometeorological measurement of the dry deposition flux of sulphate and nitrate aerosols to coniferous forest, Atmospheric Environment, 31, 333 – 343, https://doi.org/https://doi.org/10.1016/S1352-2310(96)00188-4, http://www.sciencedirect.com/science/article/pii/S1352231096001884, 1997.

Wyers, G. P. and Erisman, J. W.: Ammonia exchange over coniferous forest, Atmospheric Environment, 32, 441–451, https://doi.org/10.1016/S1352-2310(97)00275-6, http://www.sciencedirect.com/science/article/pii/S1352231097002756, 1998.

Zöll, U., Brümmer, C., Schrader, F., Ammann, C., Ibrom, A., Flechard, C. R., Nelson, D. D., Zahniser, M., and Kutsch, W. L.: Surface–atmosphere exchange of ammonia over peatland using QCL-based eddy-covariance measurements and inferential modeling, At-

mospheric Chemistry and Physics, 16, 11 283–11 299, https://doi.org/10.5194/acp-16-11283-2016, http://www.atmos-chem-phys.net/16/11283/2016/, 2016.

Zöll, U., Lucas-Moffat, A. M., Wintjen, P., Schrader, F., Beudert, B., and Brümmer, C.: Is the biosphere-atmosphere exchange of total reactive nitrogen above forest driven by the same factors as carbon dioxide? An analysis using artificial neural networks, Atmospheric Environment, 206, 108–118, https://doi.org/10.1016/j.atmosenv.2019.02.042, http://www.sciencedirect.com/science/article/pii/S1352231019301463, 2019.